Terahertz Amplification and Modulation Devices on Gallium Nitride

by

Brett Nathan Carnio

A thesis submitted in partial fulfillment of the requirements for the degree of

Master of Science

in

Electromagnetics and Microwaves

Department of Electrical and Computer Engineering

University of Alberta

Abstract

This thesis focuses on developing a high power, compact source of Terahertz (THz) radiation. An amplifier and an oscillator are designed using an active device exhibiting the Gunn Effect. The amplification properties of the amplifier and oscillator are first studied using the commercial software Comsol Multiphysics. Then, the electrical properties of the active device are studied using the commercial software Crosslight APSYS. This thesis also focuses on the modulation of THz radiation by a 2 dimensional electron gas (2DEG). THz time-domain spectroscopy (THz-TDS) experiments are performed on gallium nitride (GaN) samples in the presence and absence of a 2DEG and the measurements are used to predict the modulation introduced by the 2DEG. Additionally, THz-TDS experiments are performed on a bare sapphire wafer and GaN thin films (having various doping densities) grown on a sapphire substrate. The refractive index of the sapphire and GaN is determined from the measurements and compared to literature values. Furthermore, the GaN relative permittivity is determined from the measurements and compared to the Drude model.

Dedicated to my family, friends, and girlfriend for their love and support.

Acknowledgements

I am very thankful for the help I received from my supervisor, Dr. Abdulhakem Elezzabi. The knowledge I received from him helped me during graduate school and will undoubtedly help me in my career. His extraordinary attention to detail is something he has taught me the importance of and is a quality I hope to possess throughout my career. Dr. Elezzabi's willingness to help students is something that I experienced first-hand on many different occasions and the research in this thesis would not have been possible without his experience and knowledge. I am also very grateful for the financial support and expenses Dr. Elezzabi was willing to incur while supporting the research in this thesis.

I am equally thankful for the help I received from my supervisor, Dr. Douglas Barlage. His support motivated me to do my best and the guidance he provided always kept me on track. I am grateful for the time Dr. Barlage spent with me discussing this research and the knowledge he shared with me shaped my understanding of Gunn devices. I always looked forward to meetings with Dr. Barlage because of his optimism and easy-going personality, which made the stress of graduate school easier to manage. I am also thankful for the financial support and expenses Dr. Barlage was willing to incur while supporting the research in this thesis.

I am grateful to my colleagues, Alex Ma, Curtis Firby, Gem Shoute, Katherine Smith, Kevin Voon, Kyle Bothe, Mei Shen, Michael Nielsen, Mourad

Benlamri, Nir Katchinskiy, Shawn Greig, and Zohaib Hameed. This research would not have been possible without their willingness to help me and I would like to give a special thanks to Gem Shoute, Kyle Bothe, and Shawn Greig for training me on the equipment used during this research.

I would also like to thanks Dr. Cadien's group, especially Pouyan Motamedi, for preparing the AlN samples investigated during this research.

I also give thanks to my family who were always there for me, and my girlfriend who supported and motivated me when I needed it most.

Finally, I am grateful for the financial support provided by the Queen Elizabeth II Scholarships.

Table of Contents

List of Figures

List of Symbols and

Abbreviations

Fundamental constant

$\varepsilon_o = 8.854 \times 10^{-12}$ F/m	permittivity of free space
$e = 1.602 \times 10^{-19}$ C	elementary charge of electrons
$c = 2.99792 \times 10^{8}$ m/s	speed of light in a vacuum

Symbols

σ_{2DEG}	2DEG conductivity
G_{AC}	AC conductance
$\tilde{J}_{AC}$	AC current density
$\tilde{E}_{AC}$	AC electric field
R_{AC}	AC resistance
ρ_{AC}	AC resistivity
ω	angular frequency
V	anode voltage
fac	approximation factor
α	attenuation constant

$\tilde{\varepsilon}_b$	background relative permittivity
$\tilde{n}$	complex refractive index
d	contact (source-drain) distance
h_c	contact height
w_c	contact width
A	cross-sectional area in which electrons flow
I	current
j	current density
δ	damping term
δ_{mirror}	damping term corresponding to the lossy mirror of the resonator
μ_d	differential electron mobility
D	diffusion coefficient
m^*	effective mass of electron
E	electric field
N	electron concentration (cm^{-3})
v_d	electron drift velocity
μ	electron mobility
K	extinction coefficient
m_0	free electron mass
k_0	free space wavevector
f	frequency
L_G	gate length
V_G	gate voltage

h_r	height of resonator
ε_b''	imaginary part of background relative permittivity
ε_r''	imaginary part of relative permittivity
N_s	interface charge (cm^{-2})
L_{amp}	Length of amplifier
L_{dev}	Length of planar device (perpendicular to *x*-*y* plane)
ε_b'	real part of background relative permittivity
ε_r'	real part of relative permittivity
f_t	reciprocal of time it takes electrons to travel between device contacts
r	reflection coefficient
n	refractive index
$\tilde{\varepsilon}_r$	relative permittivity
x	spatial component
y	spatial component
z	spatial component
thickness	thickness of region in which electrons flow
t	thickness of materials
E_{th}	threshold electric field
$\tilde{E}(\omega)$	THz signal in the frequency domain
time	time
τ	time constant used in the Drude model
$\tilde{t}(\omega)$	transmission of THz radiation through a particular sample
λ	wavelength in a material

w_r	width of resonator

Abbreviations

1D	1 dimensional
2D	2 dimensional
2DEG	2 dimensional electron gas
AC	alternating current
AlGaAs	aluminum gallium arsenide
AlN	aluminum nitride
a.u.	arbitrary units
ALD	atomic layer deposition
Cr	chromium
DC	direct current
FT	Fourier Transform
GaAs	gallium arsenide
GaN	gallium nitride
Ge	germanium
GHz	gigahertz
HVPE	hydride vapor phase epitaxy
LSA	limited space-charge accumulation
MIS	metal-insulator-semiconductor
MD	modulation depth
NDC	negative differential conductivity

NDM	negative differential mobility
NDR	negative differential resistance
SI	semi-insulating
SPCT	Shockley's positive conductance theorem
Si	silicon
SA	stable amplification
THz	terahertz
TA	THz angular
THz-TDS	THz time-domain spectroscopy
TT	THz transmission
Ti	titanium
TEM	transverse electromagnetic

Chapter 1

Introduction

The terahertz (THz) regime consists of frequencies between 0.1 and 10 THz [1, 2] (or free space wavelengths between 0.03 and 3 mm) and falls between the microwave frequency regime and the infrared frequency regime. Currently, THz radiation is often generated through the use of a photoconductive antenna or by optical rectification and is detected through the use of a photoconductive antenna or by electro-optical sampling.

THz radiation is able to penetrate a number of non-conducting materials, such as clothing, plastic, and wood [3]. This is used in areas such as security and quality control of packaged goods [4]. THz radiation is also capable of exciting vibrational modes in organic and inorganic materials, which allows samples to be identified based on their chemical composition, and could be used to identify concealed drugs or explosives [4]. Furthermore, THz radiation has found a niche in medical applications. The amount of THz absorption can be used to distinguish between malignant or benign tissue [4], such that THz radiation may be used as a non-invasive cancer diagnostic technique. It is envisaged that THz radiation will find use in communication, mainly because short-range communication systems are expected to extend into the THz regime in the near future [5]. THz radiation is also

relevant to spectroscopy as THz time-domain spectroscopy (THz-TDS) is a technique often employed to study the fundamental interaction between THz radiation and a variety of materials [6].

1.1 Motivation

A major limitation associated with THz radiation is that compact, simple, and low cost sources of THz radiation are unavailable [7]. This has become known as the "THz gap" because technologies for generating microwave and infrared frequencies are well established [1], in contrast to that of THz radiation frequencies. Recently, GaN has emerged as a material capable of amplifying THz radiation, which is made possible since GaN exhibits a Gunn Effect combined with its short energy relaxation time [8-10]. GaN provided an exciting opportunity to produce a THz source, which would find use in applications such as imaging, security, quality control, material identification, medical, communications, and spectroscopy [1-7].

A modulation device attempting to extend short-range communication systems into the THz regime has been studied in [5, 11-15]. A 2 dimensional electron gas (2DEG) at a GaAs/AlGaAs interface, which may be depleted by an electrical bias voltage, modulates THz radiation transmitted through the device. This device successfully encodes an audio signal into a train of THz pulses. However, a limitation of this device is that a maximum of 3% modulation depth (MD) is achieved [12]. This is a major concern because even a small amount of noise in the channel may make it impossible to recover the signal encoded into the THz. The interface charge of a 2DEG at a GaN/AlN interface is often over an order of

magnitude larger than the interface charge of a 2DEG at a GaAs/AlGaAs interface. As such, a device with a 2DEG at a GaN/AlN interface is expected to allow for a modulation depth > 3%.

Before fabrication of THz devices it is helpful, and often necessary, to understand the properties of the material on which the device is fabricated. THz-TDS experiments have been used to study GaN [6, 10, 16-20]. However, additional research is still required to fully understand the effects of the GaN doping density and growth conditions on THz radiation.

1.2 Formation of a 2DEG at a GaN/AlN Interface

Fig. 1.1 illustrates the formation mechanism of a 2DEG at the interface of GaN (having Ga-faced polarity [21-23]) and AlN. The spontaneous and piezoelectric polarization properties of GaN and AlN [21, 22] induce a fixed positive surface charge at the GaN/AlN interface and a fixed negative surface charge at the AlN surface [24]. Electrons occupying donor-like surface states located at the AlN surface lower their energy by transferring into the GaN [24]. These electrons are attracted to the fixed positive surface charge at the GaN/AlN interface, such that a 2DEG forms a few nanometers inside the GaN. This attraction is only possible because the positive surface charge arising from the un-occupied donor-like surface states compensates for the negative surface charge at the AlN surface. The electrons in the 2DEG can only occupy discrete energy levels and the majority of the electrons occupy the ground state energy level.

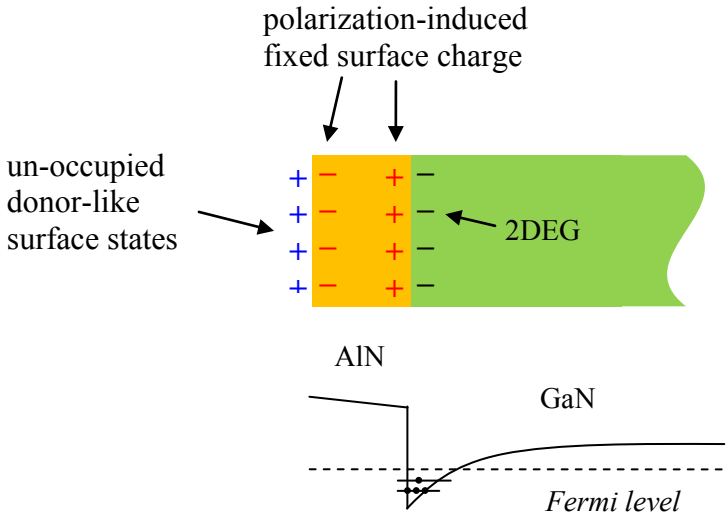

Fig. 1.1: Formation of a 2DEG at the interface of GaN and AlN. The 2DEG has discrete energy levels that are occupied by electrons.

1.3 The Gunn Effect

Devices fabricated on materials exhibiting the Gunn Effect, such as GaN and GaAs, produce a negative differential resistance (NDR) that can be used to amplify radiation. GaN exhibits a low mobility valley 0.9 eV above a higher mobility valley [25, 26], as shown in Fig. 1.2a. Electrons that gain enough energy (from an electric field) transfer to the higher energy valley and experience a reduction in their drift velocity, v_d, as seen in Fig. 1.2b. Here, E_{th} is the electric field value where the slope of the curve is zero and the portion of the curve with a negative slope has a negative differential mobility (NDM). This transfer of electrons, leading to a NDM, is referred to as the Gunn Effect.

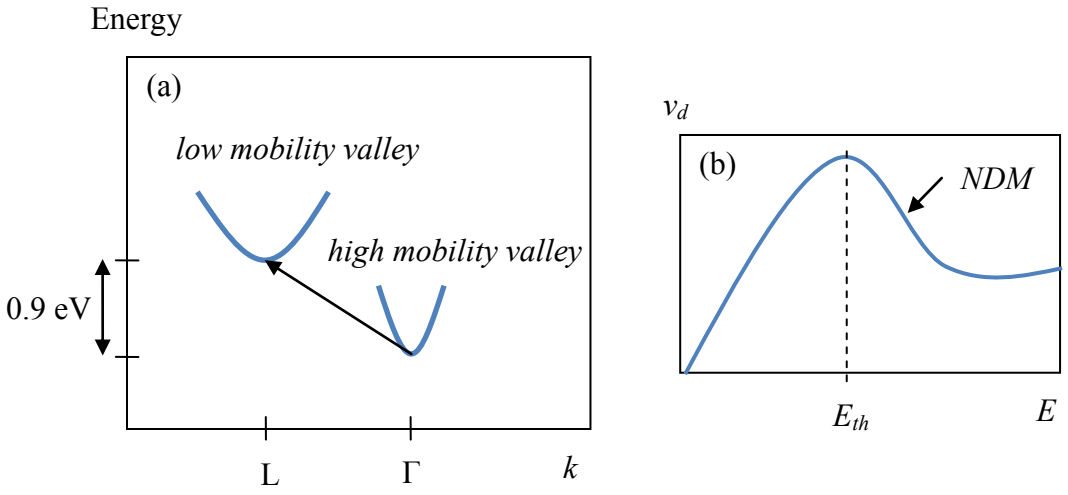

Fig. 1.2: (a) Schematic of electrons transferring from the low mobility valley to the high mobility valley in GaN, which are separated by 0.9 eV [25, 26]. (b) The electron drift velocity vs. electric field plot showing the existence of a NDM. E_{th} is the electric field value where the slope of the curve is zero.

The following sections briefly discuss Gunn and accumulation domains, Shockley's positive conductance theorem (SPCT), the stable amplification (SA) mode, the limited space-charge accumulation (LSA) mode, cathode domains, and a static NDR. All of these effects are relevant to the phenomenon of the Gunn Effect.

1.3.1 Gunn or Accumulation Domains

Devices that satisfy a specific set of conditions support Gunn or accumulation domains. When a Gunn Effect device, having ohmic contacts, is biased so the electric field is above E_{th}, a surplus of electrons arises at the cathode. This is shown by the blue curve in Fig. 1.3a and the electron bunch grows in

magnitude as it travels toward the anode. The electron bunch dissipates into the anode if the following three conditions are met [27-31],

$$N < \frac{\varepsilon_o \varepsilon_r' v_d^2}{4eD\left|\mu_{d,mimimum}\right|}, \tag{1.1a}$$

$$Nd > \frac{\varepsilon_o \varepsilon_r' v_d}{e\left|\mu_{d,minimum}\right|}, \tag{1.1b}$$

$$N * thickness > \frac{4 v_d \varepsilon_o}{e\left|\mu_{d,minimum}\right|}, \tag{1.1c}$$

where N is the electron concentration, ε_o is the permittivity of free space, ε_r' is the real part of the GaN relative permittivity, v_d is the drift velocity of the electrons in GaN, e is the electron charge, D is the diffusion coefficient of GaN, $\mu_{d,minimum}$ is the minimum electron differential mobility of GaN, d is the distance between the contacts, and *thickness* is the thickness of the region in which the electrons flow. When the electron bunch dissipates into the anode, a new bunch arises at the cathode, which later dissipates into the anode. This process is repeated, such that a steady-state is never reached and oscillations are observed in the current as a consequence of this repeated accumulation and dissipation. These electron bunches are commonly referred to as accumulation domains. However, if the cathode contact is not an ideal ohmic contact then a surplus of electrons followed by a depletion region may instead form at the cathode, which is shown by the blue curve in Fig. 1.3b. This electron concentration distribution may also occur if the doping near the cathode is less than the remainder of the device, which can be introduced

intentionally and is referred to as a doping notch. This electron distribution phenomenon is referred to as the Gunn domain, which behaves essentially identical to the accumulation domain. The time it takes for the Gunn or accumulation domains to traverse the device is equal to the velocity of the domain divided by the distance between the contacts of the device. This, thus, sets the oscillation frequency observed in the current. Clearly, by reducing the distance between the contacts of the device, this frequency can be increased. However, reducing this distance decreases the oscillation strength, which is the major limitation associated with Gunn and accumulation domains. In this mode, the NDR is supporting the propagation of the electron regions and may not be used to amplify an externally applied signal.

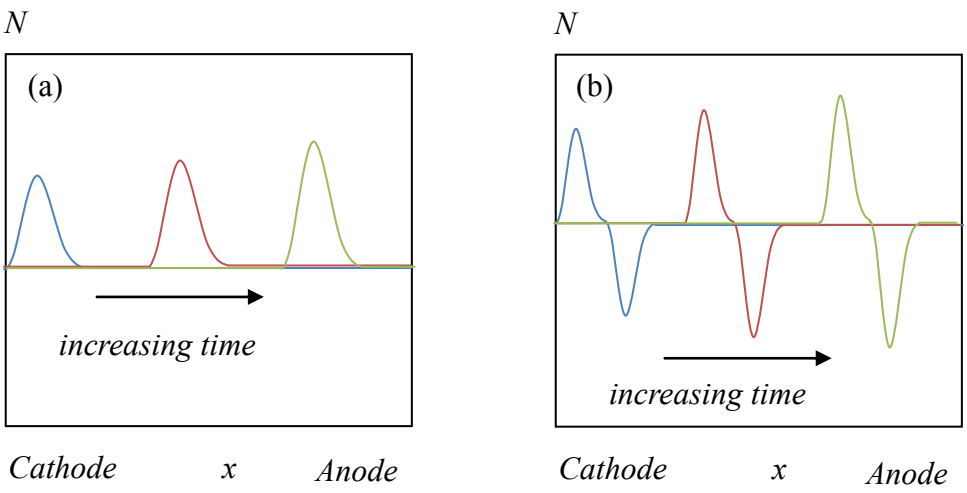

Fig. 1.3: Schematic showing (a) accumulation domains and (b) Gunn domains propagating from the cathode toward the anode. However, not shown are the accumulation and Gunn domains dissipating into the anode and the formation of a new domain at the cathode.

Devices supporting Gunn or accumulation domains with a frequency in the THz regime have been studied in detail; however, most of this research has been conducted only through simulations [32-35]. Aslan and Eastman [35] simulated a GaN-based planar device. When the distance between the contacts is 125 nm, accumulation domains oscillating at a frequency of 3.2 THz are observed at a DC to AC conversion efficiency < 2.3%. However, when the distance between the contacts is increased to 250 nm, accumulation domains oscillating at a frequency of 1.5 THz are observed (with efficiency < 3.5%). Torre et al. [34] performed Monte-Carlo simulations on GaN-based devices with a planar structure. Similarly, when the distance between the contacts is 1 μm, Gunn domains oscillating at a frequency of 0.3 THz are observed at a DC to AC conversion efficiency less than 0.5%. When the distance between the contacts is increased to 0.4 μm, Gunn domains oscillating at a frequency of 0.65 THz are observed (with efficiency ~ 0.1%). Alekseev and Pavlidis [33] performed hydro fluidic simulations on a GaN slab having contact distance of 2 μm. The device was shown to support Gunn domains oscillating at a frequency of 0.33 THz. Yang et al. [32] employed SILVACO ATLAS, which is a simulation tool capable of studying semiconductor devices, to study a slab of GaN with contacts on either end. When the distance between the contacts is 0.3 μm and the doping density is uniform, accumulation domains are observed to oscillate at a frequency of 0.70 THz. Interestingly, when a doping notch is made at the cathode, Gunn domains are observed to oscillate at a higher frequency of 0.75 THz.

1.3.2 Shockley's Positive Conductance Theorem

Devices that satisfy a specific set of conditions exhibit SPCT. When a Gunn Effect device, having ohmic contacts, is biased so the electric field is above E_{th}, a surplus of electrons arises at the cathode. This region of electrons travels along the device and, if any condition (i.e.: Eq. (1.1a), or (1.1b), or (1.1c)) is not satisfied, the electron bunch becomes "trapped" at the anode, as shown in Fig. 1.4a. Associated with this phenomenon is an accumulation of the electric field at the anode reaching a magnitude above E_{th}, as shown in Fig. 1.4b. The current in a semiconductor depends on both the electron drift velocity (which decreases as the field increases above E_{th}) and the electron concentration. SPCT states that the increase in electron concentration at the anode more than compensates for the decrease in electron drift velocity at the anode [36, 37]. This results in a DC resistance that is positive at all bias voltages.

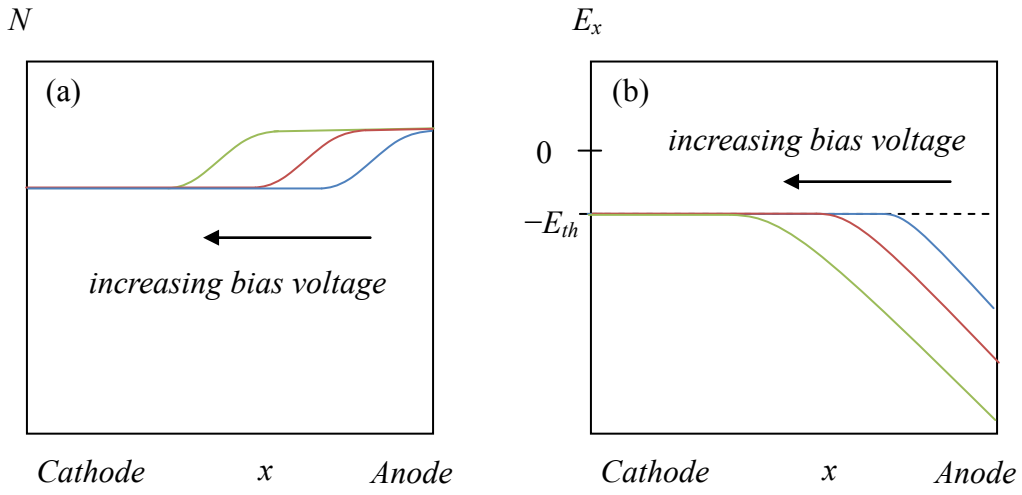

Fig. 1.4: Schematic of the (a) electron concentration and (b) electric field associated with SPCT. This schematic is designed assuming the electron drift velocity vs. electric field curve of GaN remains flat after the NDM region, as shown in [38].

SPCT was first derived in 1954, under a number of simplifying assumptions [36]. Kroemer [37] later generalized the SPCT formalism for arbitrary geometries and Hauge [39] and Döhler [40] generalized the SPCT formalism for a material having a diffusion coefficient that depends on electric field. A comprehensive theoretical analysis was performed by McCumber and Chynoweth [27], which focused on the conditions necessary to observe this effect.

1.3.3 Stable Amplification Mode

Devices that exhibit SPCT are able to operate in the SA mode. A device that operates in the SA mode supports a NDR within multiple frequency bands, as shown in Fig. 1.5. The lowest frequency band is centered at the frequency, f_t, which is equal to the reciprocal of the time it takes the electrons to traverse between the contacts of the device. The higher frequency bands are centered at the harmonics of f_t. Clearly, the largest NDR occurs at the frequency band centered at f_t [27] and the NDR is positive at DC (as required by SPCT [36]). A more detailed discussion of the SA mode is presented in section 3.2 of this thesis.

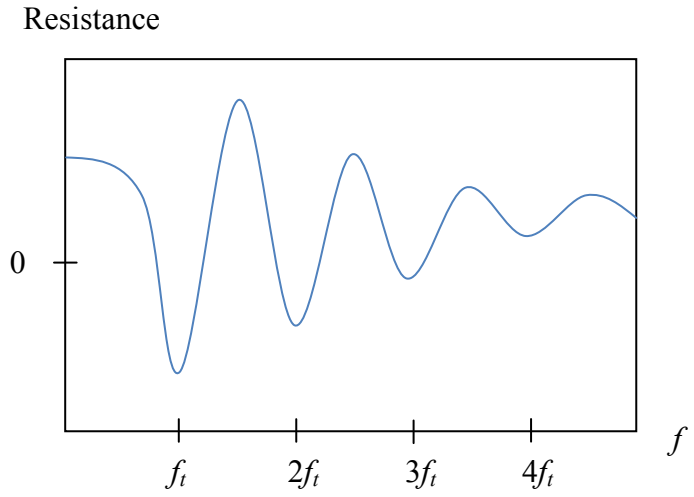

Fig. 1.5: Schematic showing a positive resistance existing at DC, and an NDR existing in frequency bands centered at f_t and its harmonics. f_t is equal to the reciprocal of the time it takes the electrons to transverse between the contacts of the device.

Thim and Barber [41, 42], Baynham and Colliver [43, 44], and Fleming et al. [45, 46] have used the SA mode to amplify frequencies in the GHz regime. In the THz regime, such devices are key interest if they are fabricated on a GaN platform. Thim and Barber [41, 42] excited a space-charge wave (i.e.: electron region) at the cathode of a device exhibiting the SA mode. Here, the wave propagated along the device and the amplified signal is extracted at the anode. Thim and Barber [42] investigated a device fabricated on GaAs and observed a positive power gain in the frequency region between 2.2 and 4.1 GHz, with maximum power gain of 10 observed at a frequency of 4 GHz. In a different investigation, Thim [41] reported on a GaAs device having a power gain ranging from 0.8 to 3.8 between frequencies of 4 and 8 GHz. Baynham and Colliver [43, 44] investigated the microstrip line structure device shown in Fig. 1.6a. The material exhibiting the Gunn Effect acts as

a cavity supporting standing wave modes, where the material-air boundaries are reflective enough to make round trip gain possible. Baynham [44] reported on a Ge-based device (another material exhibiting the Gunn Effect) and observed emission from the Ge-air boundaries with a frequency of 3.74 GHz. Baynham and Colliver [43] also studied a GaAs-based device and observed emission at frequencies ranging from 2.3-4.2 GHz. Fleming et al. [45, 46] studied the device with the co-planar waveguide structure shown in Fig. 1.6b. A signal was applied to one end of the device, which propagates along the contacts of the device, and the amplified signal is extracted from the other end. Fleming [45] studies a device fabricated on GaAs and amplification is achieved at frequencies between 15 and 22 GHz. A signal at 20 GHz experiences gain as large as 3 dB. In a later publication, Fleming et al. [46] investigated a similar device and a gain of 4.86 dB was observed at 17.5 GHz. Amplification is determined to occur between 16 and 18 GHz in this device.

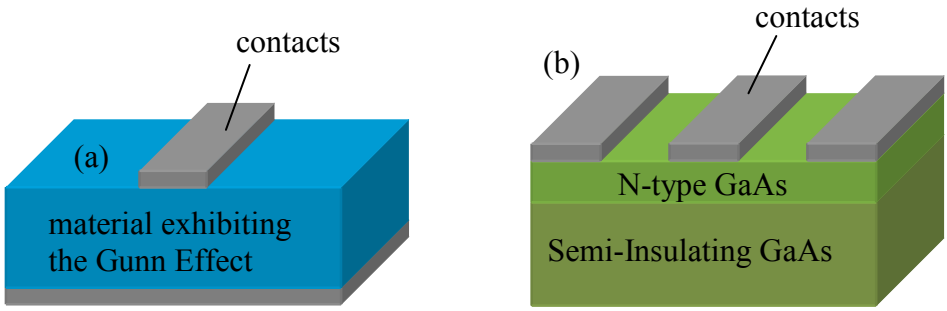

Fig. 1.6: (a) The oscillator studied by Baynham, which has a microstrip line structure (adapted from Baynham, 1970 [47]). (b) The amplifier studied by Fleming, which behaves as a co-planar waveguide (adapted from Fleming, 1975 [45]).

1.3.4 Limited Space-Charge Accumulation Mode

The LSA mode states that an AC voltage applied to a device exhibiting Gunn domains, accumulation domains, or SPCT is sustained if the following conditions are met [48],

$$\frac{N}{f} < \frac{3\varepsilon_r'\varepsilon_o}{e|\mu_{av}|}, \tag{1.2a}$$

$$\frac{N}{f} > \frac{\varepsilon_r'\varepsilon_o}{e\mu_o}, \tag{1.2b}$$

where f is the frequency of the AC voltage applied by a resonant circuit, μ_{av} is the average negative electron mobility, and μ_o is the electron mobility of GaN at low electric fields. Equation (1.2a) places a restriction on the length of time the electric field in the semiconductor can remain above E_{th}. If Eq. (1.2a) is satisfied then the electric field in the semiconductor does not remain above E_{th} long enough for accumulation domains, Gunn domains, or the electron bunch discussed in section 1.3.2 to completely form. Furthermore, Eq. (1.2b) places a restriction on the length of time the electric field in the semiconductor can remain below E_{th}. If Eq. (1.2b) is satisfied then the electric field in the semiconductor remains below E_{th} long enough for accumulation domains, Gunn domains, or the electron bunch discussed in section 1.3.2 to completely dissipate [48, 49]. If Eq.'s (1.2a) and (1.2b) are satisfied, then the electric field remains approximately uniform in the device and the electron concentration remains approximately constant with increasing bias voltage.

The AC voltage is sustained because it is essentially operating on a current vs. voltage curve with an NDR [50], as illustrated in Fig. 1.7.

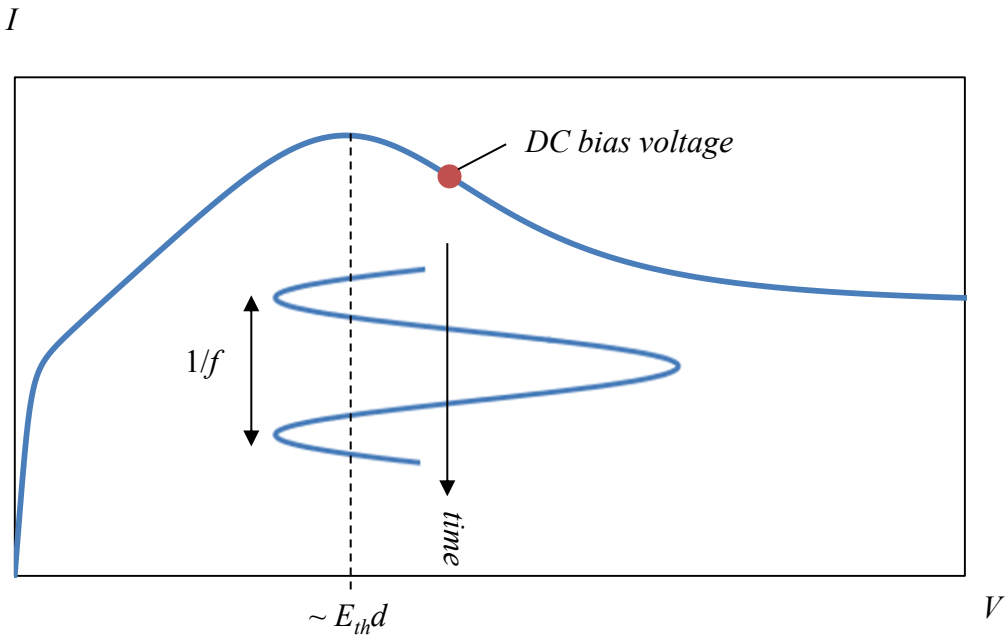

Fig. 1.7: Schematic showing an AC voltage superimposed onto the anode current vs. anode voltage curve associated with the LSA mode. The peak current occurs at a voltage of ~ $E_{th}d$, since the electric field in the device remains approximately uniform.

Devices supporting the LSA mode at a frequency in the THz regime have been studied; however, this has only been done through simulations. Sokolov et al. [51] studied a device fabricated on GaN using a transport model and a quasistatic large-signal approach. When the distance between the contacts is 100 nm, a DC to AC conversion efficiency of up to 8.9% is predicted and this device is capable of sustaining oscillations with frequencies between 0.14 and 1.6 THz. Barry [52] simulates a device fabricated on GaN and that has a distance between the contacts of 100 nm. This device supports frequencies between 0.5 and 2.3 THz and the

maximum DC to AC conversion efficiency is about 1.7%, which is obtained at 2.1 THz. Barry et al. [53] investigated a GaN device using a high-field electron transport model and the local quasistatic approximation. When the distance between the contacts of the device is 0.5 μm, they reported THz oscillation in the region of 0.33-0.88 THz. A maximum DC to AC conversion frequency of nearly 1.2% was obtained at 0.6 THz.

1.3.5 Cathode Domain

When the material exhibiting the Gunn Effect has an "imperfect" cathode contact, a surplus of electric field may form at the cathode. This is commonly referred to as a cathode domain [54, 55] and is illustrated in Fig. 1.8a. Cathode domains increase in width with additional bias voltage and a depletion region exists in the electron concentration at the location where the electric field equals E_{th}, as shown in Fig. 1.8b. This phenomenon occurs because the electron drift velocity is largest at this point, such that a small electron concentration is required to satisfy current continuity. The depletion region shifts towards the anode region with increasing bias voltage and seems to "propagate" as the bias voltage increases. At a bias voltage slightly below $E_{th}d$ the cathode domain often breaks away from the cathode and initiates Gunn or accumulation domains [54]. If the cathode domain does not break away from the cathode then the device remains in a steady-state, which results in a DC resistance that is positive at all bias voltages.

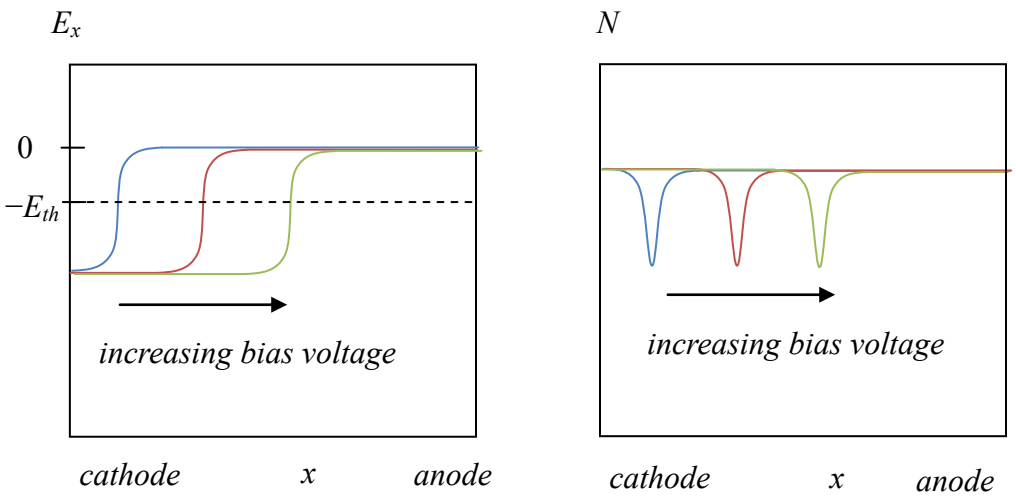

Fig. 1.8: A schematic of the (a) electric field and (b) electron concentration associated with a cathode domain.

Böer et al. [54] used the field of directions to show that cathode domains form if a slightly blocking schottky contact exists at the cathode. Böer et al. [54] also considers the situation when a strongly blocking schottky contact exists at the cathode. At low bias voltages a depletion region exists near the cathode, which arises due to the strongly blocking cathode, and the electric field accumulates in the depletion region only. This is the normal operation of a device with a strongly blocking cathode contact. However, at larger bias voltages a cathode domain appears adjacent to the electric field that accumulated in the depletion region. Böer et al. [54] showed that the cathode domains that occur due to a slightly blocking cathode contact can lead to Gunn domains; however, cathode domains that occur due to a strongly blocking cathode are expected to remain stable. Gunn [56] observed cathode domains experimentally in GaAs. At large bias voltage values, the

domain breaks away from the cathode and a cyclic propagation of domains is observed.

1.3.6 Static Negative Differential Resistance

The current density in a semiconductor, assuming diffusion current is negligible, is described by the equation,

$$j = eNv_d(E)\,, \tag{1.3}$$

where E is the electric field. If the electron concentration, N, does not change with bias voltage and the electric field between the contacts of the device increases uniformly with the bias voltage, then the NDM directly results in an NDR. This is often referred to as a static NDR. A device structure for exhibiting NDM is shown in Fig. 1.9a, which is studied in [58]. The primary axis of Fig. 1.9b shows the current vs. voltage obtained from this device and the secondary axis shows the electron drift velocity vs. electric field of GaN. The NDR is a result of the Gunn Effect and is expected to exist up to THz due to the small energy relaxation time of GaN [8-10]. Huang et al. [38] also measured a static NDR from a planar device fabricated on low-doped GaN, while Yilmazoglu et al. [57] measured a static NDR from a device with a vertical structure and a doping density of 10^{17} cm^{-3}.

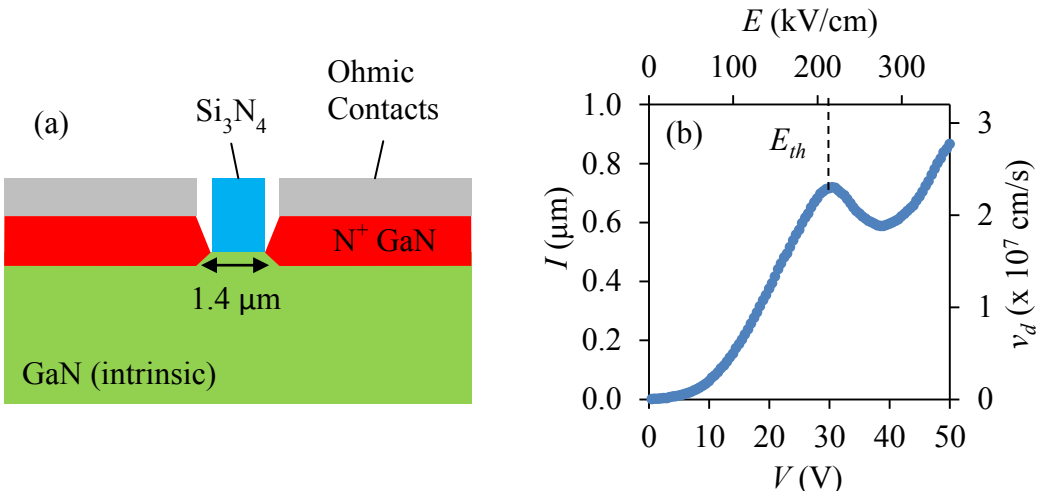

Fig. 1.9: (a) The gateless device studied in [58], which is fabricated on low-doped GaN (adapted from Ceroici et al., 2012 [58]). (b) The current vs. voltage curve clearly showing a NDR region and the electron drift velocity vs. electric field curve clearly showing a NDM region [58].

A device exhibiting a NDR has the ability to amplify a signal. A semiconductor device exhibits a NDR when the current flowing into the anode decreases with increasing bias voltage. This means the current density flowing in the semiconductor decreases as the electric field in the semiconductor increases. As such, the semiconductor exhibits a negative differential conductivity (NDC). However, this NDC only exists at the specific anode bias voltage and only exists in the specific region of the semiconductor that the current is flowing. Radiation interacting with this NDC region experiences amplification if the gain provided by the region of the semiconductor exhibiting a NDC overcomes the losses experienced by the radiation. Due to the low electron concentration of the GaN, the NDR measured in [58] is unable to overcome the THz losses. It should be noted that the electron concentration in the device may be increased significantly by inducing a 2DEG (i.e.: a channel), as shown in Fig. 1.10. This proposed device can: (1) amplify

THz radiation by exciting a wave on the contacts of the device and allowing it to propagate and, (2) be placed into a resonator to sustain THz oscillations.

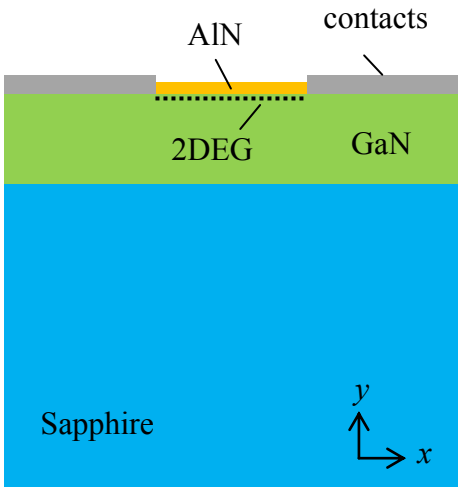

Fig. 1.10: The gateless device fabricated on GaN and that has a 2DEG (i.e.: a channel), which is a result of polarization effects between the AlN and GaN [24].

1.4 THz Modulation Device

A modulation device is used to encode signals containing information into a higher frequency signal (known as the carrier signal) to be transmitted to another location [59]. Kleine-Ostmann et al. [13] designed and tested the THz modulation device illustrated in Fig. 1.11a. THz modulation is achieved by electrically-controlling the presence or depletion of a 2DEG. To fully understand how this device operates, consider the example in Fig. 1.11b, which shows a train of THz pulses being transmitted through the modulator. The voltage on the Cr contact is large and negative at the time of the first pulse through the device. The 2DEG is depleted, such that the pulse is transmitted through the device with large amplitude. However, the voltage on the Cr contact is at an intermediate negative value at the

time of the second pulse through the device. The 2DEG is partially depleted and, therefore, the pulse is transmitted through the device with slightly smaller amplitude then the first pulse. Finally, there is no voltage applied to Cr contact at the time the third pulse is through the device. The 2DEG is fully present and the pulse is transmitted through the device with the smallest amplitude of the three pulses. Thus, the signal applied to the Cr contact is encoded into the amplitude of the THz pulses.

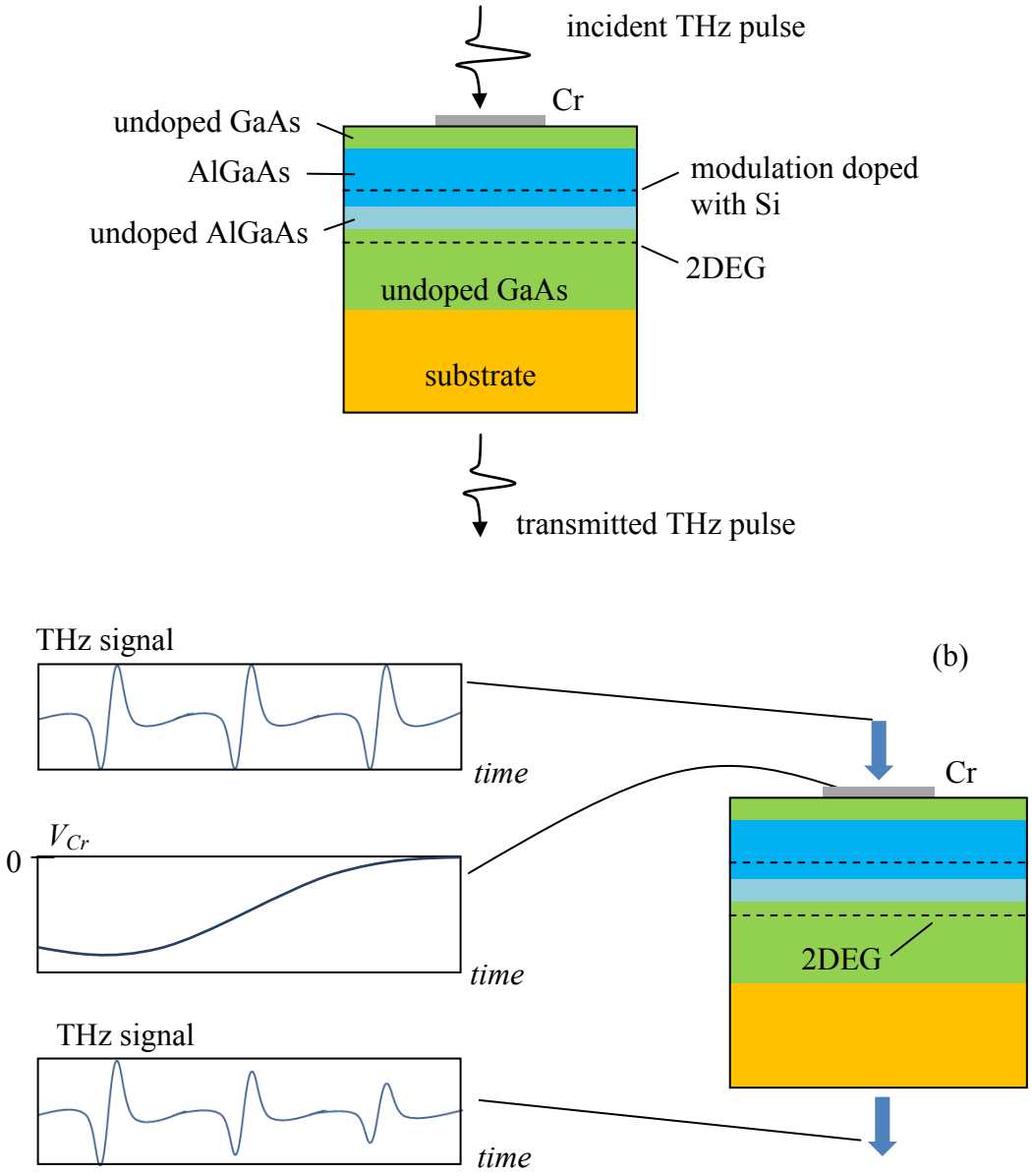

Fig. 1.11: (a) Schematic of the THz modulator fabricated on GaAs (adapted from Kleine-Ostmann et al., 2004 [13]). (b) A simple example showing the operation of the THz modulator. The amplitude of the transmitted pulses depends on the 2DEG concentration and, therefore, on the voltage applied to the Cr. V_{Cr} is the voltage, *time* is the time, and the blue arrows represent transmission of THz radiation through the device.

1.5 Research Objectives

The main objectives of this thesis are:

- To design a high-power THz amplifier and/or oscillator that is inexpensive and compact using a GaN platform.
- To investigate the static NDR mode and the SA mode and their potential to amplify THz radiation.
- To provide a better understanding of devices fabricated on GaN that incorporate a channel configuration. A more specific objective is to determine if a static NDR can be obtained from these devices.
- To improving the modulation depth obtained from the THz modulation devices based on a 2DEG at a GaAs/AlGaAs interface.
- To study the interaction of THz radiation with GaN having various doping densities.

1.6 Thesis Outline

This thesis consists of 5 chapters, which consider THz amplification devices, THz modulation from a 2DEG, and THz spectroscopy of GaN.

In chapter 2, a commercial software package (Comsol Multiphysics) is used to simulate THz amplification devices, under the assumption of a static NDR. The simulations are performed to determine the feasibility of THz amplification.

In chapter 3, a commercial software package (Crosslight APSYS) is used to simulate a GaN-based, gateless device having ohmic contacts to determine if a static NDR occurs. A gated device employing ohmic contacts and a gateless device employing metal-insulator-semiconductor (MIS) contacts are also simulated for the

same reason. Furthermore, Crosslight APSYS is used to determine the resistivity of a non-planar GaN-device based and to determine if a planar GaN-device (and having a channel) is able to exhibit the SA mode.

In chapter 4, THz pulses are transmitted through (and reflected from) GaN samples in the presence and absence of a 2DEG. The measurements are used to predict the amount of modulation that occurs from a 2DEG at an AlN/GaN interface. In addition, THz pulses are transmitted through GaN thin films (grown on sapphire), as well as a bulk sapphire wafer. The GaN and sapphire complex refractive index is determined, as well as the GaN relative permittivity.

In chapter 5, the results of this research are summarized. This chapter also presents suggestions for continuing this research.

Chapter 2

THz Amplifier and Oscillator

COMSOL Multiphysics software is used to simulate an amplifier and oscillator, which amplifies THz radiation using the active device shown in Fig. 1.10. The main objective of this chapter is to determine if THz amplification is achieved in the amplifier and/or the oscillator, under the assumption that the active device exhibits a static NDR. Another objective is to determine possible techniques to increase the amplification observed in the amplifier and the oscillator.

2.1 Active Device

This section discusses the techniques and approximations used to implement the active device into COMSOL. Voon et al. [60] determined that a 2DEG at the interface of low-doped GaN and 5.7 nm of AlN has an interface charge of 1.9×10^{13} cm^{-2}. Implementing this interface charge into Crosslight APSYS software produces a 2DEG having a concentration of 85×10^{18} cm^{-3} and a thickness of

approximately 1 nm. As such, the 2DEG in COMSOL is modelled as a rectangular region with a thickness of 1 nm and a 2DEG concentration $\leq 85 \times 10^{18}$ cm^{-3}. Furthermore, the 2DEG conductivity, σ_{2DEG}, must be anisotropic because only the component of the electric field in the direction of current flow is amplified [61, 62]. This is achieved by defining the tensor,

$$[\sigma_{2DEG}] = \begin{bmatrix} eN\mu_{d,2DEG}(E) & 0 & 0 \\ 0 & 0 & 0 \\ 0 & 0 & 0 \end{bmatrix}, \tag{2.1}$$

where $\mu_{d,2DEG}$ is the differential mobility of the electrons in the 2DEG. The top-left component in this equation is the only non-zero component because the electrons in the 2DEG are assumed to flow entirely in the *x*-direction (see Fig. 1.10). This is a valid assumption since the 2DEG is only 1 nm thick. Moreover, this component has a value of $eN\mu_{d,2DEG}(E)$ because the 2DEG is assumed to have a static NDR. The 2DEG electron mobility is defined as −100 cm^2/(Vs), which is determined from the slope of the curve in Fig. 1.9b at an electric field value of ~ 240 kV/cm.

The GaN and sapphire are defined by a complex refractive index of 3 + *i**0, which is based on the assumption that low-doped GaN and sapphire have a similar complex refractive index at THz [6, 63]. The contacts of the active device are assumed to be gold having a complex refractive index described by the function [64],

$$\tilde{n} = 300 + i1020.5\left(\frac{f}{10^{12}}\right)^{-0.94}, \tag{2.2}$$

where f is the radiation frequency. This equation is only valid for frequencies between 0.5 and 2 THz.

Considering the factors outlined above, the device shown in Fig. 1.10 is transformed into the device shown in Fig. 2.1, which can now be implemented into COMSOL. The contact width (w_c), the contact height (h_c), and the contact distance (d) are design parameters that influence THz amplification.

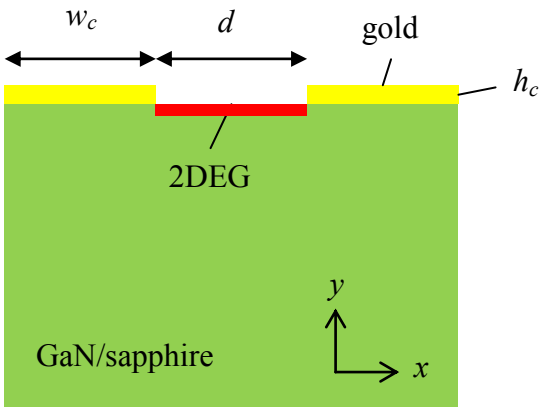

Fig. 2.1: Schematic of the active device used in the simulations. w_c, h_c, and d are design parameters.

2.2 THz Amplifier

A THz signal may be amplified by DC biasing the active device into the NDR region and applying a THz wave to the contacts. This excites a transverse electromagnetic (TEM) mode that propagates along the contacts perpendicular to the x-y plane. Amplification occurs if the gain that the TEM mode experiences

overcome the loss it experiences. The active device in Fig. 2.1 is referred to as the THz amplifier when used in this manner.

Details of the simulation are discussed in section 2.2.1. Amplification of the TEM mode, as well as techniques to improve this amplification, is discussed in sections 2.2.2-2.2.4.

2.2.1 Simulation Details

The TEM mode of the amplifier is obtained and analysed using COMSOL's 2D "Mode Analysis" study, which solves Maxwell's equations using the finite element method. The amplifier is enclosed in a rectangular region defined by perfect electric conductor boundaries. These boundaries are carefully placed far enough from the amplifier that they have no effect on the TEM mode. Amplification of the TEM mode is studied using the attenuation constant, α, which is defined in the equation,

$$\frac{|E_{out}|}{|E_{in}|} = e^{-\alpha L_{amp}}, \tag{2.3}$$

where E_{out} is the electric field at the end of the amplifier, E_{in} is the electric field at the beginning of the amplifier, and L_{amp} is the length of the amplifier in the direction perpendicular to the *x*-*y* plane. It is worth noting that this equation does not consider saturation of the TEM mode's amplification.

The reliability of the simulation is checked by simulating the amplifier that has a 2DEG conductivity of 0 S/m and ignoring the loss of the contacts. An attenuation constant of $0\ \mathrm{mm}^{-1}$ is obtained, confirming that the simulation environment is properly set up under these simplified conditions. It is very easy to introduce too few mesh points in regions thinner than about 1 μm, which could lead to incorrect results. Therefore, the mesh in the 2DEG and the mesh in the contacts are reduced (in a few select simulations) and the attenuation constant remains essentially unchanged, which confirms that the mesh in these regions is satisfactory.

2.2.2 Basic THz Amplifier

The optimal contact width (w_c), contact height (h_c), and contact distance (d) are determined by simulating the amplifier at a 2DEG concentration of $85 \times 10^{18}\ \mathrm{cm}^{-3}$ and an operating frequency of 1 THz. Amplification of the TEM mode increases as the contact width and contact distance decreases because the TEM mode interacts better with the 2DEG at smaller dimensions. The optimal value for both parameters is 1 μm, since this is the smallest dimension that can be fabricated at the University of Alberta. Maximum amplification is achieved when the contact height is 200 nm. This could be because the mode interacts best with the 2DEG at this value, or it could be related to the fact that THz radiation experiences more loss from metals having smaller dimensions [65]. The amplifier studied in this section, as well as in sections 2.2.3 and 2.2.4, is defined by the optimal dimensions stated above.

The amplifier is investigated at an operating frequency of 1 THz. Amplification is achieved at 2DEG concentrations $> 7.8 \times 10^{18}$ cm^{-3}, as seen in Fig. 2.2a, and an attenuation constant of -5.8 mm^{-1} is achieved at a 2DEG concentration of 85×10^{18} cm^{-3}. The TEM mode supported by the amplifier is shown in Fig. 2.2b and the radiation interacts well with the 2DEG.

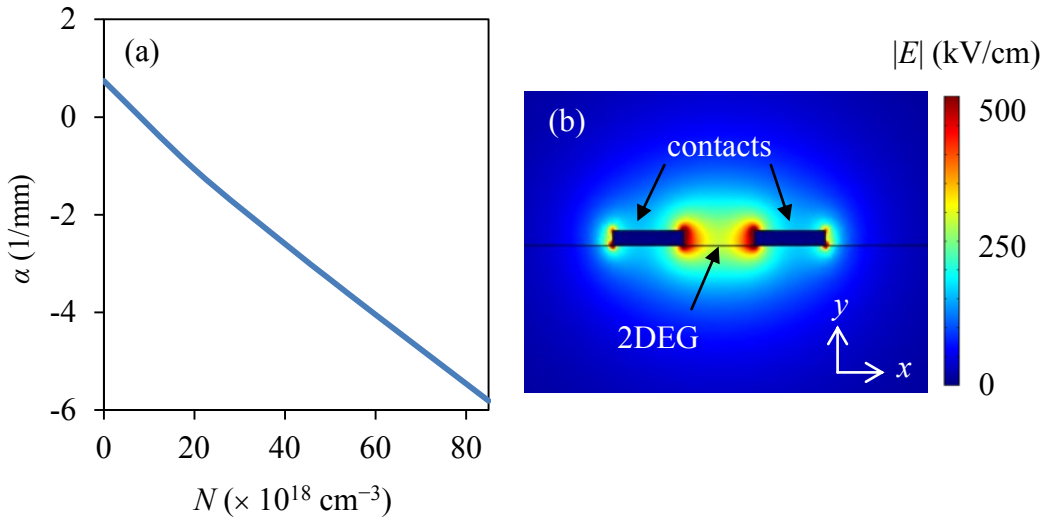

Fig. 2.2: (a) The attenuation constant vs. 2DEG concentration, obtained at $f = 1$ THz. (b) The TEM mode supported by the amplifier.

The amplifier is investigated at a 2DEG concentration of 50×10^{18} cm^{-3}. The TEM mode experiences amplification at frequencies between 0.5 and 2 THz, as shown in Fig. 2.3.

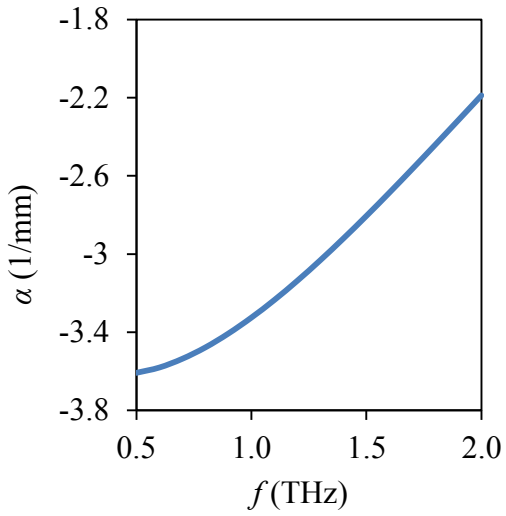

Fig. 2.3: The attenuation constant vs. operating frequency, obtained at $N = 50 \times 10^{18}$ cm^{-3}.

Amplification of the TEM mode vs. amplifier length is obtained from Eq. (2.3) and plotted in Fig. 2.4. This plot is created using an attenuation constant of -3.3 mm^{-1} and the electric field magnitude grows by a factor of 10 for an amplifier having a length of ~ 700 μm.

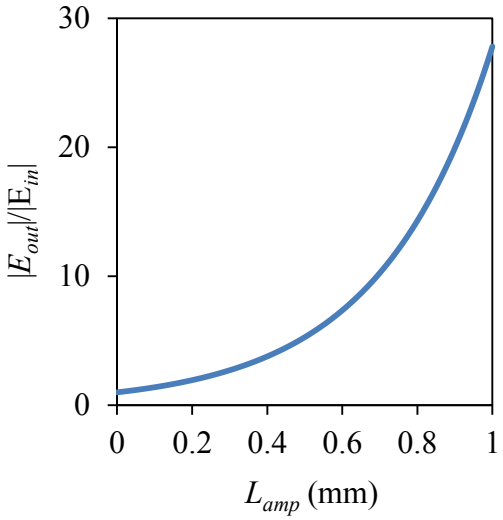

Fig. 2.4: Amplification of the TEM mode vs. amplifier length, obtained at $\alpha = 50 \times 10^{18}$ cm^{-3}.

2.2.3 Moving the Contacts into the GaN

The amplifier shown in Fig. 2.1 is investigated at an operating frequency of 1 THz. A 2DEG having an isotropic conductivity allows for larger amplification than a 2DEG having an anisotropic conductivity, as shown in Fig. 2.5a. This is because the *y*-component of the electric field in the 2DEG is amplified by the isotropic 2DEG conductivity, but not by the anisotropic 2DEG conductivity. The contacts of the amplifier are moved into the GaN, such that the middle of the contacts is aligned with the middle of the 2DEG. The amplifier is simulated at an operating frequency of 1 THz and, as seen in Fig. 2.5b, amplification is the same for a 2DEG having an anisotropic and isotropic conductivity. This is because the electric field in the 2DEG has no *y*-component, such that the anisotropic and isotropic 2DEG conductivities have the exact same effect on the TEM mode. This technique was believed to increase the amplification, since all the radiation in the

2DEG is experiencing gain. However, amplification is not increased, which is evident by comparing the curves labelled "anisotropic" in Fig. 2.5a and b.

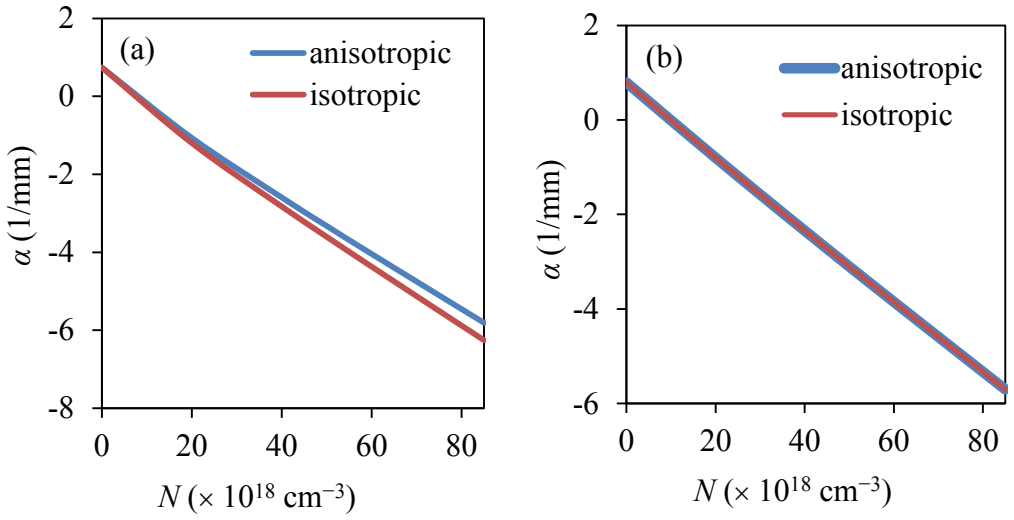

Fig. 2.5: The attenuation constant vs. 2DEG concentration, obtained at $f = 1$ THz. The 2DEG has either an anisotropic or isotropic 2DEG conductivity. The contacts are sitting on the GaN in (a), and are moved into the GaN in (b).

2.2.4 Multi-Contact THz Amplifier

COMSOL is unable to simulate the multi-contact THz amplifier (with a 2DEG thickness of 1 nm) due to an exceedingly large number of mesh points. This issue is overcome by simulating the multi-contact oscillators having a 2DEG thickness of 1 nm**fac* and having a 2DEG concentration of *N*/*fac* (where $fac \geq 1$). The attenuation constant obtained from this simulation approximates the attenuation constant of the amplifier having a 2DEG concentration of *N* and a 2DEG thickness of 1 nm. Increasing the 2DEG thickness allows the simulation to run, while decreasing the 2DEG concentration avoids overestimation of the amplification.

The multi-contact THz amplifier is investigated to operate at a frequency of 1 THz and with *fac* equal to 10. As shown in Fig. 2.6a, the 6 contact amplifier

achieves amplification at 2DEG concentrations > 7.0×10^{18} cm^{-3} and an attenuation constant of -7.9 mm^{-1} is achieved at a 2DEG concentration of 85×10^{18} cm^{-3}. Moreover, increasing the number of contacts from 2 to 6 causes the attenuation constant to become more negative by a factor of 1.5 at a 2DEG concentration of 85×10^{18} cm^{-3}. The TEM mode supported by the 6 contact amplifier is shown in Fig. 2.6b and the radiation interacts most strongly with the center 2DEG region.

The multi-contact amplifier is simulated at an operating frequency of 1 THz, having a 2DEG concentration of 50×10^{18} cm^{-3}, and with *fac* equal to 10. The curve saturates as the number of contacts increases, as shown in Fig. 2.6c, and there is essentially no benefit to producing an amplifier with more than 6 contacts.

The 6-contact amplifier is simulated at an operating frequency of 1 THz. Decreasing *fac* increases the amplification, as shown in Fig. 2.6d, which suggests that the approximation implemented in this section underestimates the amplification.

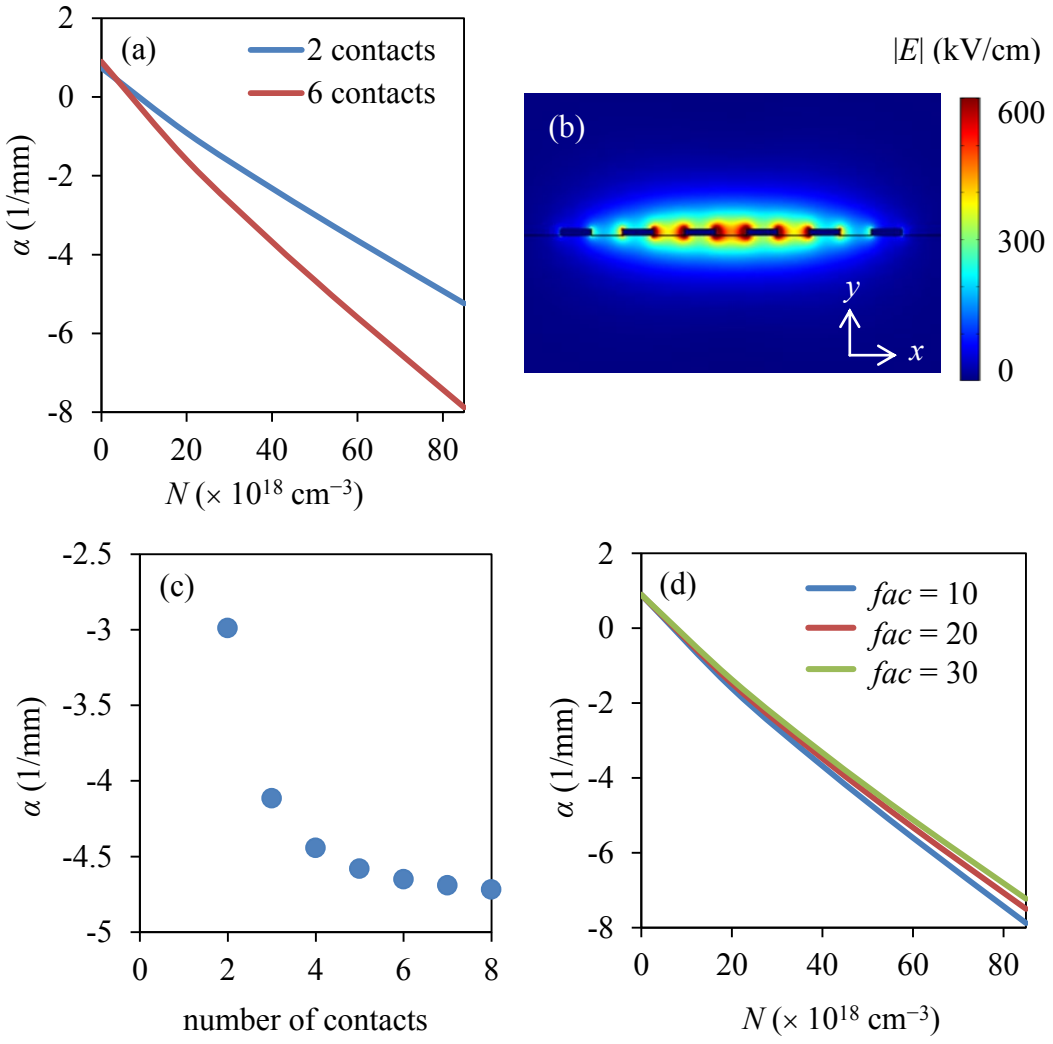

Fig. 2.6: (a) The attenuation constant vs. 2DEG concentration of the multi-contact amplifier, obtained at $f = 1$ THz and $fac = 10$. (b) The TEM mode supported by the 6-contact amplifier. (c) The attenuation constant vs. number of contacts, obtained at $f = 1$ THz, $N = 50 \times 10^{18}$ cm^{-3}, and $fac = 10$. (d) The attenuation constant vs. 2DEG concentration of the 6-contact amplifier, obtained at $f = 1$ THz.

2.3 THz Oscillator

The resonator shown in Fig. 2.7a is able to support standing waves equal to integer multiples of $\lambda/2$, where λ is the wavelength of radiation in the dielectric. The standing wave of half a wavelength is shown in Fig. 2.7b (obtained using COMSOL's "Eigenfrequency" study, which is discussed in detail below). The active

device shown in Fig. 2.1 can be used to sustain the standing wave supported by this resonator. This device is referred to as the THz oscillator and is shown in Fig. 2.7c. The distance between the upper and lower metal regions is $\lambda/2$ and the active device is covered with a dielectric that has the same refractive index as the GaN. The standing wave with polarization in the *x*-direction passes through the contacts of the active device and experiences gain by interacting with the 2DEG (assuming the active device is biased into the NDR region). The thickness of the GaN and the thickness of the overlaying dielectric are equal, such that the anti-node of the standing wave occurs at the location of the 2DEG. Radiation is extracted from the oscillator by making the top metal region partially transparent (lossy). The amount of transmission through this lossy region is controlled by defining it as having a reflection coefficient, *r*.

Details of the simulation are discussed in section 2.3.1. Amplification of the standing wave, as well as techniques to improve this amplification, is discussed in sections 2.3.2-2.3.4.

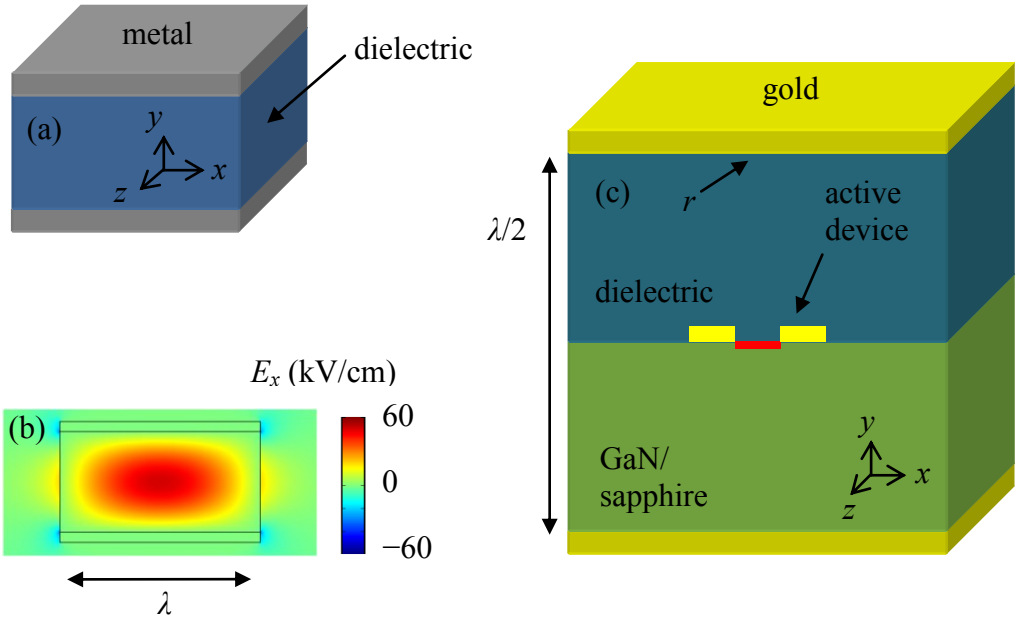

Fig. 2.7: (a) The resonator that supports a standing wave in the *y*-direction. (b) COMSOL simulation showing the standing wave of half a wavelength supported by the GaN-resonator. This simulation is performed at 1 THz. (c) Schematic of the THz oscillator.

2.3.1 Simulation Details

The standing wave of the oscillator is obtained and analysed using COMSOL's 2D "Eigenfrequency" study, which solves Maxwell's equation using the finite element method. Initially, the THz oscillator in Fig. 2.7c was implemented into COMSOL. However, the very large number of mesh points (which is a consequence of the 1 nm thick 2DEG region) makes simulating this oscillator unrealistic. Instead, a cross section of the oscillator in the *x*-*y* plane is considered, which accurately describes the 3D oscillator that is sufficiently long in the *z*-direction. Likely, a length of ~ 3λ will satisfy this requirement. In order to simplify the simulation further, gold regions are placed at the boundaries intersecting the

x-axis, as shown in Fig. 2.8. This likely overestimates amplification when the width of the resonator is $\lesssim \lambda$, since the GaN-air boundaries do not effectively confine the standing wave to the resonator. However, these simulations may actually underestimate the amplification when the width of the resonator is $\gtrsim \lambda$, since the loss associated with the metal boundaries could be greater than the loss associated with the GaN-air boundaries. The width of the resonator is 100 μm in all simulations performed, which is approximately equal to the wavelength of radiation in GaN at 1 THz.

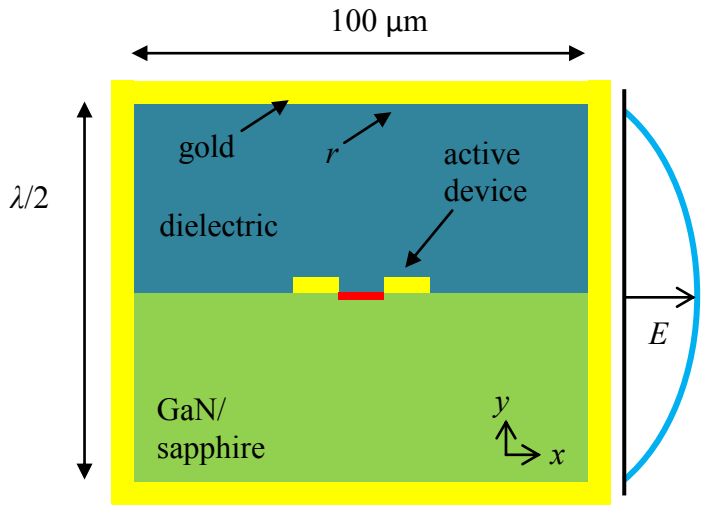

Fig. 2.8: The 2D THz oscillator that is simulated in COMSOL.

Amplification of the standing wave is studied using the damping term, δ, which is defined in the equation,

$$\frac{|E(time)|}{|E(time_0)|} = e^{-\delta(time-time_0)}, \tag{2.4}$$

where $E(time)$ is the electric field in the oscillator at time, *time,* and $E(time_0)$ is the electric field in the oscillator at some arbitrarily chosen time, $time_0$. It is important to note that this equation does not consider saturation of the standing wave's amplification. The damping term, δ, can be obtained by simulating the oscillator having a perfectly reflective upper gold region and adding the simulation damping term to the equation,

$$\delta_{mirror} = -fln(r)\,, \tag{2.5}$$

where δ_{mirror} is the damping term that results from the upper lossy region and f is the frequency supported by the resonator. This equation is derived by considering the standing wave as a travelling wave that is reflecting back and forth inside the resonator. The damping term, δ, obtained using Eq. (2.5) and obtained by including the upper lossy region directly into the simulation is compared for various cases. The results are identical, verifying the accuracy of Eq. (2.5). In this chapter, the lossy gold region is described by Eq. (2.5) with a reflection coefficient of 0.99.

The reliability of the simulation is checked by simulating the resonator with lossless boundaries. The resonant frequencies agree with the equation [66],

$$f_{m,p} = \frac{c}{2\sqrt{\varepsilon_r'}}\sqrt{\frac{m}{h_r^2}+\frac{p}{w_r^2}}\,, \tag{2.6}$$

where $f_{m,p}$ is the resonant frequency of the mode, m and p are the indexes representing the different modes the resonator supports, c is the speed of light, ε_r' is the real part of the relative permittivity of the material filling the resonator, h_r is the height of the resonator, and w_r is the width of the resonator. This confirms that the simulation environment is set up properly under these simplified conditions. Additionally, the mesh in the 2DEG and the mesh in the contacts are reduced (in a few select simulations) and the damping term remains essentially unchanged, which confirms that the mesh in these regions is satisfactory.

2.3.2 Basic THz Oscillator

The optimal contact width (w_c), contact height (h_c), and contact distance (d) are determined by simulating the oscillator at a 2DEG concentration of $85 \times 10^{18}\ \mathrm{cm}^{-3}$ and at an operating frequency of 1 THz. Amplification of the standing wave increases as the contact height and contact distance decreases, since the standing wave interacts better with the 2DEG as these dimensions decrease. The optimal contact height is 100 nm because a value below this may lead to issues during fabrication or testing. The optimal contact distance is 1 μm because this is the smallest dimension that can be fabricated at the University of Alberta. Amplification increases as the width of the contacts increases because larger widths cause the electric field to increase in the 2DEG. The optimal width is 8 μm, since larger values lead to significant distortion of the standing wave. The oscillator studied in this section, section 2.3.3, and section 2.3.4 is defined by the dimensions stated above.

The oscillator is investigated at an operating frequency of 1 THz. Amplification is achieved at 2DEG concentrations $> 68 \times 10^{18}$ cm^{-3}, as seen in Fig. 2.9a, and a damping term of -2.6×10^{9} s^{-1} is achieved at a 2DEG concentration of 85×10^{18} cm^{-3}. The standing wave supported by the oscillator is shown in Fig. 2.9b and the radiation interacts well with the 2DEG.

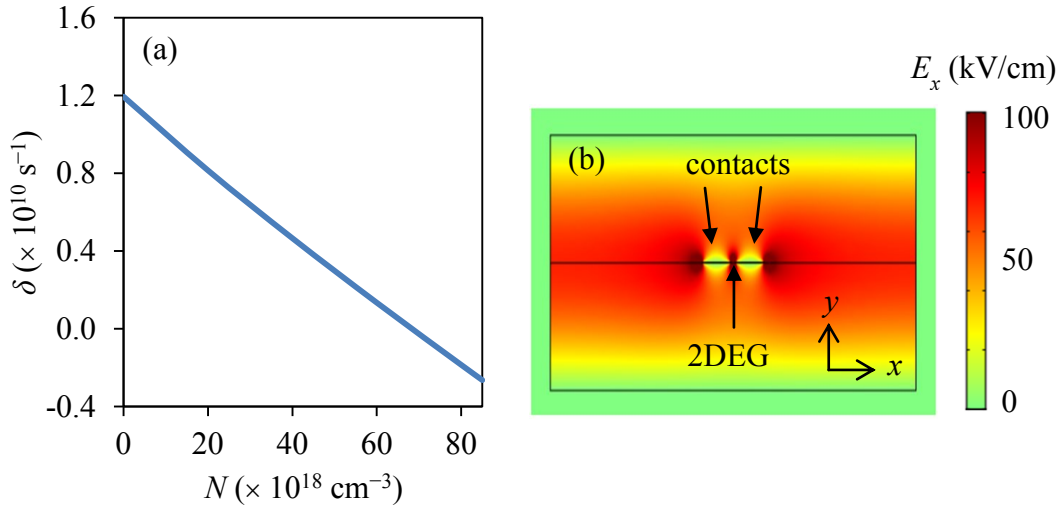

Fig. 2.9: (a) The damping term vs. 2DEG concentration, obtained at $f = 1$ THz. (b) The standing wave supported by the oscillator.

The oscillator is investigated at a 2DEG concentration of 50×10^{18} cm^{-3}. The standing wave experiences amplification at frequencies between 0.5 and 2 THz, as shown in Fig. 2.10. However, the damping term drops to a value of -2×10^{8} s^{-1} at a frequency of 0.5 THz.

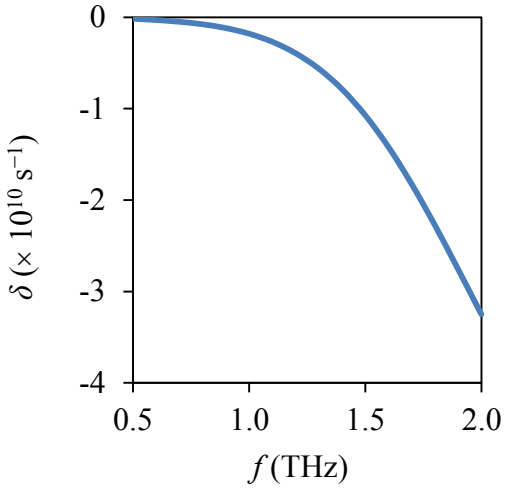

Fig. 2.10: The damping term vs. operating frequency, obtained at $N = 80 \times 10^{18}$ cm^{-3}.

Amplification of the standing wave vs. amplifier lengths is obtained from Eq. (2.4) and plotted in Fig. 2.11. This plot is created using a damping term of -1.85×10^{9} s^{-1} and the electric field magnitude increases by a factor of 10 in ~ 1.25 ns.

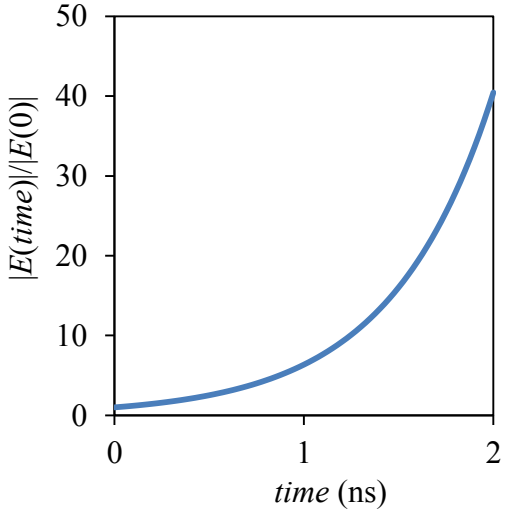

Fig. 2.11: Amplification of the standing wave vs. time, obtained at $\delta = -1.85 \times 10^{9}$ s^{-1}.

2.3.3 Moving the Contacts into the GaN

The oscillator shown in Fig. 2.8 is investigated at an operating frequency of 1 THz. A 2DEG having an isotropic conductivity allows for larger amplification then a 2DEG having an anisotropic conductivity, as shown in Fig. 2.12a. This means that the electric field in the 2DEG has a *y*-component. The contacts of the active device are moved into the GaN, such that the middle of the contacts is aligned with the middle of the 2DEG. This oscillator is simulated at an operating frequency of 1 THz and, as seen in Fig. 2.12b, amplification is the same for a 2DEG having an anisotropic and isotropic conductivity. This confirms that the electric field in the 2DEG is oriented entirely in the *x*-direction. This technique causes the damping term to become more negative by a value of $-1 \times 10^9\ \mathrm{s}^{-1}$, which is observed by comparing the curves labelled "anisotropic" in Fig. 2.12a and b.

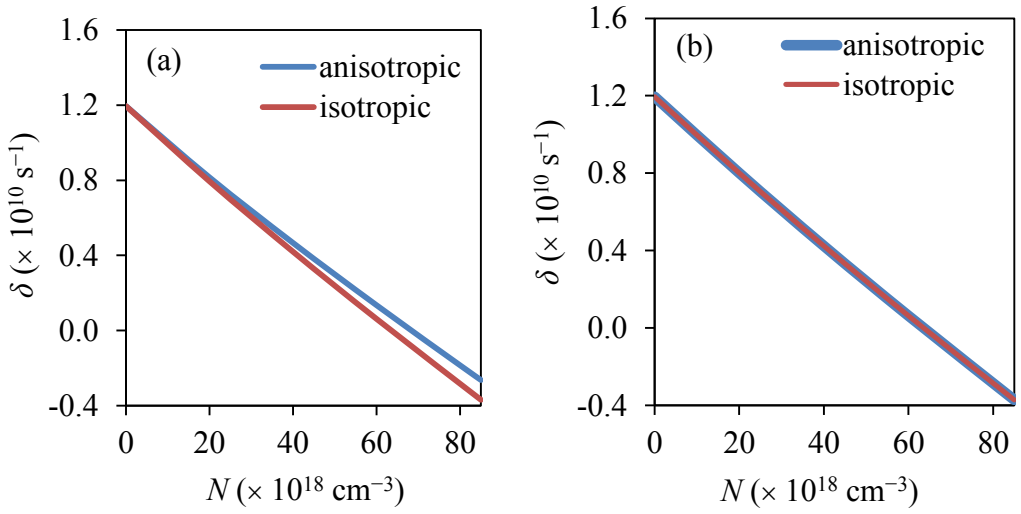

Fig. 2.12: The damping term vs. 2DEG concentration, obtained at $f = 1$ THz. The 2DEG has either an anisotropic or isotropic 2DEG conductivity. The contacts are sitting on the GaN in (a), and are moved into the GaN in (b).

2.3.4 Multi-Contact THz Oscillator

COMSOL is unable to simulate the multi-contact THz oscillator (with a 2DEG thickness of 1 nm) due to the extremely large number of mesh points. The approximation used in section 2.2.4 is again used in this section. This approximation consists of increasing the 2DEG thickness by a factor, *fac*, and decreasing the 2DEG concentration by this same factor.

Here, a multi-contact THz oscillator is investigated to operate at a frequency of 1 THz and with *fac* equal to 10. As shown in Fig. 2.13a, the oscillator with an active device that has 11 contacts (which is the maximum number of contacts that fit in the resonator) shows amplification at 2DEG concentrations $> 5.0 \times 10^{18}\ \mathrm{cm}^{-3}$. Additionally, a damping term of $-17.3 \times 10^{10}\ \mathrm{s}^{-1}$ is achieved at a 2DEG concentration of $85 \times 10^{18}\ \mathrm{cm}^{-3}$. Furthermore, increasing the number of contacts from 4 to 11 causes the damping term to become more negative by a factor of 4 at a 2DEG concentration of $85 \times 10^{18}\ \mathrm{cm}^{-3}$. Figure 2.13b shows the standing wave supported by the 4-contact oscillator and the mode interacts with the three 2DEG regions equally.

The 4-contact THz oscillator is simulated at an operating frequency of 1 THz. Decreasing *fac* increases the amplification, as shown in Fig. 2.13d, which suggests that the approximation implemented in this section underestimates the amplification.

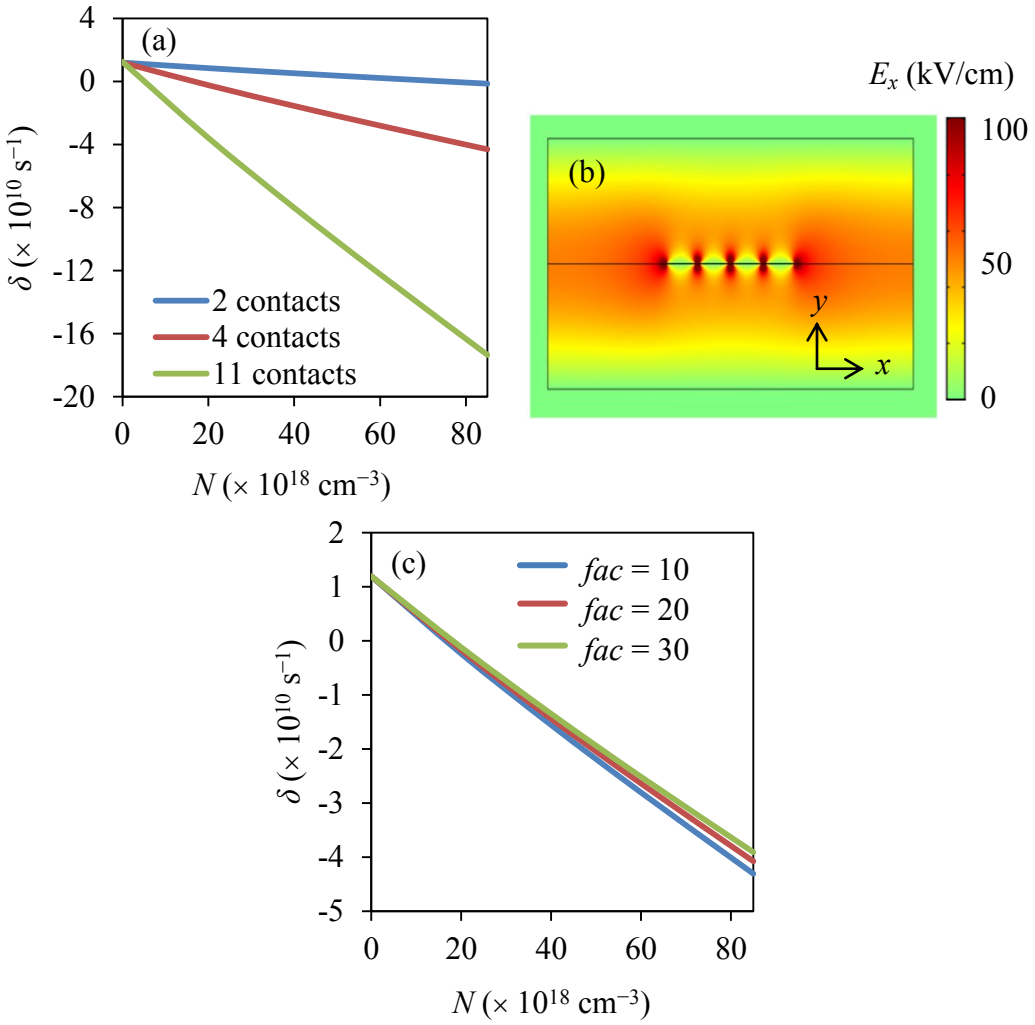

Fig. 2.13: (a) The damping term vs. 2DEG concentration of the multi-contact oscillator, obtained at $f = 1$ THz and $fac = 10$. (b) The standing wave supported by the 4-contact oscillator. (c) The damping term vs. 2DEG concentration of the 4-contact amplifier, obtained at $f = 1$ THz.

2.4 Conclusions

COMSOL is used to simulate an amplifier supporting a TEM mode and amplification is possible over a frequency range of 0.5-2 THz. Increasing the amplifier's number of contacts increase amplification of the TEM mode; however, there is a limit to which this improvement. The minimum 2DEG concentration

necessary to achieve amplification at 1 THz is 7.0×10^{18} cm^{-3}. COMSOL is also used to simulate an oscillator supporting a standing wave and amplification is possible over a frequency range of 0.5-2 THz. Increasing the active device's number of contacts increase amplification of the standing wave; however, the number of contacts is limited by the width of the resonator. The minimum 2DEG concentration necessary to achieve amplification at 1 THz is 5.0×10^{18} cm^{-3}.

Chapter 3

Static NDR and the SA Mode

The previous chapter determined that THz radiation can be amplified if the active device in Fig. 1.10 exhibits a static NDR. The first objective of this chapter is to determine if GaN-based, planar devices that incorporate a channel are able to exhibit a static NDR. Another objective of this chapter is to study a planar device (having a channel) and a non-planar device that operate in the SA mode. Crosslight APSYS software is used to perform all simulations in this chapter.

3.1 Static NDR

A static NDR, due to the Gunn Effect of GaN, has been separately measured by Ceroici et al. [58], Huang et al. [38], and Yilmazoglu et al. [57]. However, the conditions required to obtain this static NDR are not well understood. A gateless GaN-device with ohmic contacts (section 3.1.2), a gated GaN-device with ohmic contacts (section 3.1.3), and a gateless GaN-device with MIS contacts (section 3.1.4)

are investigated in an effort to observe a static NDR. The details of the simulations are discussed in section 3.1.1.

3.1.1 Simulation Details

Crosslight APSYS uses the drift-diffusion model and the finite element method to simulate the electrical properties of semiconductor devices. The electron drift velocity vs. electric field curve describing the GaN is shown in Fig. 3.1 [67] and the Gunn Effect is incorporated into the simulations by the NDM region. The 2DEG is included into the simulations by defining a fixed positive charge at the GaN/AlN interface (which attracts electrons). The discrete energy levels of the 2DEG are determined by solving the drift-diffusion equations and Schrödinger's equation self-consistently. Furthermore, intraband quantum tunnelling of electrons through the AlN [68] is taken into account using the techniques discussed in [69].

Ohmic contacts are implemented into the simulation using Crosslight's pre-defined "ohmic contact" boundary condition, which is a Dirichlet boundary condition that allows electrons to flow across the boundary undisturbed. This boundary condition must be in contact with a highly doped region ($\gtrsim 5 \times 10^{18}$ cm^{-3}) to function properly. Schottky contacts can be implemented into the simulations using Crosslight's pre-defined "schottky contact" boundary condition. The user must define the contacts work function, which Crosslight uses to determine the surface potential at the boundary condition. Alternatively, schottky contacts can be implemented by placing a metal in contact with a semiconductor. Crosslight uses the

work function of the metal to determine the electron energy barrier at the metal-semiconductor interface.

Hot electron effects and self-heating effects are ignored in the simulations. These effects can produce an NDR at DC [70-73], but the NDR does not remain into the THz regime. Breakdown effects [74], trapping effects [73], surface states [24], current leaking into the gate, and the sapphire substrate are also ignored in the simulations.

Time-independent simulations are performed to determine the steady-state of the devices. Time-independent simulations are capable of simulating a static NDR, but are unable to simulate Gunn and accumulation domains (since a steady-state is never reached). As such, a device exhibiting a static NDR requires further analyses to test for Gunn or accumulation domains; however, a device not exhibiting a static NDR does not need to be analysed further.

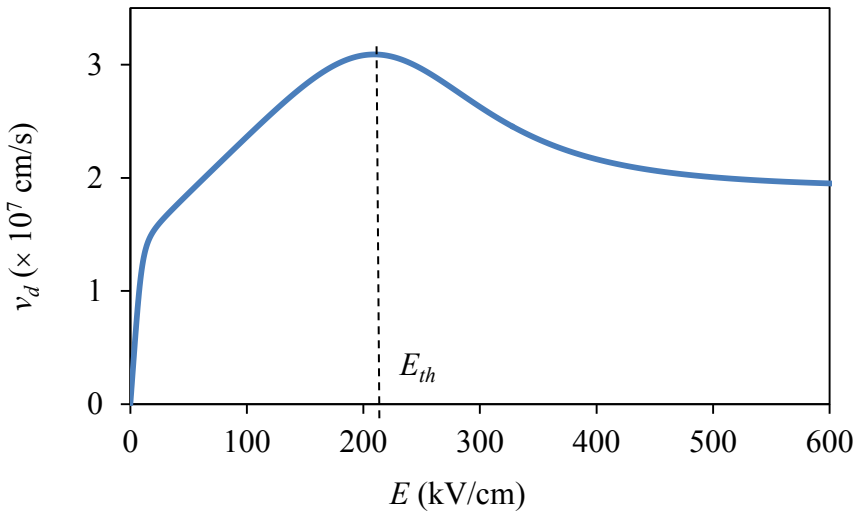

Fig. 3.1: The electron drift velocity vs. electric field of GaN. This curve is obtained using the model discussed in [67].

3.1.2 Gateless GaN-Device with Ohmic Contacts

The GaN-based device studied in this section is shown in Fig. 3.2a, which has ohmic contacts and no gate. The GaN has a thickness of 5 μm and a doping density of 1×10^{15} cm^{-3}. The N^+ doping regions have a width of 1 μm, a height of 300 nm, and a doping density of 1×10^{19} cm^{-3}. Furthermore, the contacts are implemented into the simulations using Crosslight's pre-defined "ohmic contact" boundary condition.

The device is investigated at an interface charge, N_s, of 1×10^{12} cm^{-2} and having a contact distance, d, of 1 μm. At anode voltages $\gtrsim 20$ V, a surplus of electric field and a surplus of electrons exist at the anode end of the 2DEG. This is shown in Fig. 3.2b and c, respectively. Furthermore, the current density magnitude at the anode end of the 2DEG decreases as the anode voltage increasing from 20 V to 20.5 V, which is represented by the blue region seen in Fig. 3.2d. However, this decrease in current is more than compensated for by the current increase represented by the yellow region seen in Fig. 3.2d. This means that the DC resistance of the device is positive and suggests the presence of SPCT.

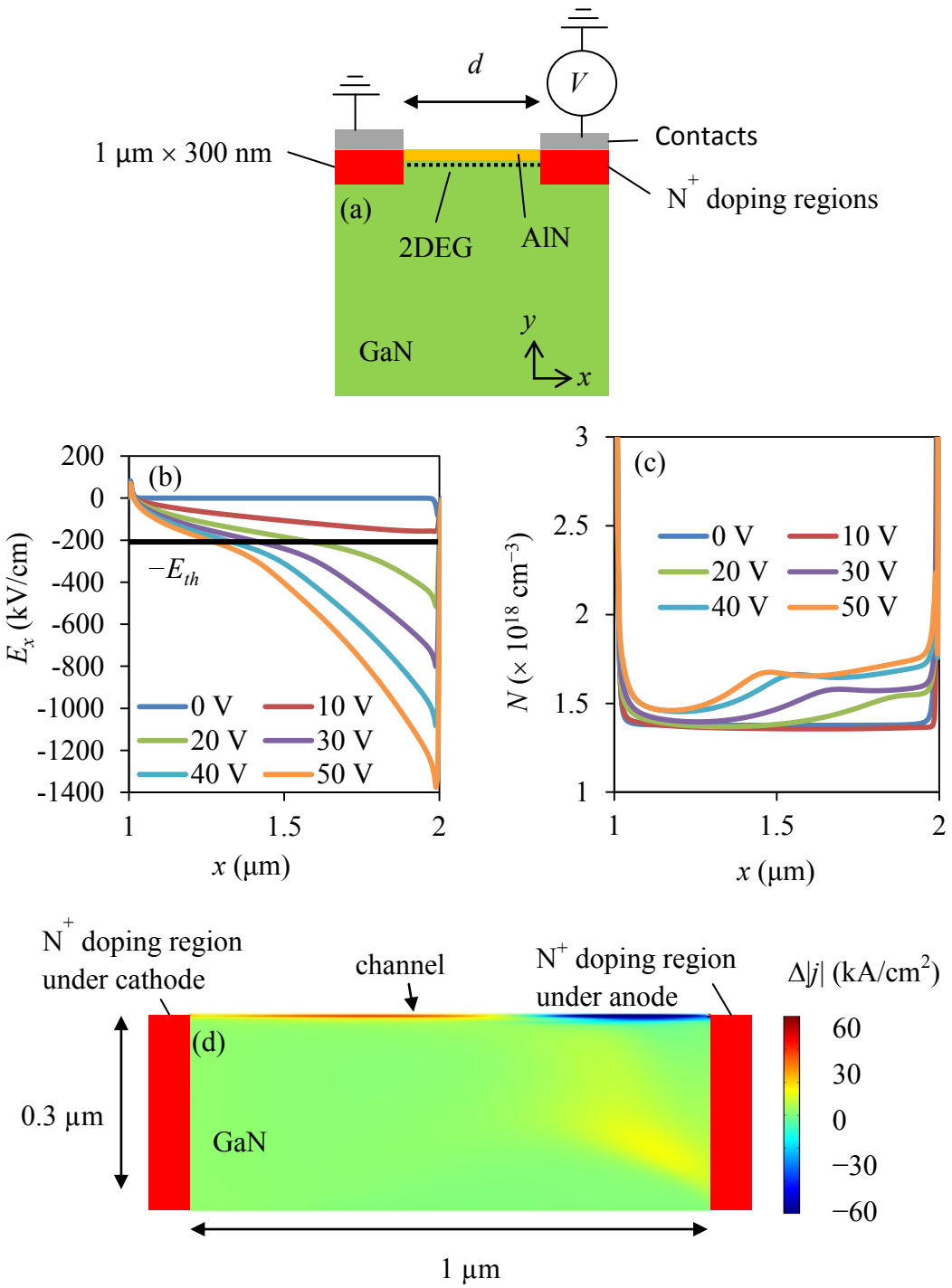

Fig. 3.2: (a) Schematic of the GaN-device with ohmic contacts and no gate. (b) The electric field and (c) the electron concentration plotted along the 2DEG, obtained at $N_s = 1 \times 10^{12}$ cm^{-2} and $d = 1$ μm. (d) The current density magnitude at an anode voltage of 20 V subtracted from the current density magnitude at an anode voltage of 20.5 V, $\Delta|j| = |j(20.5\text{ V})| - |j(20\text{ V})|$, obtained at $N_s = 1 \times 10^{12}$ cm^{-2} and $d = 1$ μm.

The anode current is investigated at various interface charges and having various contact distances. The device exhibits a positive DC resistance at all anode voltages, as shown in Fig. 3.3, which confirms the presence of SPCT. This agrees with literature, which states that SPCT occurs in devices having ohmic contacts [36], independent of the device geometry [37]. The second point where the anode current saturates, as seen in Fig. 3.3, corresponds to the onset of SPCT. The first point of saturation is due to the knee occurring ~ 16 kV/cm in Fig. 3.1.

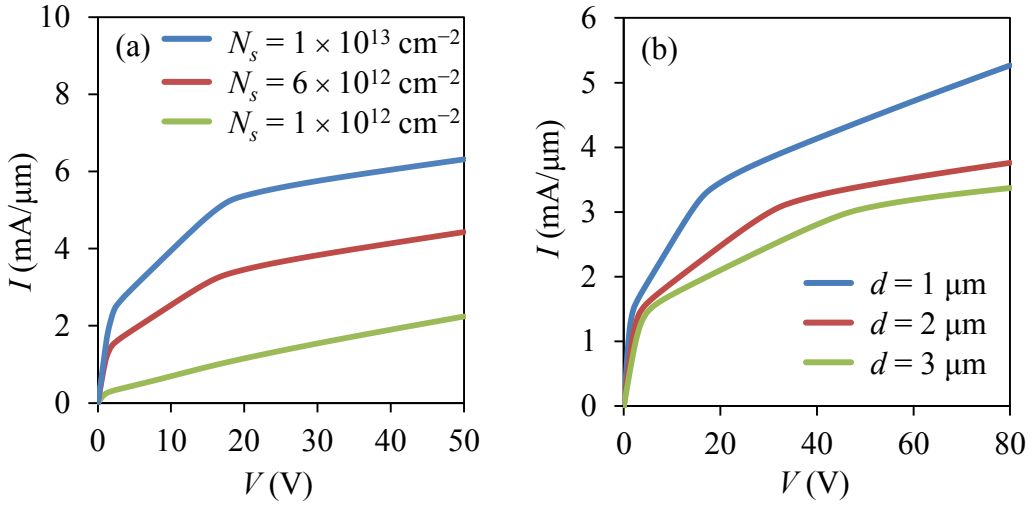

Fig. 3.3: (a) The anode current vs. anode voltage, obtained at $d = 1$ μm. (b) The anode current vs. anode voltage, obtained at $N_s = 6 \times 10^{12}$ cm^{-2}.

3.1.3 Gated GaN-Device with Ohmic Contacts

The GaN-based device simulated in this section is shown in Fig. 3.4a, which has a gate and ideal ohmic contacts. The GaN has a thickness of 5 μm and a doping density of 1×10^{15} cm^{-3}. The N^+ doping regions have a width of 1 μm, a height of 300 nm, and a doping density of 1×10^{19} cm^{-3}. Furthermore, the gate contact has a work function of 4.6 eV and 6.6 nm of SiO_2 exists between the gate contact and the

AlN. The cathode to gate spacing and the gate to anode spacing are both 0.5 μm. Additionally, the anode and cathode contacts are implemented into the simulations using Crosslight's pre-defined "ohmic contact" boundary condition. The gate contact is implemented into the simulations using Crosslight's pre-defined "schottky contact" boundary condition.

The device is investigated at an interface charge (N_s) of 1×10^{13} cm^{-2}, a gate length (L_G) of 5 μm, and a gate voltage (V_G) of 0 V. The electron concentration is depleted under the anode edge of the gate and the electric field accumulates in this region, as shown in Fig. 3.4b and c, respectively. This confirms the device is operating in the pinch-off regime [75].

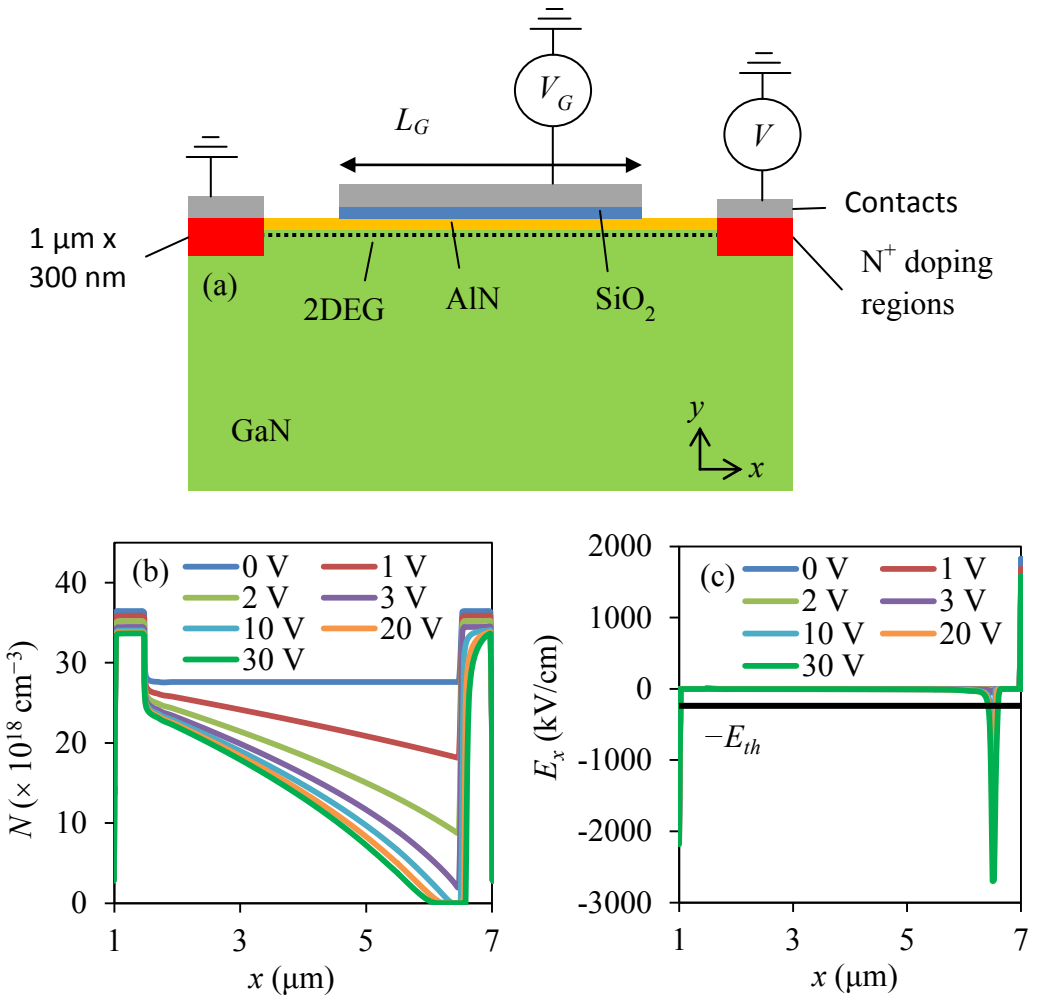

Fig. 3.4: (a) Schematic of the gated GaN-device with ohmic contacts. (b) The electron concentration and (c) the electric field plotted along the 2DEG of the device, obtained at $N_s = 1 \times 10^{13}$ cm^{-2}, $L_G = 5$ µm, and $V_G = 0$ V.

The device is investigated at an interface charge of 1×10^{13} cm^{-2}, a gate length of 5 µm, a gate voltage of 0 V, and at an anode voltage (V) of 30 V. In the region of the device under the anode edge of the gate, the channel spreads away from the GaN/AlN interface (consistent with the analysis in [75]) and the electric field magnitude is above the threshold electric field (E_{th}). This is shown in Fig. 3.5a and b, respectively. The current density magnitude in this region increases with

increasing anode voltage, due to an increase in electron concentration. Therefore, SPCT suppresses the occurrence of an NDR in this device.

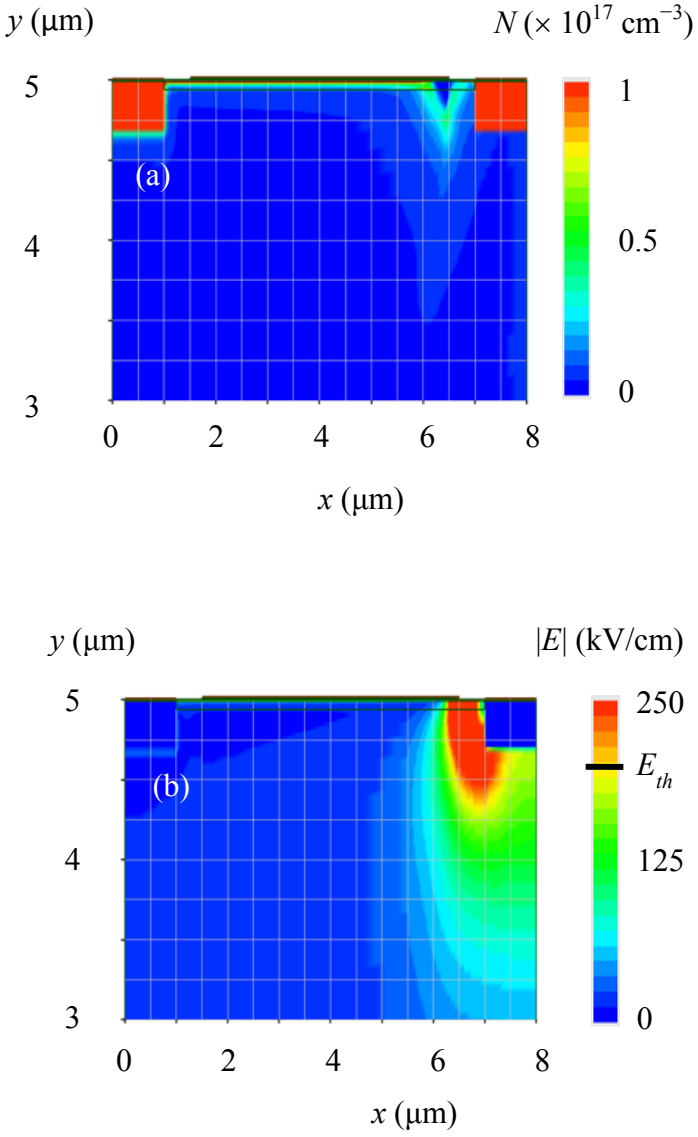

Fig. 3.5: (a) The electron concentration and (b) the electric field, obtained at $N_s = 1 \times 10^{13}$ cm^{-2}, $L_G = 5$ μm, $V_G = 0$ V, and $V = 30$ V.

The anode current is determined at various interface charges, having various gate lengths, and at various gate voltages. The current saturates, as shown in

Fig. 3.6, since the device is operating in the pinch-off regime. Furthermore, a static NDR does not occur due to the presence of SPCT in this device.

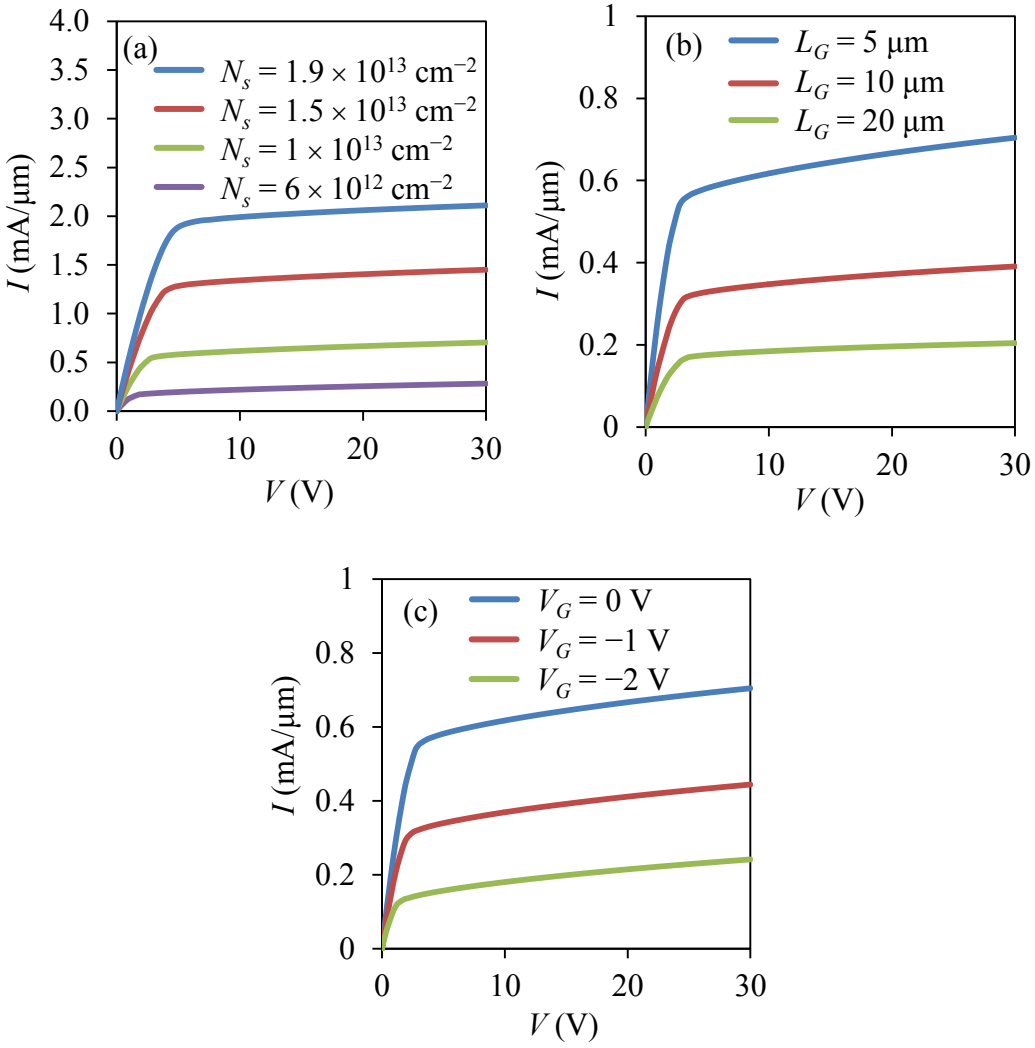

Fig. 3.6: (a) The anode current vs. anode voltage, obtained at $L_G = 5$ μm and $V_G = 0$ V. (b) The anode current vs. anode voltage, obtained at $N_s = 1 \times 10^{13}$ cm^{-2} and $V_G = 0$ V. (c) The anode current vs. anode voltage, obtained at $N_s = 1 \times 10^{13}$ cm^{-2} and $L_G = 5$ μm.

3.1.4 Gateless GaN-Device with MIS Contacts

The GaN-based device simulated in this section is shown in Fig. 3.7a, which has no gate and contacts with an MIS structure. The GaN has a thickness of 5 μm

and a doping density of 1×10^{15} cm^{-3}. Moreover, the contacts of the device are implemented into the simulations as metal having a width of 1 μm, a thickness of 100 nm, and a work function of 4.6 eV.

The device is investigated at an interface charge, N_s, of 1×10^{13} cm^{-2} and having a distance between the contacts, d, of 1 μm. The schottky cathode contact depletes the cathode end of the 2DEG, as seen in Fig. 3.7b, and the electric field accumulates within this region, thus producing the large spike seen in Fig. 3.7c. The depletion regions observed in Fig. 3.7b are directly related to the existence of cathode domains. As seen in Fig. 3.7c, cathode domains are observed at anode bias voltages $\gtrsim$ 30 V.

Böer and Döhler [54] use the field of directions to study a non-planar device that is based on a material having an NDM and that has a cathode contact that strongly blocks the flow of electrons. The electric field distribution supported by this device is extremely similar to the electric field distribution shown in Fig. 3.7c, regardless of the difference in geometry.

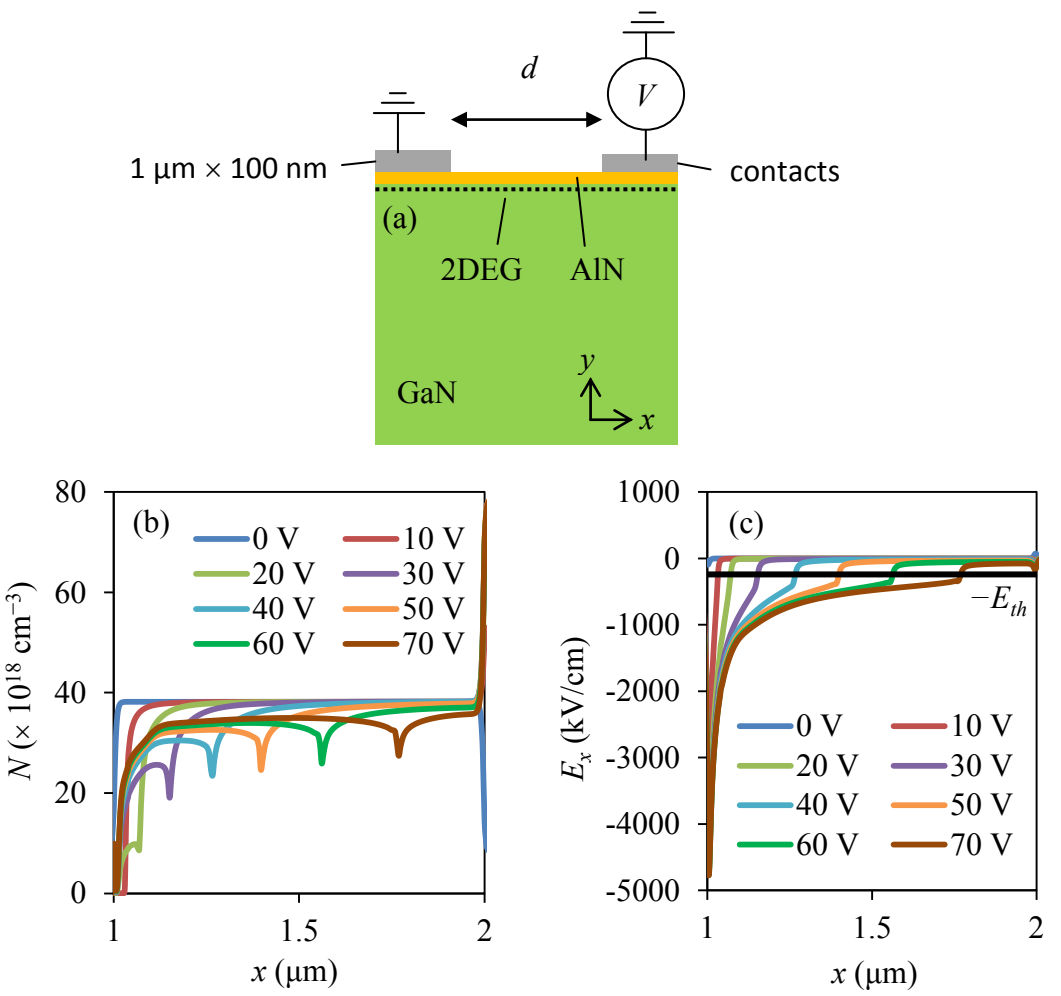

Fig. 3.7: (a) Schematic of the gateless GaN-device with MIS contacts. (b) The electric field and (c) the electron concentration plotted along the 2DEG of the device, obtained at $N_s = 1 \times 10^{13}$ cm^{-2} and $d = 1$ µm.

The anode current is investigated at various interface charges and having various contact distances. The current saturates, as seen in Fig. 3.8, due to the formation of a cathode domain. Additionally, the low current region is due to the energy barrier introduced at the cathode contact by the AlN, which prevents electrons from entering the GaN at anode voltages below $\lesssim 15$ V. However, $\gtrsim 15$ V the width of the barrier becomes sufficiently thin that electrons can tunnel through

the AlN and into the GaN. This effect is known as Fowler-Nordheim tunneling [76] and the existence of a low current region with this contact structure is consistent with the experimental data in [68]. As the interface charge increases the low current region remains up to larger anode voltages, as seen in Fig. 3.8a. This is because the AlN is thicker in these simulations. In addition, the anode current vs. anode voltage curves in Fig. 3.8b are essentially identical. This is because the electric field distribution remains largely unchanged with increasing contact distance.

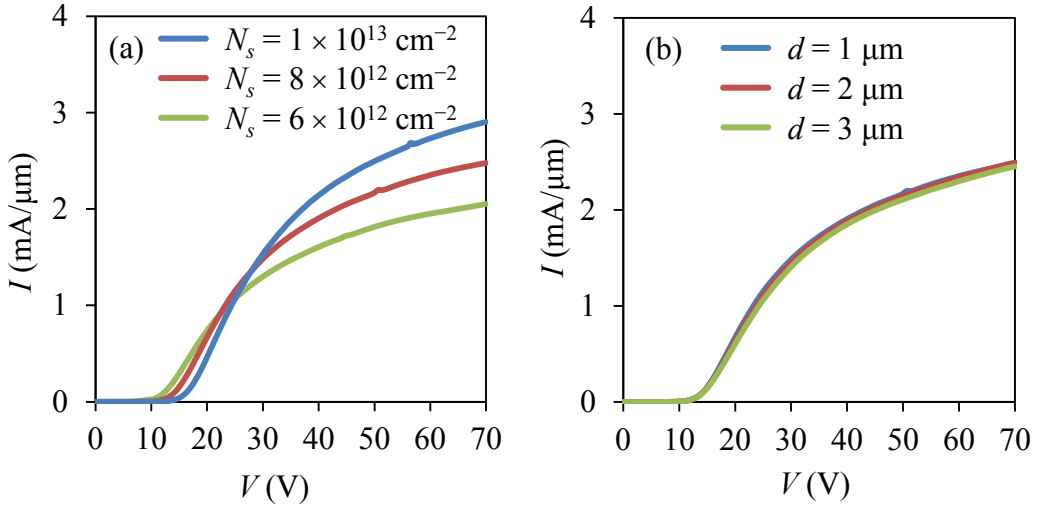

Fig. 3.8: (a) The anode current vs. anode voltage, obtained at $d = 1$ μm. (b) The anode current vs. anode voltage, obtained at $N_s = 1 \times 10^{13}$ cm^{-2}. There always exists a small bump in the curves with a contact distance of 1 μm. This seems to occur as a result of the cathode domain getting too close to the anode end of the channel. This is the reason it is not observed in the plots with a contact distance of 2 μm and 3 μm.

3.2 SA Mode

McCumber and Chynoweth [27] determined the AC conductance of a non-planar device operating in the SA mode. In section 3.2.3, their analysis is expanded upon by determining the AC resistivity of a non-planar device operating in the SA mode. Additionally, Fleming [45, 77] and Fleming et al. [46] have shown

that the SA mode occurs in planar devices without a channel. In section 3.2.4, Crosslight is used to verify that a planar device having a channel is also capable of operating in the SA mode. The simulation details are discussed in section 3.2.1 and a technique that can determine whether a device supports Gunn or accumulation domains is introduced in section 3.2.2.

3.2.1 Simulation Details

The simulation details discussed in section 3.1.1 hold for the simulations performed in this section. However, it has not been previously discussed that Crosslight has a small signal analysis tool, which determines the AC resistance of a DC biased device. This tool solves the drift-diffusion equations in response to a sinusoidal voltage with a magnitude of 1 V. The AC parameters (AC electric field, electron concentration, current, etc.) are approximated by their first order Taylor series expansion.

3.2.2 Testing for Gunn and Accumulation Domains

A device can only operate in the SA mode if Gunn and accumulation domains do not form. Time-dependent simulations can be performed to test if a device supports Gunn or accumulation domains, as follows:

1. Apply a step voltage to the anode contact, which has a magnitude larger than the threshold electric field times contact distance ($> E_{th}d$) and that has a rise time equal to 1 fs. The electrons are unable to respond to this change in 1 fs,

such that the electric field is uniformly distributed between the contacts of the device.

2. Hold the anode voltage at the value applied in step 1 and allow time to progress. The electrons in the device redistribute, which leads to fluctuations in the electric field and the electron concentration. These fluctuations initiate Gunn or accumulation domains if, and only if, the device is able to support Gunn or accumulation domains.

The device shown in fig. 3.9a is investigated, which is known to support Gunn domains [54, 56, 78]. This device has a length of 5 μm, a homogenous doping density of 1×10^{17} cm^{-3}, and contacts with shallow schottky barriers. These contacts are implemented into the simulations using Crosslight's pre-defined "schottky contact" boundary condition. The device is simulated using the technique outlined above (using a step voltage of 160 V) and Gunn domains propagate towards the anode, as shown in Fig. 3.9b. This confirms that the technique presented in this section can successfully determine if a device supports Gunn or accumulation domains.

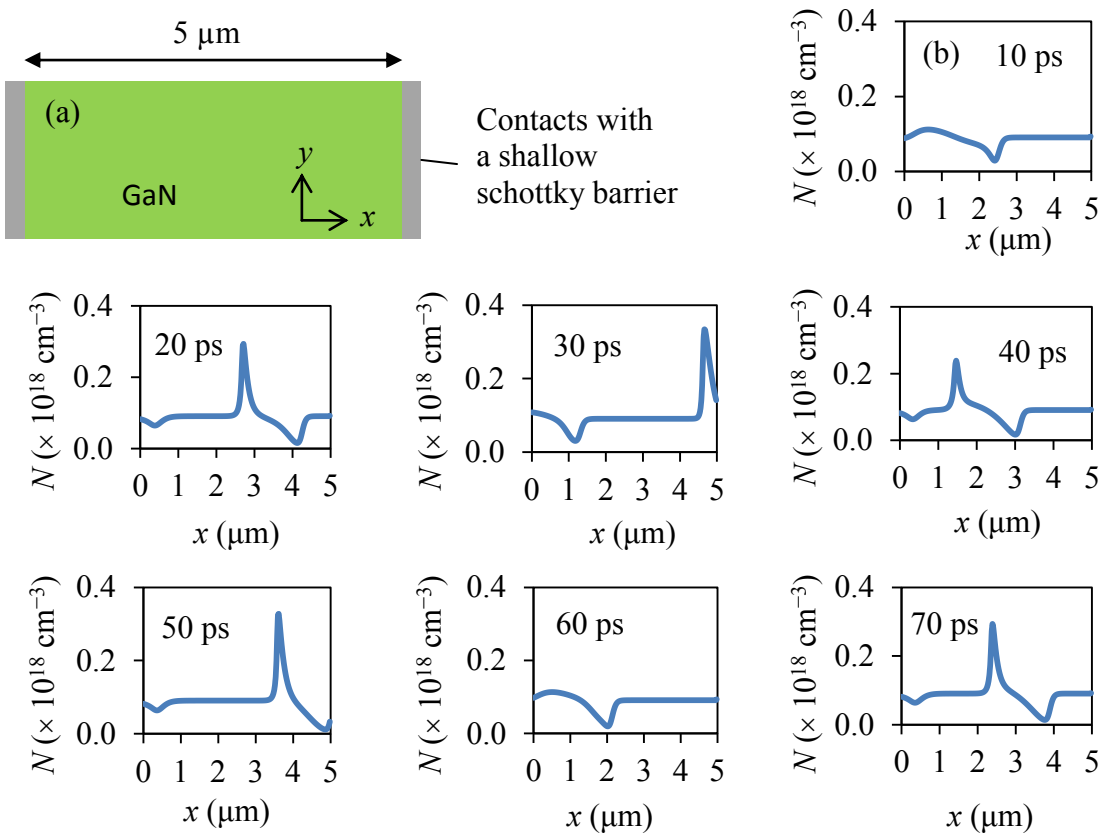

Fig. 3.9: (a) Schematic of the device that supports Gunn domains. (b) The electron concentration vs. distance between the contacts, at different instances in time.

3.2.3 Non-planar GaN-Device

The non-planar GaN-device studied in this section is shown in Fig. 3.10a, which has ohmic contacts. The N^+ doping regions have a width of 100 nm and a doping density of 1×10^{19} cm^{-3}. The distance between the N^+ doping regions is 1 µm and the GaN doping density is 3×10^{17} cm^{-3}. The contacts are implemented using Crosslight's pre-defined "ohmic contact" boundary condition.

The device is simulated using the technique discussed in section 3.2.2 (having a step voltage of 45 V). Electrons are injected into the GaN at the cathode

contact and settle to a steady-state near the anode contact, as shown in Fig. 3.10b, which confirms that the device does not support Gunn or accumulation domains.

The device is further investigated by performing time-independent simulations. At an anode voltage (V) of 45 V, a surplus of electric field and a surplus of electrons are observed near the anode contact, as shown in Fig. 3.10c. Additionally, the DC resistance of the device is positive at all anode bias voltages, as shown in Fig. 3.10d, confirming that the device exhibits SPCT.

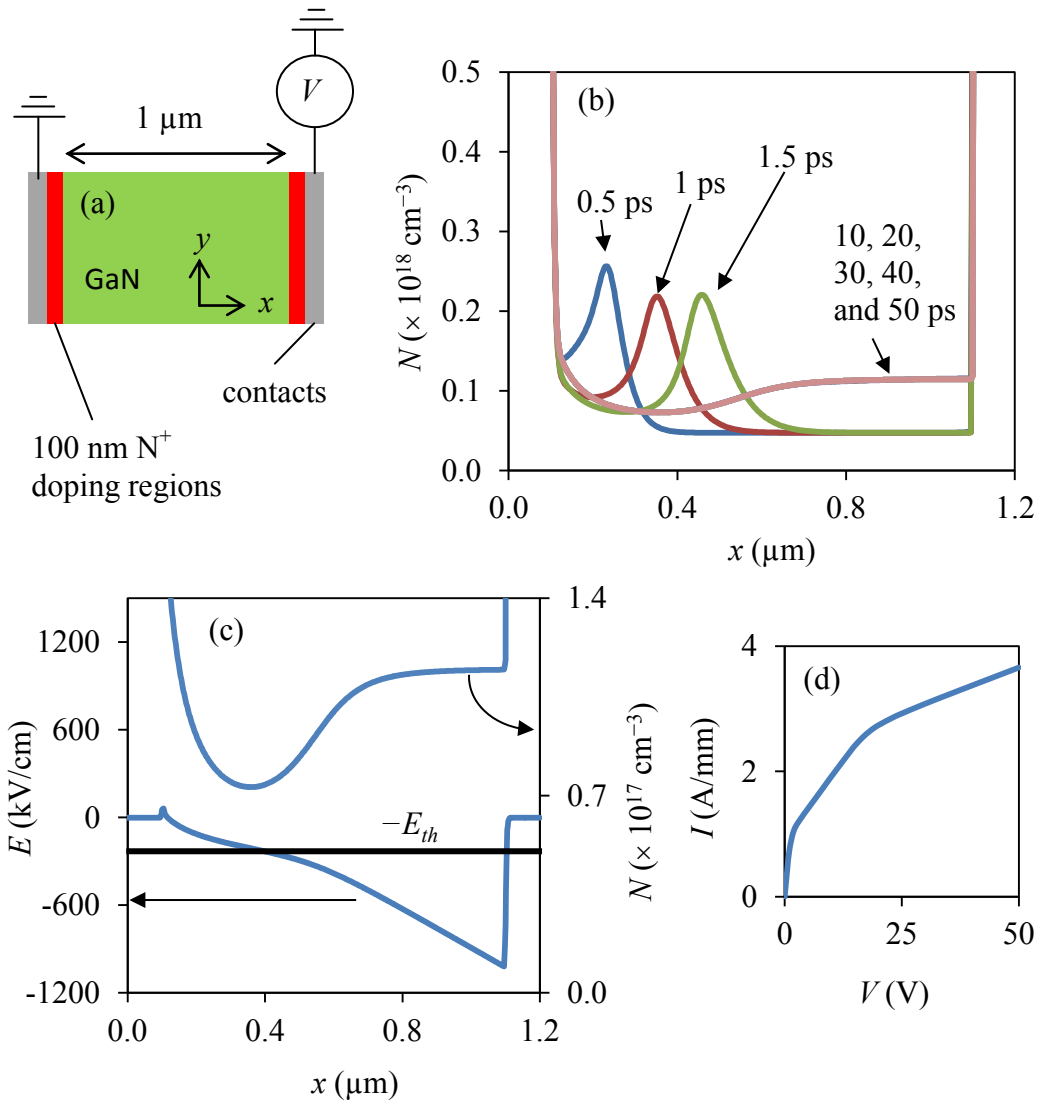

Fig. 3.10: (a) Schematic of the non-planar GaN-device. (b) The electron concentration plotted along the *x*-axis of the device, at various instances in time. (c) The electric field and electron concentration plotted along the *x*-axis of the device, obtained at $V = 45$ V. (d) The anode current vs. anode voltage.

The device, having an anode voltage of 45 V, is analysed using Crosslight's AC small signal analysis tool. The AC resistance of the device is negative at frequencies equal to ~ 0.2 THz and ~ 0.46, which is shown by the line-plot in Fig. 3.11a. The lower frequency is approximately equal to the reciprocal of the time

it takes the electrons to travel between the contacts of the device (f_t), while the higher frequency is approximately equal to $2f_t$. This confirms that this device is operating in the SA mode.

The device is investigated at a DC anode voltage of 45 V with a sinusoidal anode voltage (having frequency f and an amplitude of 1 V). Time-dependent simulations determine the complex AC electric field ($\tilde{E}_{AC}$) and the complex AC current density ($\tilde{J}_{AC}$). This, in turn, can be used to determine the AC resistivity of GaN from the equation,

$$\rho_{AC}(x,f) = real\left(\frac{\tilde{E}_{AC}(x,f)}{\tilde{J}_{AC}(x,f)}\right), \tag{3.1}$$

where *real* is the real part of the argument. The AC resistivity near the cathode (left) contact always remains positive, as seen in Fig. 3.11b, since the electric field magnitude is below the threshold electric field. However, negative resistivity values can exist near the anode (right) contact, since the electric field magnitude is above the threshold electric field. Furthermore, the resistivity near the anode can be either positive or negative because of variations in the electron concentration. However, a detailed discussion of this is not within the scope of this research.

The AC resistance times area of the device is determined from the AC resistivity shown in fig. 3.11b, using the relationship,

$$R_{AC}(f)A = \int_{cathode}^{anode} \rho_{AC}(x,f)\,dx, \tag{3.2}$$

The results are represented by the discrete points in Fig. 3.11a and they are in agreement with the line-plot presented in this figure.

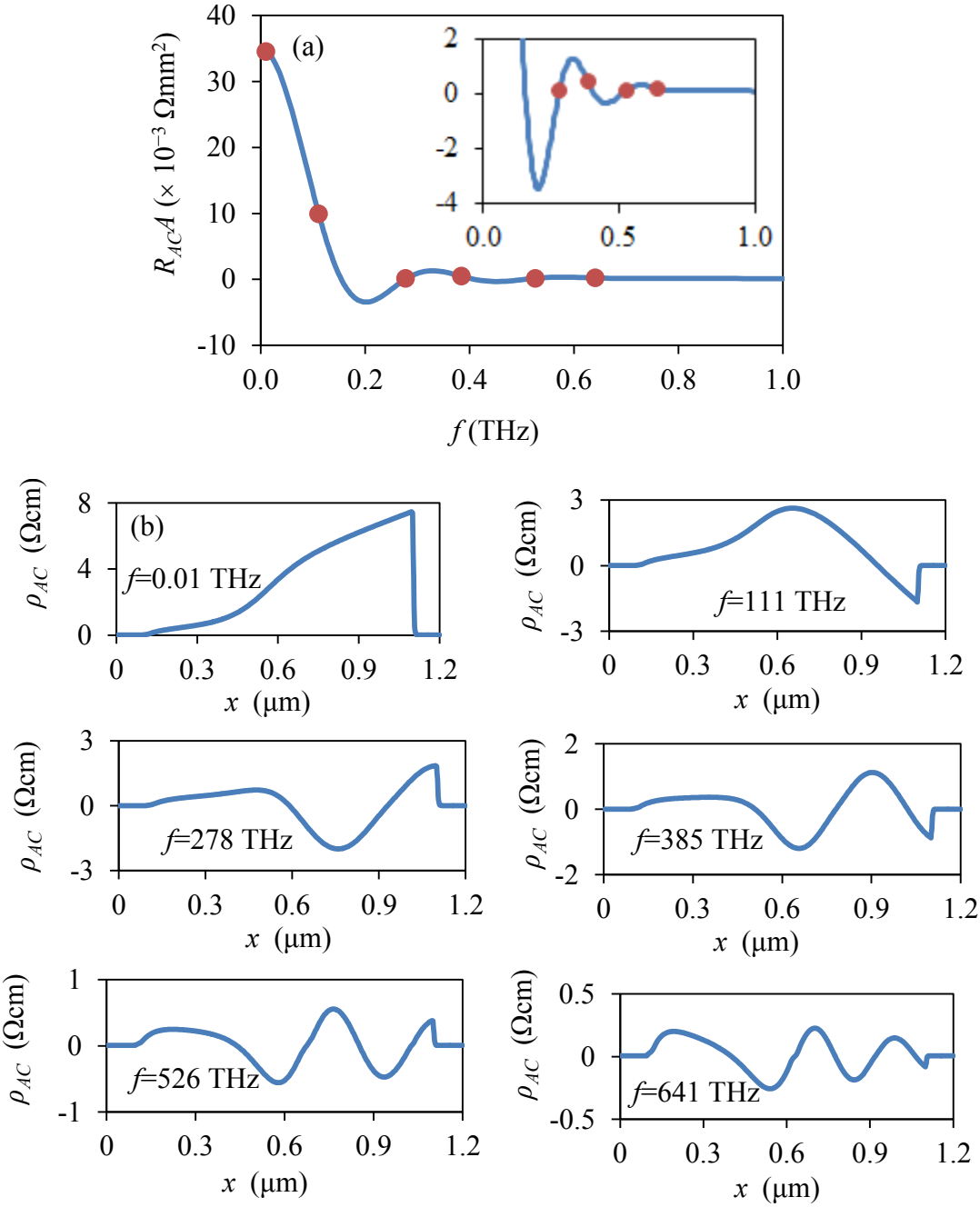

Fig. 3.11: (a) The AC resistance times area of the device, obtained at $V = 45$ V. The line-plot is obtained using Crosslight's small signal analysis tool and the discrete points are obtained from the curves in (b). (b) The GaN resistivity, obtained at $V = 45$ V and various frequencies.

3.2.4 Planar GaN-Device

The planar GaN-device studied in this section is shown in Fig. 3.2a, which was also the focus of section 3.1.2. The technique outlined in section 3.2.2 (having a step voltage of 30 V) is used to simulate the device having an interface charge, N_s, of 1×10^{12} cm^{-2} and a contact distance, d, of 1 μm. The electron concentration reaches a steady-state, as shown in Fig. 3.12a. This confirms that the device does not support Gunn or accumulation domains. A doping notch is added into the 2DEG (which is shown in the inset of Fig. 3.12b) to study the effects of an inhomogeneous 2DEG concentration. This device is simulated using the technique discussed in section 3.2.2 and, as shown in Fig. 3.12b, a steady-state is reached. Devices with an interface charge of 2×10^{12} cm^{-2}, 4×10^{12} cm^{-2}, and 6×10^{12} cm^{-2} are also simulated (both having and not having a doping notch) and Gunn or accumulation domains are not observed. Furthermore, this device is known to exhibit SPCT, which was discussed in section 3.1.2.

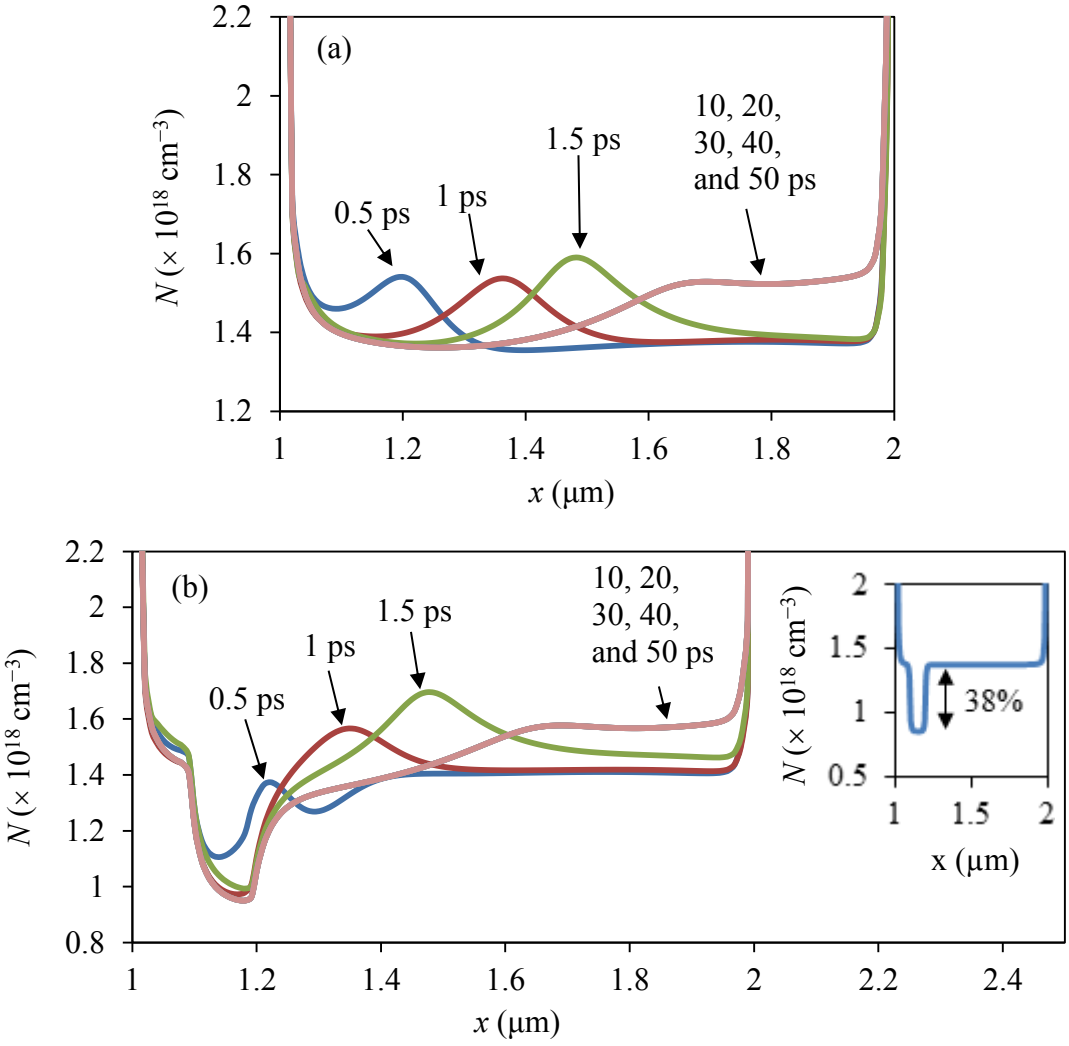

Fig. 3.12: The electron concentration plotted along the 2DEG of the device, obtained at $N_s = 1 \times 10^{12}$ cm^{-3}, $d = 1$ μm, and $V = 30$ V. The 2DEG concentration is homogenous in (a). In (b), the 2DEG has a doping notch near the cathode. The inset in (b) shows the doping notch at equilibrium.

The AC resistance was presented in section 3.2.3, since it relates well to the semiconductor's resistivity. In this section, the AC conductance is obtained in order to be consistent with literature [27]. The device is investigated (using Crosslight's AC small signal analysis tool) at an anode voltage of 45 V. The existence of a negative conductance, as shown in Fig. 3.13, confirms that the device is operating in

the SA mode. The minimum conductance in Fig. 3.13 is −3 S/m at an interface charge of 1×10^{12} cm^{-3} and decreases to −52.3 S/m at an interface charge of 1×10^{13} cm^{-3}. This decrease is likely a result of the increase in current, which is due to the increase in 2DEG concentration. Furthermore, the minimum conductance in Fig. 3.13 is located at a frequency of 0.2 THz when the interface charge is 1×10^{12} cm^{-3} and increases to 0.33 THz when the interface charge is 1×10^{13} cm^{-3}. This shift in frequency may be explained by the effect illustrated in Fig. 3.2d, which shows a portion of the channel spreading away from the GaN/AlN interface. This spreading becomes more pronounced as the interface charge increases, such that the time it takes for electrons to travel between the contacts of the device also increases.

The complex conductivity (or resistivity) of GaN must be obtained in order to determine whether or not this device is able to amplify THz radiation. However, the technique used in section 3.2.3 is only effective in 1D and future work should focus on determining a technique that can be applied in 2D.

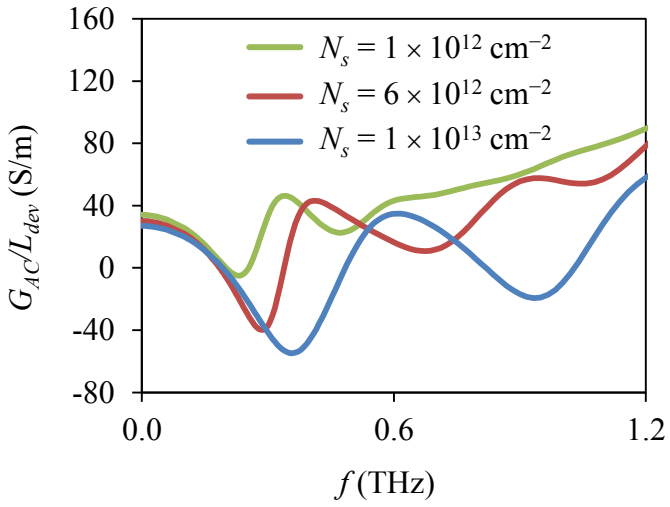

Fig. 3.13: The conductance per length of the device, obtained at $d = 1$ µm and $V = 45$ V. The length is measured in the direction perpendicular to the x-y plane.

3.3 Conclusions

Various GaN-based devices are simulated that have a planar structure and a 2DEG. The devices with ohmic contacts exhibit SPCT, regardless of the presence or absence of a gate contact, while a cathode domain exists in the device with MIS contacts and no gate. The AC resistivity of GaN is determined from a non-planar device with ohmic contacts. Negative resistivity regions may exist at the anode, while the resistivity near the cathode is always positive. A planar GaN-device with a channel and ohmic contacts is shown to support the SA mode. The next step in this research is to determine the complex conductivity of this device, which can be used to determine if the device has the ability to amplify THz radiation.

Chapter 4

THz Modulation and Spectroscopy Experiments

This chapter discusses modulation of THz radiation by a 2DEG at a GaN/AlN interface. THz pulses are transmitted through (and reflected from) GaN samples in the presence and absence of a 2DEG. This chapter also presents several THz spectroscopy experiments performed on GaN thin films (grown on a sapphire substrate) and a bulk sapphire wafer.

4.1 THz Systems

Three different time-domain THz spectroscopy systems are used to perform the experiments. The THz systems are briefly discussed in this section.

(a) The THz Transmission (TT) system

This setup consists of a THz pump-optical probe system that allows time-domain THz radiation transmission measurements to be performed at normal incidence. The setup is composed of: A mode-locked Ti:sapphire laser that produces femtosecond optical pulses having a duration of 10 fs, a wavelength of 794 nm, at a repetition rate of 75 MHz. The THz time-domain pulses are generated using a GaAs photoconductive antenna and these pulses are detected using an electro-optic sampling detector. This system has a measuring bandwidth between 0.2 and 1.5 THz.

(b) Zomega's THz system

This THz system is owned and operated by a US company, Zomega (www.zomega-terahertz.com, East Greenbush, New York). Zomega was kind enough to perform measurements on a number of samples, the results of which are presented in this chapter. The experiments were performed by the company's staff and were sent to us for comparison with our measurements. Zomega's THz system has a measuring bandwidth between 0.2 and 1.5 THz.

(c) The THz Angular (TA) system

This system is a THz pump-optical probe system that allows either transmission or reflection measurements to be performed at any angle. A mode-locked Ti:sapphire laser produces femtosecond optical pulses having a duration of 10 fs, a wavelength of 800 nm, at a repetition rate of 80 MHz. The THz

time-domain pulses are generated using a GaAs photoconductive antenna and these pulses are detected using an electro-optic sampling detector. This system has a measuring bandwidth between 0.2 and 0.8 THz. A full description of this system is provided in [79].

The measurements obtained by the TT system are considered the primary set of data. The measurements obtained using Zomega's system and the TA system is used to supplement the measurements of the TT system.

4.2 Materials

THz measurements are performed on the various samples discussed below. These samples are purchased from a US company, KYMA (www.kymatech.com, Raleigh, North Carolina).

- *Sapphire*

This sample consists of a bare 435 μm thick sapphire wafer. The upper surface of the wafer is optically polished and the backside of the sapphire is unpolished. The unpolished sapphire surface has a peak-to-peak surface roughness $\lesssim$ 6 μm, as is determined using the KLA Tencor P-6 Profilometer.

- *Semi-insulating (SI) GaN*

This sample consists of SI 5 μm (±1 μm) GaN grown on a sapphire substrate using Hydride Vapour Phase Epitaxy (HVPE) with a low growth rate. The total thickness of the sample (GaN and sapphire) is 424 μm. A surface roughness

measurement of sapphire's backside was not performed on this sample; however, it is expected to be $\lesssim 6$ μm. The doping density is estimated to be $< 10^{12}$ cm^{-3}, which is obtained from the SI GaN resistivity value stated on the KYMA website.

- *N^- GaN*

The N-type GaN is grown on a sapphire substrate in a two-step process. First, high growth rate HVPE is used to grow ~ 2 μm of GaN that is un-intentionally doped with Si. Then, low growth rate HVPE is used to grow ~ 3 μm of GaN that is also un-intentionally doped with Si. The total thickness of the sample (GaN and sapphire) is measured to be 440 μm. Similarly, the sapphire has an unpolished backside with a peak-to-peak surface roughness $\lesssim 5$ μm, as determined using the KLA Tencor P-6 Profilometer. The doping density is estimated to be $\sim 4 \times 10^{14}$ cm^{-3} [68].

- *N^+ GaN*

The N-type GaN is grown on a sapphire substrate in a two-step process. First, high growth rate HVPE is used to grow ~ 2 μm of GaN that is un-intentionally doped with Si. Then, low growth rate HVPE is used to grow ~ 3 μm of GaN that is intentionally doped with Si. The total thickness of the sample is measured to be 440 μm. The sapphire has an unpolished backside with a peak-to-peak surface roughness $\lesssim 5$ μm, as measured using the KLA Tencor P-6 Profilometer. The doping density is estimated to be 7×10^{17} cm^{-3} [68].

- *AlN-N^- GaN*

This sample consists of the N^- GaN sample discussed above, but with 5.7 nm of AlN deposited on the GaN surface using atomic layer deposition (ALD). The AlN induces a 2DEG at the GaN/AlN interface having an interface charge of 1.9×10^{13} cm^{-3} [68].

- *AlN-N^+ GaN*

This sample consists of the N^+ GaN sample discussed above, but with 4.5 nm of AlN deposited on the GaN surface using ALD. The AlN induces a 2DEG at the GaN/AlN interface having an interface charge of ~ 2.2×10^{13} cm^{-3} [68].

4.3 THz Modulation by a 2DEG

Kleine-Ostmann et al. [13] performed experiments on the GaAs-based THz modulation device outlined in section 1.4. This device operates on the principle of modulating the THz radiation by electrically controlling the presence/absence of a 2DEG of sheet density 1.12×10^{12} cm^{-3}. At a voltage of −10 V, the authors demonstrated a maximum MD of 3%.

The 2DEG at a GaN/AlN interface is expected to significantly increase the MD due to the large interface charges that can be achieved [68]. THz transmission and reflection experiments are performed on the N^- and N^+ AlN-GaN samples, as well as the N^- and N^+ GaN samples, which are discussed in section 4.2. The AlN deposited on the GaN is sufficiently thin that, under ideal conditions, such a ~ 5 nm thick layer does not affect the THz radiation. As such, the modulation of THz radiation, due to a 2DEG in GaN, can be detected by these experiments.

4.3.1 THz Radiation Transmission Through N^- GaN and AlN-N^- GaN

THz transmission and reflection experiments are performed on the N^- GaN sample and the AlN-N^- GaN sample. The transmission measurements are performed at normal incidence and the reflection measurement is performed at 45°. Transmission experiments are performed using the TT system and the time-domain pulses are shown in Fig. 4.1a. The Fourier Transform (FT) of these pulses is obtained and the amplitude is shown in Fig. 4.1b. The blue curves represent measurements performed on the AlN-N^- GaN sample and the red curves represent measurements performed on the N^- GaN sample. Presenting the runs separately, opposed to the averaged pulse, allows the scan-to-scan error in identical runs to be determined (see insets). There is no measureable difference between the two samples, indicating that even in the presence of the 2DEG, the interface free electron plasma does not couple to the incident THz radiation

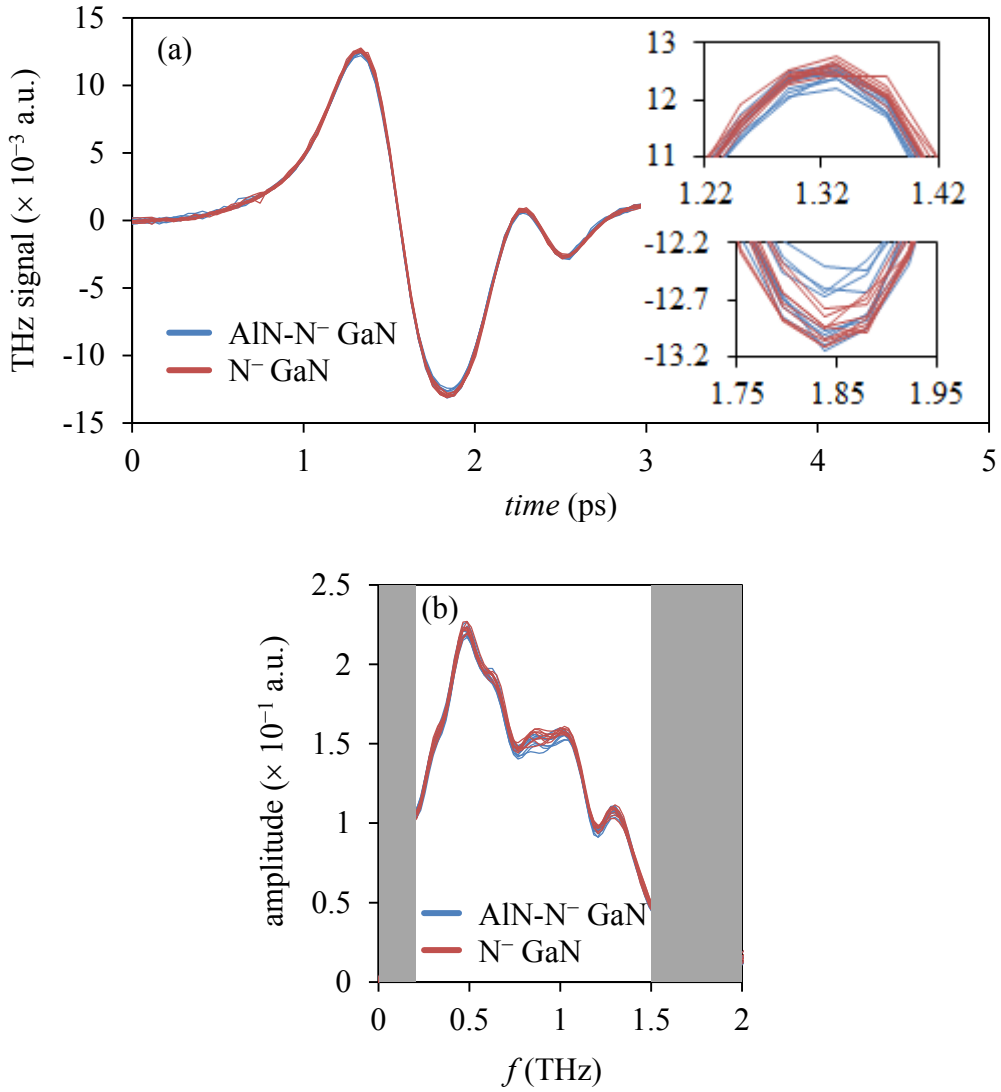

Fig. 4.1: Measurements performed using the TT system. (a) The THz time-domain pulses transmitted through the N^- GaN sample and the AlN-N^- GaN sample. The upper inset shows the positive peak of the pulse between 11 and 13×10^{-3} a.u.. Similarly, the lower inset shows the negative peak of the pulse between −13.2 and -12.2×10^{-3} a.u.. (b) The spectral power of the FT of the time-domain pulses.

Fig. 4.2a depicts the THz radiation transmission measurements performed at the Zomega facility. The time-domain signals are averaged over multiple runs. The THz radiation pulse transmitted through the AlN-N^- GaN sample experiences significant attenuation in comparison to the THz radiation pulse transmitted through

the N^- GaN sample. Clearly, these results are in direct disagreement with those presented in Fig. 4.1a.

The THz radiation transmission through the N^- GaN sample relative to transmission through free space, analysed in the frequency domain, is given by the equation,

$$\tilde{t}_{GaN,FS}(\omega) = \frac{\tilde{E}_{GaN}(\omega)}{\tilde{E}_{free\ space}(\omega)}, \tag{4.1}$$

where $\tilde{E}_{GaN}(\omega)$ is the FT of the main THz pulse transmitted through the GaN sample, $\tilde{E}_{free\ space}(\omega)$ is the FT of the pulse transmitted through free space, and ω is the angular frequency. Similarly, transmission through the AlN-N^- GaN sample relative to transmission through free space is given by the equation,

$$\tilde{t}_{AlN-GaN,FS}(\omega) = \frac{\tilde{E}_{AlN-GaN}(\omega)}{\tilde{E}_{free\ space}(\omega)}, \tag{4.2}$$

where $\tilde{E}_{AlN-GaN}(\omega)$ is the FT of the main pulse transmitted through the AlN-GaN sample. The magnitude of $\tilde{t}_{N^-\ GaN,FS}(\omega)$ and $\tilde{t}_{AlN-N^-\ GaN,FS}(\omega)$ is displayed in Fig. 4.2b. The 2DEG introduces absorption at all frequencies; however, the absorption is strongest in a frequency range centered at ~ 0.55 THz. The phase of $\tilde{t}_{N^-\ GaN,FS}(\omega)$ is subtracted from the phase of $\tilde{t}_{AlN-N^-\ GaN,FS}(\omega)$ and the results are

plotted in Fig. 4.2c. The change in sign at ~ 0.55 THz implies that the absorption occurring at this frequency is due to a resonance.

The origin of the absorption/resonance depicted in Fig. 4.2 is unknown; however, there are a number of possible explanations. There is a possibility that this might be due to artefact of the THz system, and is not a product of the THz radiation interacting with the sample. Another possibility is that the location spot on the AlN-N^{-} GaN surface where the measurement was taken consists of a defect at the back of the sapphire substrate. This defect region would need to be comparable to the spot size of the THz beam (~ 800 μm) in order to significantly distort the pulses. However, THz pulses which are transmitted through the same AlN-N^{-} GaN sample at a number of different locations (using both the TT system and the TA system) did not show this feature.

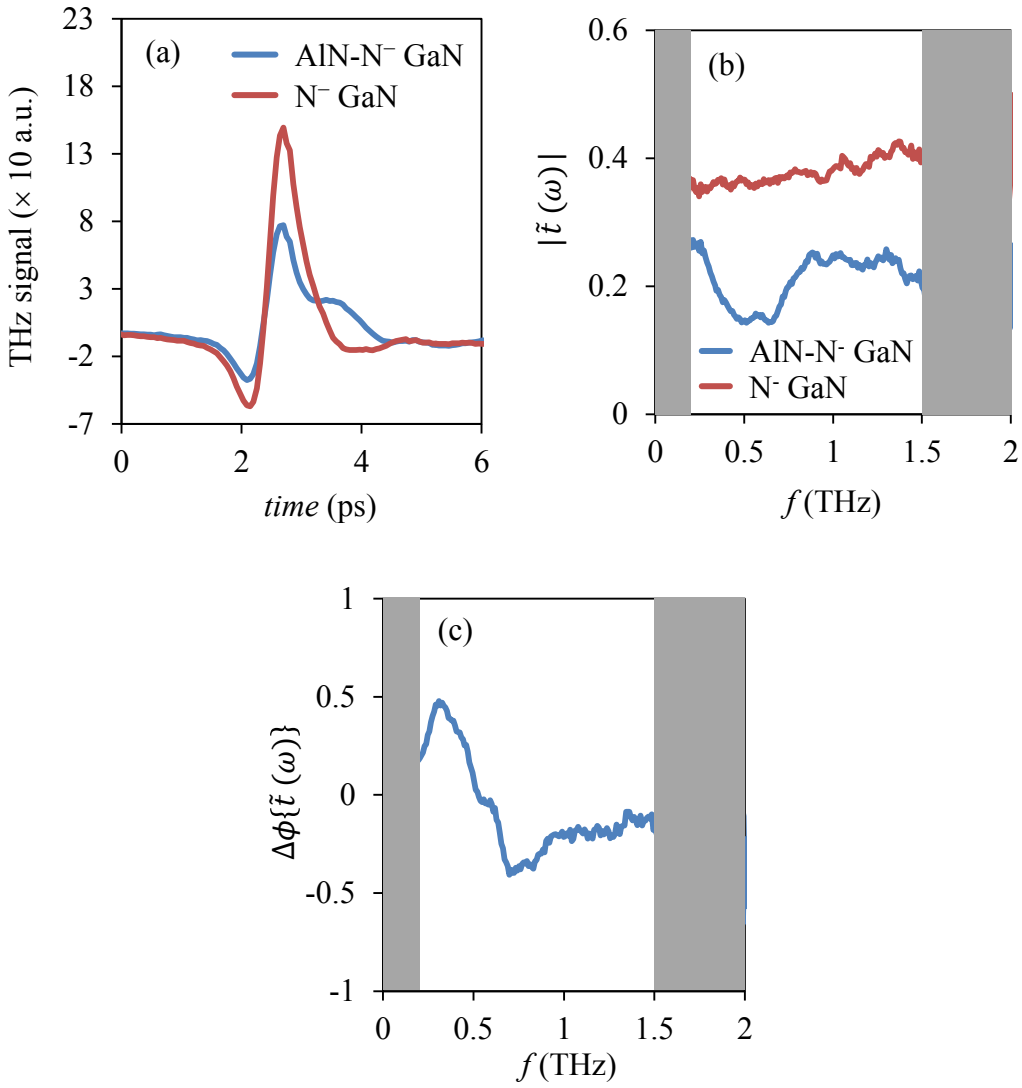

Fig. 4.2: Measurements performed by Zomega. (a) The THz time-domain pulses transmitted through the N⁻ GaN sample and the AlN-N⁻ GaN sample. (b) The magnitude of $\tilde{t}_{N^- GaN,FS}(\omega)$ and $\tilde{t}_{AlN-N^- GaN,FS}(\omega)$ (c) The phase difference between the samples, $\Delta\phi\{\tilde{t}(\omega)\} = \phi\{\tilde{t}_{AlN-N^- GaN,FS}(\omega)\} - \phi\{\tilde{t}_{N^- GaN,FS}(\omega)\}$.

The transmission and reflection measurements using the TA system are shown in Fig. 4.3a and Fig. 4.3b, respectively. The temporal shift seen in the reflection measurements is due to an un-intentionally change in the path length when switching between the N⁻ GaN sample and the AlN-N⁻ GaN sample. Although there

is a substantial amount of noise in the measurements, it is clear that no significant modulation is present in either the transmission or reflection signals. This is in agreement with the measurements obtained using the TT system.

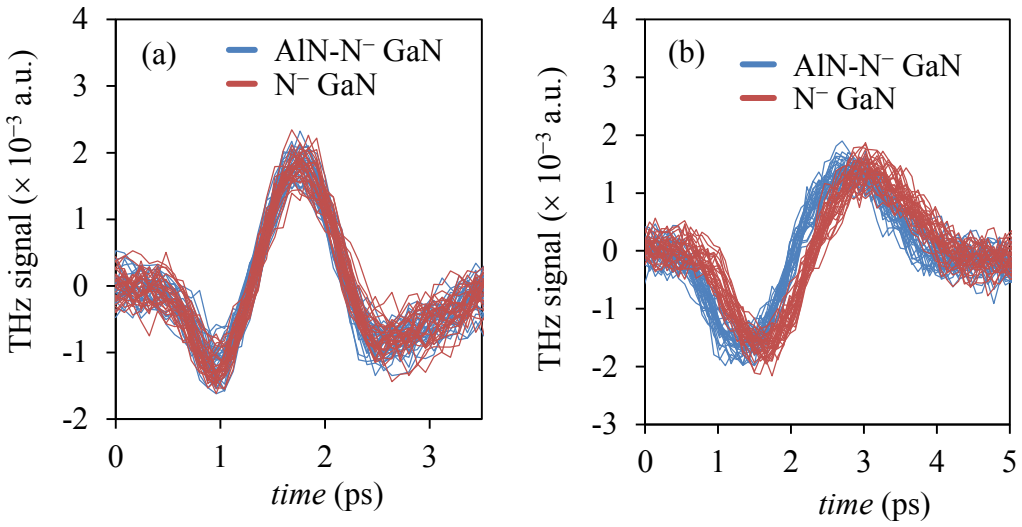

Fig. 4.3: Measurements performed using the TA system. (a) The THz time-domain pulses transmitted through the N^- GaN sample and the AlN-N^- GaN sample. (b) The THz time-domain pulses reflected from the N^- GaN sample and the AlN-N^- GaN sample.

4.3.2 THz Radiation Transmission Through N^+ GaN and AlN-N^+ GaN

THz transmission experiments performed on the N^+ GaN sample and the AlN-N^+ GaN sample. The transmission experiments are performed using the TT system and the time-domain pulses are shown in Fig. 4.4a. The FT of the corresponding time-domain pulses is obtained and the amplitude is shown in Fig. 4.4b. Similar to the AlN-N^- GaN and the N^- GaN, no significant modulation is observed.

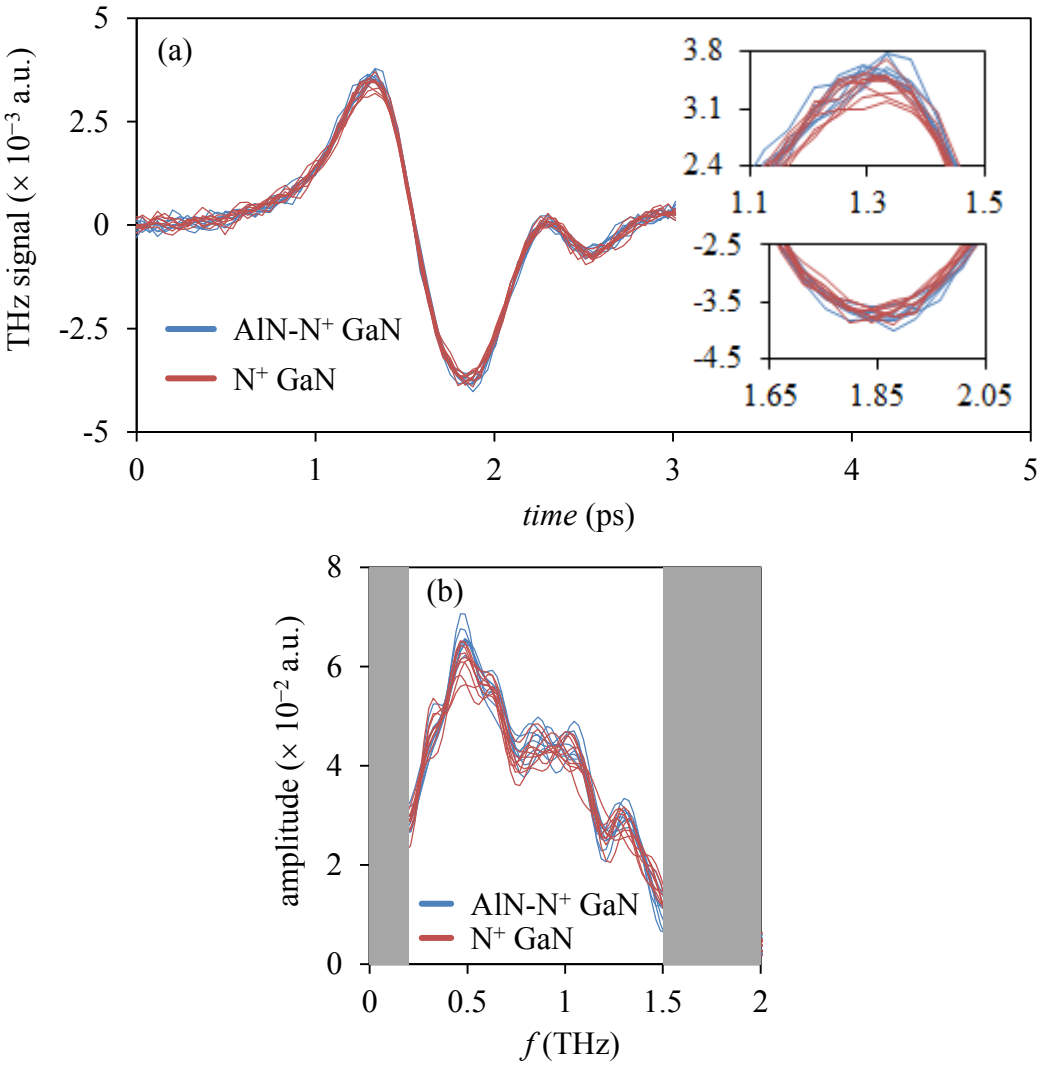

Fig. 4.4: Measurements performed using the TT system. (a) The THz time-domain pulses transmitted through the N^+ GaN sample and the AlN-N^+ GaN sample. The upper inset shows the positive peak of the pulse between 2.4 and 3.8×10^{-3} a.u.. Similarly, the lower inset shows the negative peak of the pulse between −4.5 and -2.5×10^{-3} a.u.. (b) The magnitude of the FT of the time-domain pulses.

Zomega performed transmission measurements and the time-domain pulses (averaged over multiple runs) are shown in Fig. 4.5a. The pulses are nearly identical. Transmission through the N^+ GaN sample relative to transmission through free space, analysed in the frequency domain, is given by Eq. (4.1). Similarly, transmission through the AlN-N^+ GaN sample relative to transmission through free

space is given by Eq. (4.2). The magnitude obtained from these two equations is displayed in Fig. 4.5b and show no significant modulation.

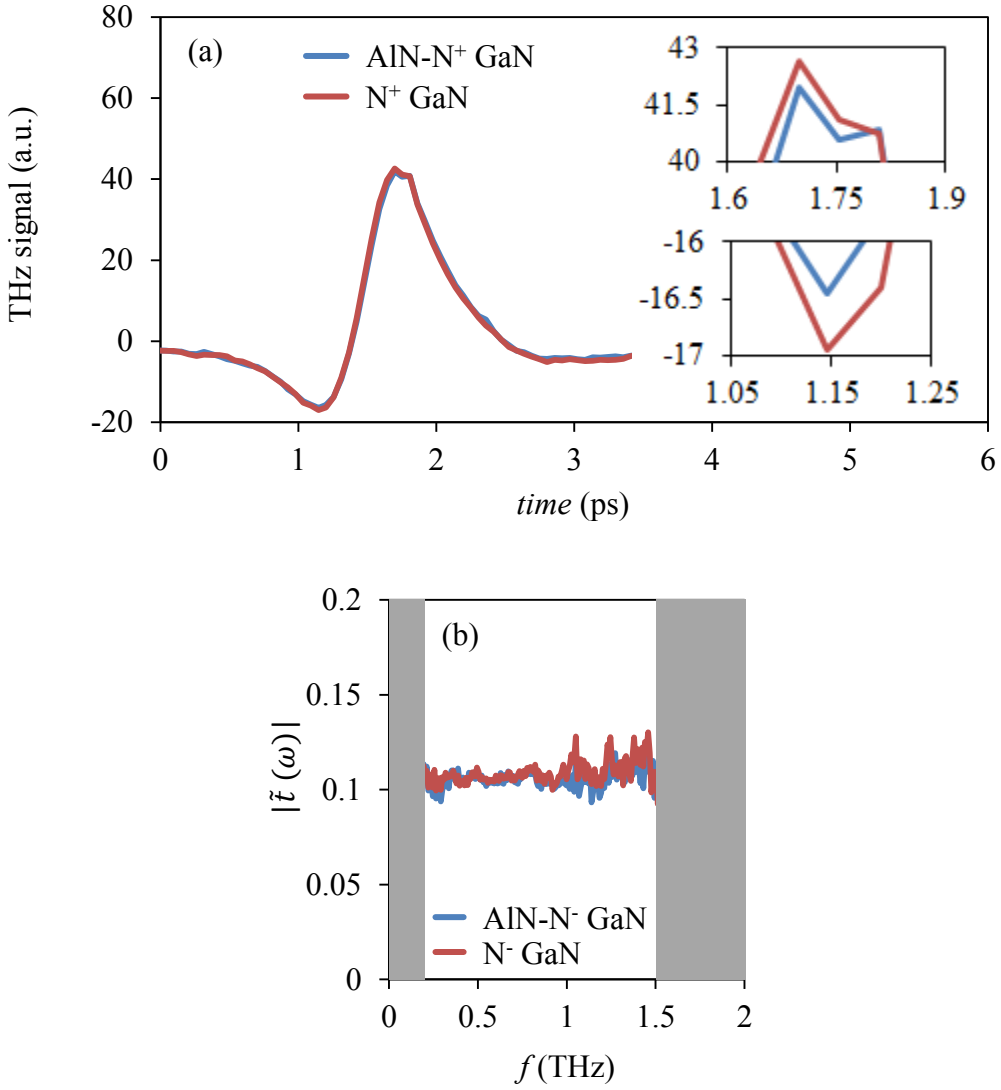

Fig. 4.5: Measurements performed by Zomega. (a) The THz time-domain pulses transmitted through the N^+ GaN sample and the AlN-N^+ GaN sample. The upper inset shows the positive peak of the pulse between 40 and 43 a.u.. Similarly, the lower inset shows the negative peak of the pulse between −17 and −16 a.u.. (b) The magnitude of $\tilde{t}_{N^+\ GaN,FS}(\omega)$ and $\tilde{t}_{AlN-N^+\ GaN,FS}(\omega)$.

4.4 THz Spectroscopy Experiments

THz spectroscopy experiments are performed on the GaN samples, as well as the bare sapphire sample. The complex refractive index of sapphire and GaN is obtained. Additionally, the relative permittivity of the GaN is determined and compared to the Drude model.

4.4.1 Bulk sapphire

THz time-domain pulses are transmitted through the sapphire sample, as well as through free space. The pulses obtained using the TT system is shown in Fig. 4.6a. On such traces there is a noticeable low-amplitude THz noise after the main pulse's arrival. This signal is attributed to the water absorption in the air and can be removed by purging the system with nitrogen. The pulses obtained from Zomega's system are also shown in Fig. 4.6b. The two after pulses transmitted through the sapphire sample are due to reflections from the sample faces. Furthermore, the THz pulses obtained from the TA system are shown in fig. 4.6c.

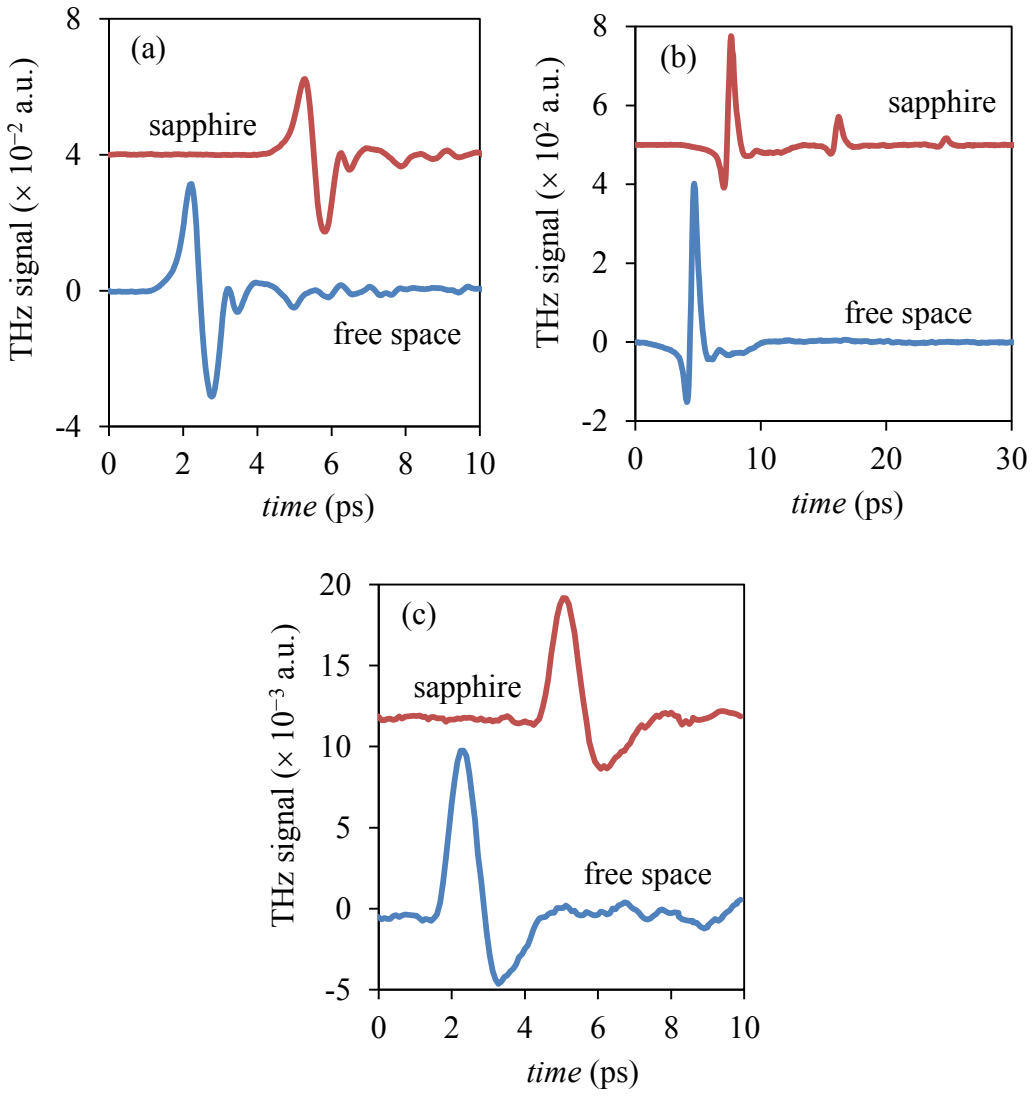

Fig. 4.6: The time-domain pulses transmitted through sapphire, as well as free space. These pulses are measured using (a) the TT system, (b) Zomega's system, and (c) the TA system.

The THz transmission through the sapphire sample relative to transmission through free space, analysed in the frequency domain, is given by the equation,

$$\tilde{t}_{S,FS}(\omega) = \frac{\tilde{E}_{sapphire}(\omega)}{\tilde{E}_{free\ space}(\omega)}, \tag{4.3}$$

where $\tilde{E}_{sapphire}(\omega)$ is the FT of the main pulse transmitted through the sapphire sample. In order to isolate the main THz pulse in the Zomega measurements, the signal is truncated at ~ 14.6 ps. The magnitude of $\tilde{t}_{S,FS}(\omega)$ is plotted in Fig. 4.7a and there are significant fluctuations in the TT system measurement, as well as the TA system measurement. The fluctuations in the TT system measurement are due to the low amplitude THz noise present in the pulses (see Fig. 4.6a). Similarly, the fluctuations in the TA system measurement are due to the system's low signal-to-noise ratio. The phase of $\tilde{t}_{S,FS}(\omega)$ is plotted in Fig. 4.7b. Both the transmission magnitude and phase differ depending on which system is used to perform the measurements; however, this dependence is more evident in the magnitude data.

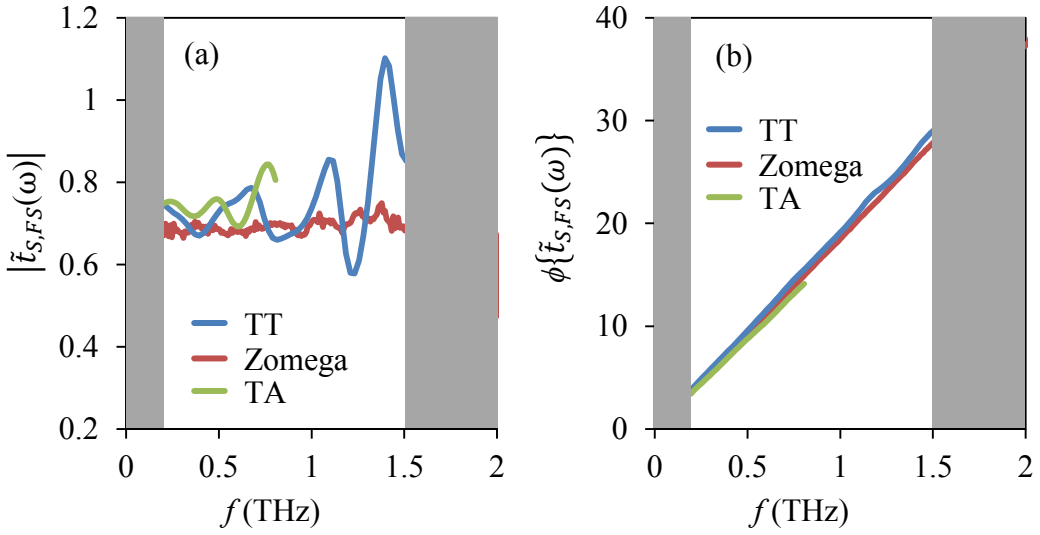

Fig. 4.7: (a) The magnitude and (b) phase of $\tilde{t}_{S,FS}(\omega)$. This is determined from the measurements obtained using the TT system, Zomega's system, and the TA system.

The sapphire complex refractive index, $\tilde{n}_S$, is obtained from the following equation,

$$\tilde{t}_{S,FS}(\omega) = \frac{\tilde{E}_{sapphire}(\omega)}{\tilde{E}_{free\ space}(\omega)} = \frac{4\tilde{n}_S e^{ik_0(\tilde{n}_S - 1)t_S}}{(1+\tilde{n}_S)^2}, \tag{4.4}$$

where k_0 is the free space wavevector and t_S is the thickness of the sapphire wafer. The refractive index of sapphire is shown in Fig. 4.8a, which is obtained using the data from each of the three THz systems. The refractive index determined from the TT system measurements is ~ 3.11 between 0.2 and 1.5 THz, while the refractive index determined from the measurements provided by Zomega is ~ 3.03 between 0.2 and 1.5 THz. Grischkowsky et al. [63] determined that sapphire has a refractive index between 3.066 and 3.077 (over the frequency range of 0.2-1.5 THz). The refractive index determined by Grischkowsky et al. [63] is within the range of that determined from the TT system measurements and Zomega's measurements. The sapphire extinction coefficient shown in Fig. 4.8b, for all three measurement systems, is almost zero. The fact that sapphire is essentially lossless at THz agrees with the results of Grischkowsky et al. [63].

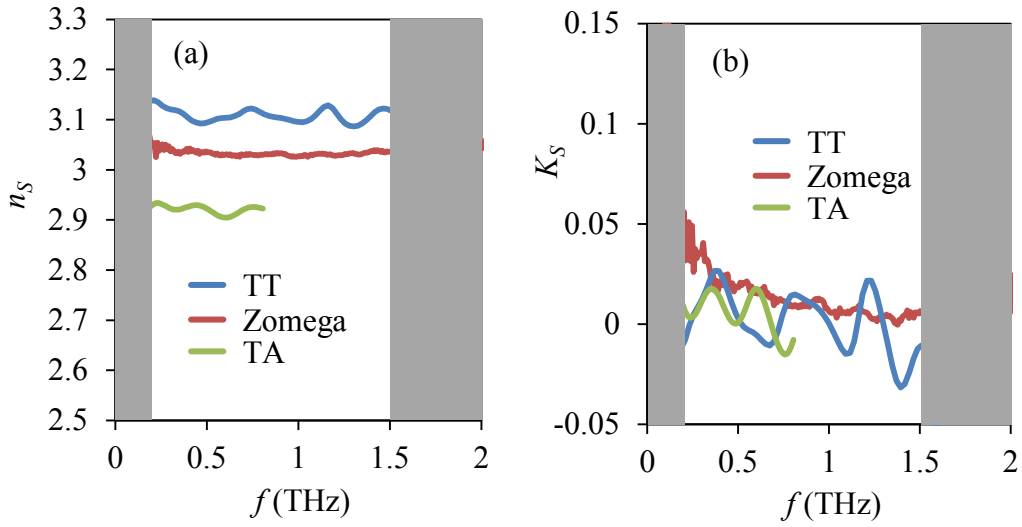

Fig. 4.8: (a) The refractive index and (b) extinction coefficient of sapphire. The curves are determined from the measurements obtained using the TT system, Zomega's system, and the TA system.

4.4.2 Thin Film GaN

THz pulses are transmitted through the GaN and sapphire samples using the TT system. The time domain THz signals are presented in Fig. 4.9a. THz pulses transmitted through the GaN and sapphire samples using Zomega's system are shown in Fig. 4.9b. Notably, the after pulses that arrive shortly after 20 ps are due to multiple reflections from the faces of the samples. The THz pulses transmitted through the GaN samples, as well as free space, using the TA system are shown in Fig. 4.9c.

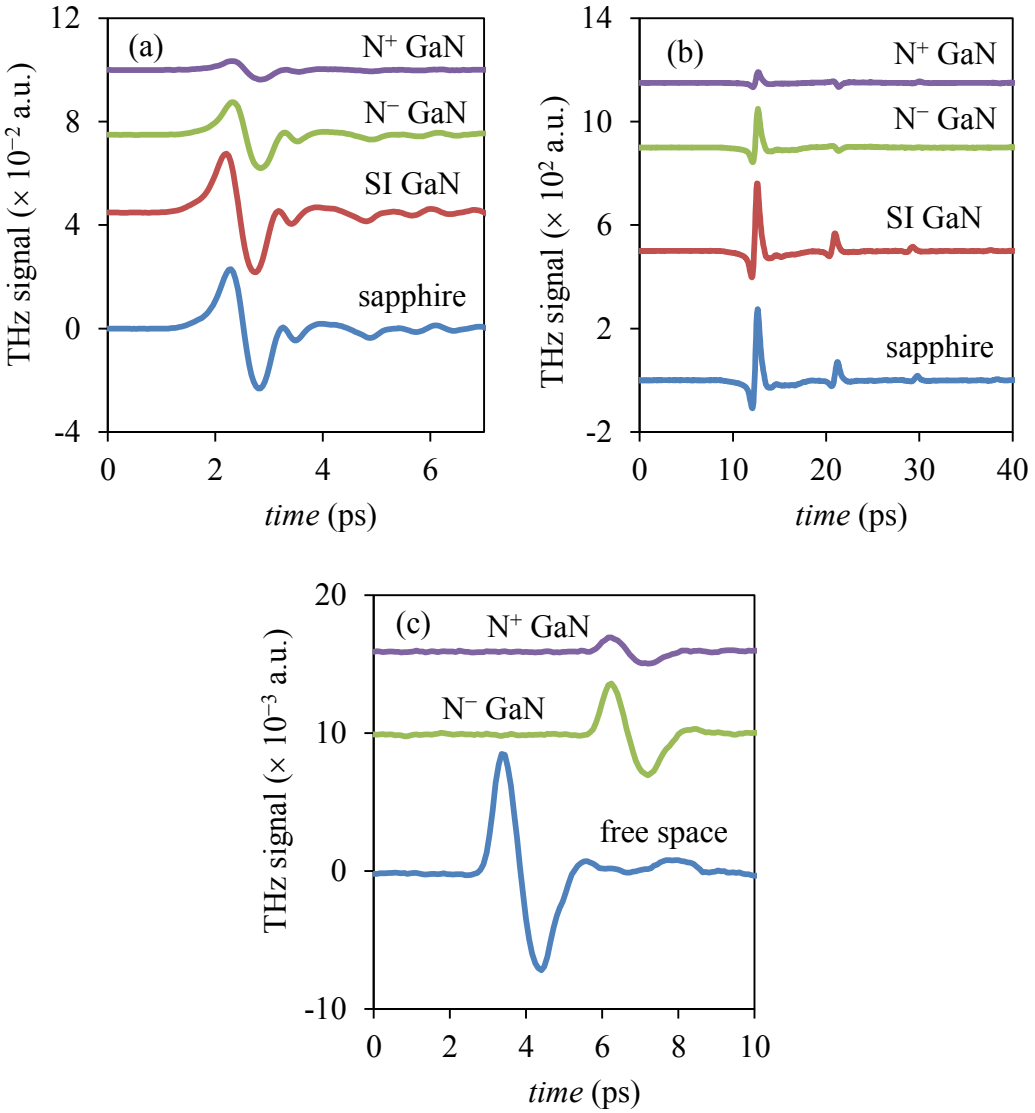

Fig. 4.9: The time-domain pulses transmitted through the GaN samples, as well as a reference sample. These pulses are obtained using (a) the TT system, (b) Zomega's system, and (c) the TA system.

The THz transmission through GaN relative to transmission through sapphire, analysed in the frequency domain, is given by,

$$\tilde{t}_{GaN,S}(\omega) = \frac{\tilde{E}_{GaN}(\omega)}{\tilde{E}_{sapphire}(\omega)}, \tag{4.5a}$$

$$\tilde{t}_{GaN,S}(\omega) = \frac{\tilde{E}_{GaN}(\omega)}{\tilde{E}_{free\ space}(\omega)} \frac{\tilde{E}'_{free\ space}(\omega)}{\tilde{E}'_{sapphire}(\omega)}, \quad (4.5b)$$

where Eq. (4.5a) is used for both the TT system measurements and the Zomega measurements, Eq. (4.5b) is used for the TA system measurements, the un-primed symbols ($\tilde{E}(\omega)$) correspond to the traces shown in Fig. 4.9, and the primed symbols ($\tilde{E}'(\omega)$) correspond to the traces shown in Fig. 4.6c. In order to isolate the main THz pulse in the Zomega measurements, the signal is truncated at ~ 19.3 ps. The magnitude and phase of $\tilde{t}_{GaN,S}(\omega)$ (obtained for SI GaN) is plotted in Fig. 4.10a and b, respectively. A significant discrepancy exists in both the magnitude and phase depending upon the system used to perform the measurements. The negative phase means that the THz time-domain pulses transmitted through the SI GaN sample arrive before the pulses transmitted through the sapphire sample. This occurs because the SI GaN sample is thinner than the sapphire sample. The magnitude and phase of $\tilde{t}_{GaN,S}(\omega)$ (obtained for N^- GaN) is plotted in Fig. 4.10c and d, respectively. In addition, the magnitude and phase of $\tilde{t}_{GaN,S}(\omega)$ (obtained for N^+ GaN) is plotted in Fig. 4.10e and f, respectively. The positive phase means that the THz pulses transmitted through the N^- and N^+ GaN samples arrive after the pulses transmitted through the sapphire sample. This is due to the additional 5 μm of GaN present in the N^- and N^+ GaN samples.

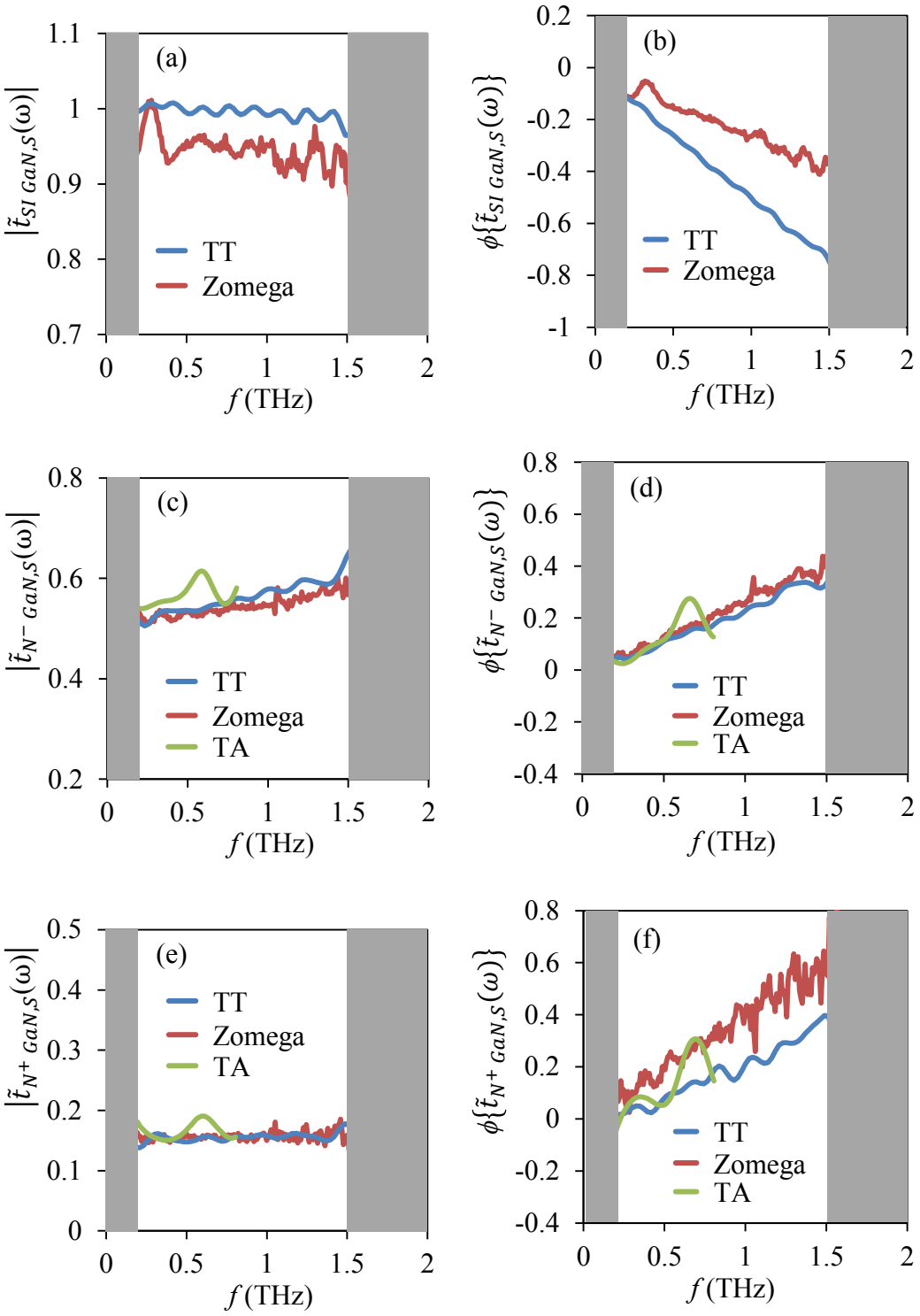

Fig. 4.10: (a) The magnitude and (b) phase of $\tilde{t}_{SI\ GaN,S}(\omega)$. (c) The magnitude and (d) phase of $\tilde{t}_{N^-\ GaN,S}(\omega)$. (e) The magnitude and (f) phase of $\tilde{t}_{N^+\ GaN,S}(\omega)$ obtained using the N^+ GaN measurements.

The complex refractive index of GaN, $\tilde{n}_G$, is determined (using the measurements obtained by the TT system and Zomega's systems) from the equation,

$$\tilde{t}_{GaN,S}(\omega) = \frac{\tilde{E}_{GaN}(\omega)}{\tilde{E}_{sapphire}(\omega)} = \frac{2\tilde{n}_G(1+\tilde{n}_S)e^{ik_0(\tilde{n}_G-1)t_G}e^{ik_0(\tilde{n}_S-1)t_S}}{[(1+\tilde{n}_G)(\tilde{n}_G+\tilde{n}_S)+(1-\tilde{n}_G)(\tilde{n}_G-\tilde{n}_S)e^{i2k_0\tilde{n}_G t_G}]e^{ik_0(\tilde{n}_S-1)t_S'}}, \quad (4.6)$$

where t_G is the thickness of the GaN, t_S is the thickness of the sapphire in the GaN sample, and t_S' is the thickness of the bare sapphire (reference) sample. The refractive index and extinction coefficient of SI GaN are presented in Figs. 4.11a and b, respectively. The discrepancy in the refractive index is due to the large difference in the experimental data (see Fig. 4.10a and b). Zhang et al. [6] determined that low-doped GaN has a refractive index very nearly equal to 3 in the THz regime, which agrees with the refractive index obtained from the TT system measurements.

The refractive index and extinction coefficient of N^- GaN is obtained from Eq. (4.6) and the results are shown in Fig. 4.11c and d, respectively. The refractive index and extinction coefficient obtained using the measurements from both systems are in agreement. The refractive index and extinction coefficient of N^+ GaN is obtained from Eq. (4.6) and the results are shown in Fig. 4.11e and f, respectively. There is a noticeable discrepancy in the results depending upon which system is used to perform the measurements, which is slightly more noticeable in the refractive index.

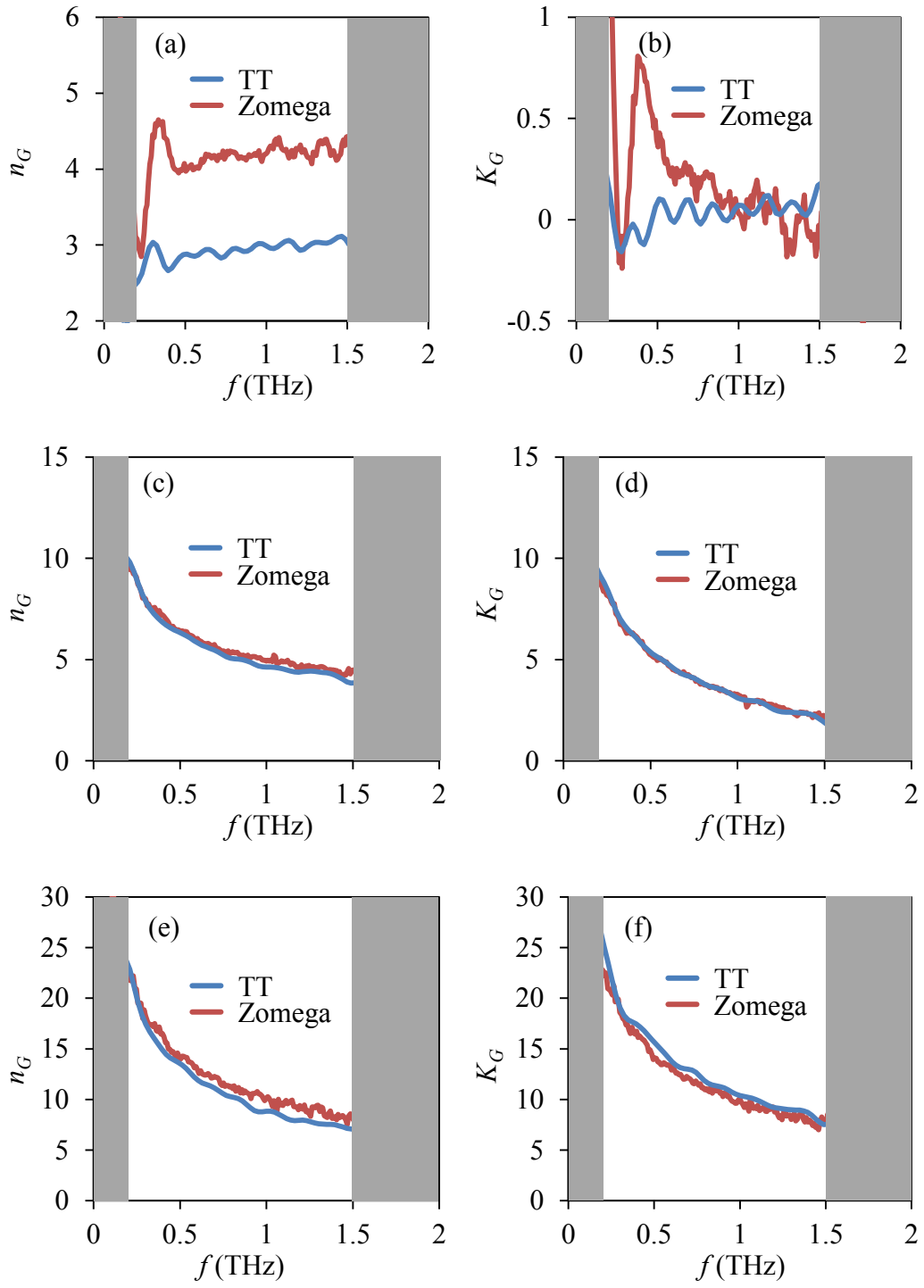

Fig. 4.11: (a) The refractive index and (b) extinction coefficient of SI GaN. (c) The refractive index and (d) extinction coefficient of N^- GaN. (e) The refractive index and (f) extinction coefficient of N^+ GaN.

It is interesting to compare our measured results with other groups. Gauthier-Brun et al. [80] presented a plot that compares the refractive index and extinction coefficient of GaN collected from various papers. These figures are displayed in Fig. 4.12a and b. Each curve is labelled with the GaN doping density and, for the most part, the refractive index and extinction coefficient decrease with decreasing doping density. The refractive index and extinction coefficient of the GaN (obtained from the TT system measurements) is plotted on Fig. 4.12a and b, respectively. Clearly, the SI GaN curve on the refractive index plot is comparable to the curve corresponding to GaN having a doping density of 9×10^{15} cm^{-3}. In addition, the SI GaN curve on the extinction coefficient plot is below all the other curves that are presented. This behaviour is expected since SI GaN has the lowest estimated doping density ($< 10^{12}$ cm^{-3}). However, the curves corresponding to N^+ GaN are above the GaN curves having a doping density of 3.3×10^{17} cm^{-3}, 2.0×10^{17} cm^{-3}, and 3.3×10^{17} cm^{-3}. Clearly, this does not agree with the estimated doping density of N^+ GaN, which is 7×10^{17} cm^{-3}. In addition, the curves corresponding to N^- GaN are above the curves corresponding to GaN having a doping density of 9×10^{15} cm^{-3} and 2.5×10^{17} cm^{-3}. Again, this trend does not agree with the estimated doping density of N^- GaN, which is $\sim 10^{14}$ cm^{-3}.

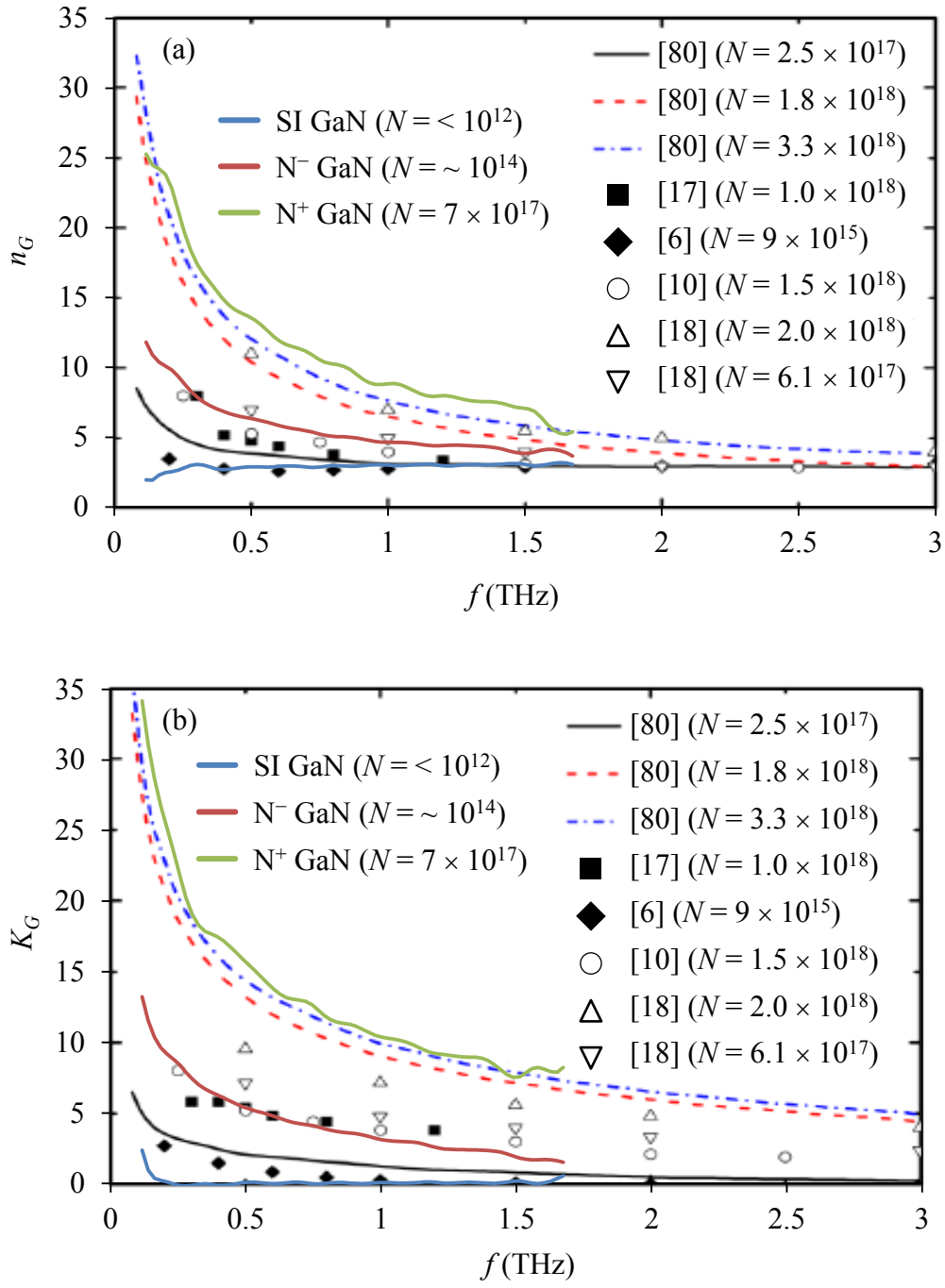

Fig. 4.12: (a) The refractive index and (b) extinction coefficient of GaN with various doping densities (adapted from Gauthier-Brun et al., 2012 [80]). The refractive index and extinction coefficient of SI, N^-, and N^+ GaN (obtained using the TT system) is added to the plot in (a) and (b), respectively.

Clearly, according to the measured refractive index and extinction coefficient, the reported doping levels cannot be correct. As such, to estimate the doping levels, one must refer to a model representing the material property. Here, we employ the Drude model to fit to the GaN relative permittivity and infer the doping density, as in [6, 10, 16-20, 80]. The Drude relative permittivity is given by the equation [6, 10],

$$\tilde{\varepsilon}_{r,drude} = \tilde{\varepsilon}_b + \frac{i\tau N e^2}{\omega \varepsilon_0 m^* (1 - i\omega\tau)}, \tag{4.7}$$

where $\tilde{\varepsilon}_b$ is the background relative permittivity, m^* is the effective mass of GaN, N is the doping density, and τ is the time constant of the electrons in GaN. $\tau = m^*\mu/e$ and $m^* = 0.22m_0$ [6, 10], where μ is the electron mobility in GaN and m_0 is the mass of a free electron. The Drude relative permittivity reduces to the background relative permittivity when the doping is equal to zero. Additionally, the Drude relative permittivity can be separated into its real, $\varepsilon'_{r,drude}$, and imaginary, $\varepsilon''_{r,drude}$, components as follows,

$$\varepsilon'_{r,drude} = \varepsilon_b' - \frac{\tau^2 N e^2}{\varepsilon_0 m^* (1 + \omega^2\tau^2)}, \tag{4.8a}$$

$$\varepsilon''_{r,drude} = \varepsilon_b'' + \frac{\tau N e^2}{\omega \varepsilon_0 m^* (1 + \omega^2\tau^2)}, \tag{4.8b}$$

where ε_b' is the real component of the background relative permittivity and ε_b'' is the imaginary component of the background relative permittivity. Notably, when fitting the Drude model to experimental data to determined relative permittivity, there is an inherent assumption that the background relative permittivity is considered to be constant, [6, 10, 18-20, 80]. In this case, the doping density and electron mobility controls the shape of the Drude relative permittivity vs. frequency curves. In addition, the background relative permittivity introduces a constant shift into the Drude relative permittivity vs. frequency curves.

The complex refractive index of a material is related to its relative permittivity through the relationship, $\tilde{\varepsilon}_r = \tilde{n}^2$. This relationship is used to obtain the SI GaN relative permittivity and the real and imaginary components are plotted in Fig. 4.13a and b, respectively. The Drude relative permittivity is fit to these results as follows. First, the background relative permittivity is set to $9.4 + i*0$, [6, 10, 18-20, 80]. Then, the doping density is set as 10^{15} cm^{-3} and the electron mobility is chosen to be 2000 cm^2/(Vs). For the best fit, it is clear that the doping density obtained from the Drude model (10^{15} cm^{-3}) is larger than the estimated doping density ($< 10^{12}$ cm^{-3}).

The real and imaginary components of the N^- GaN relative permittivity are plotted in Fig. 4.13c and d, respectively. The Drude model cannot be fit to these curves when the background relative permittivity is $9.4 + i*0$. Instead, the proper shape of the Drude relative permittivity curves is obtained by choosing a doping density of 2.4×10^{23} cm^{-3} and an electron mobility of 500 cm^2/(Vs). Then, the proper shift in the Drude relative permittivity curves is obtained by choosing a

background relative permittivity of 23.5 + *i**0. The Drude model only considers free carrier scattering. Thus, the real part of the background relative permittivity having a value of 23.5 suggests that there are additional effects present in the GaN that is influencing the transmission of THz radiation through the sample. It is possible that impurities, defects, or traps are introduced into the GaN during the growth process and interact with the THz radiation transmitted through the sample.

The real and imaginary components of the N^+ GaN relative permittivity are plotted in Fig. 4.13e and f, respectively. Again, the Drude model cannot be fit to these curves when the background relative permittivity is 9.4 + *i**0. The best fit is achieved by choosing a doping density of 1.5×10^{18} cm^{-3}, an electron mobility of 500 $cm^2/(Vs)$, and a relative permittivity of 45 + *i**0. The real part of the background relative permittivity is much larger than 9.4 and this suggests that additional effects are influencing the THz radiation, as in the case of N^- GaN. Again, it is possible that impurities, defects, or traps are introduced into the GaN during the growth process, which interacts with the THz radiation transmitted through the sample.

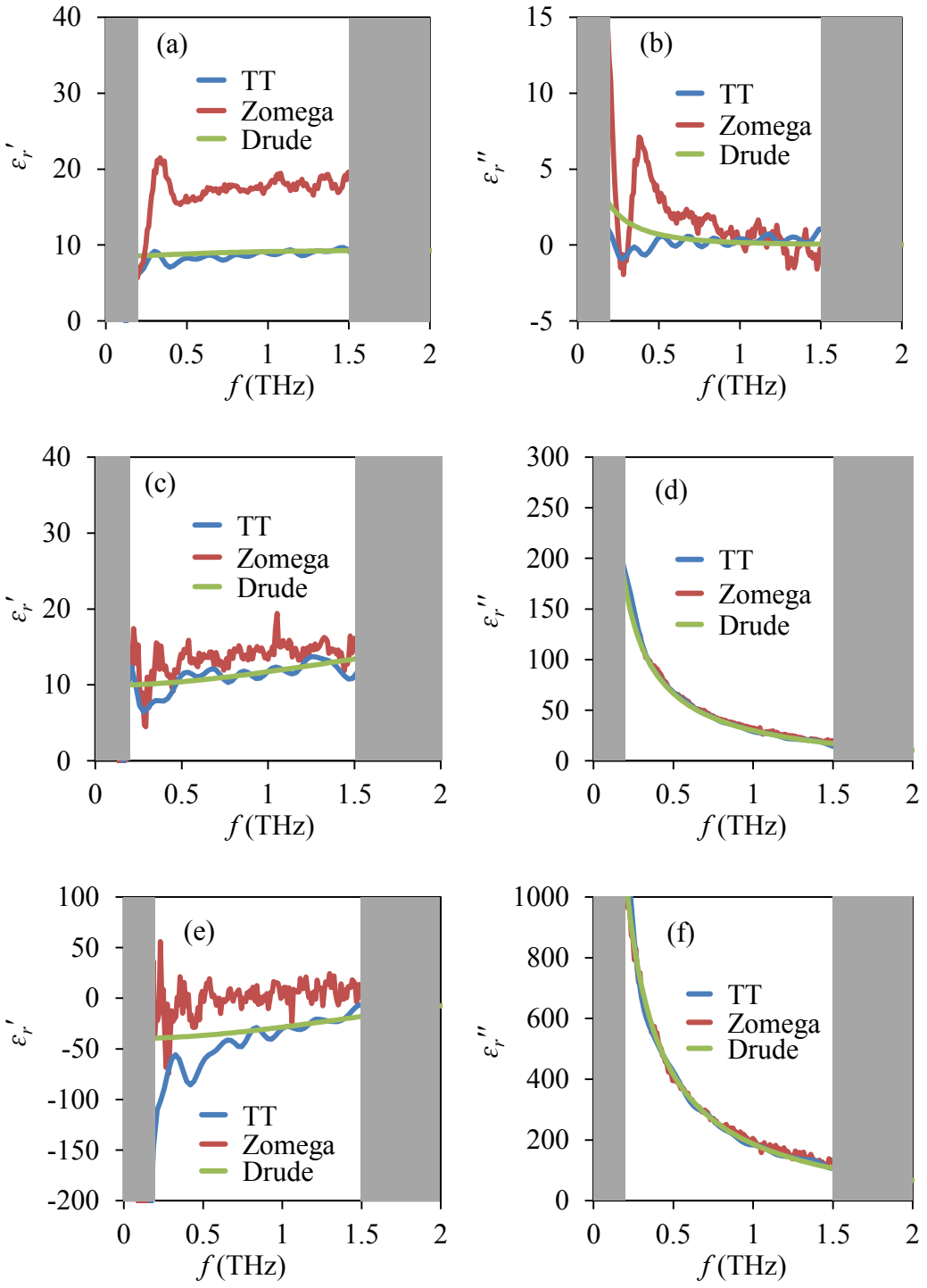

Fig. 4.13: (a) The real part and (b) imaginary part of the SI GaN relative permittivity. (c) The real part and (d) imaginary part of the N^- GaN relative permittivity. (e) The real part and (f) imaginary part of the N^+ GaN relative permittivity. The Drude model is fit to the results.

4.5 Conclusions

THz experiments performed on the N^- GaN and AlN-N^- GaN sample, using the TT system and the TA system, shows no modulation. However, experiments performed on these samples using Zomega's system shows a resonance at ~ 0.55 THz. This resonance could be spurious or the THz beam could be interacting with a defect that is located at the back surface of the sapphire wafer. THz modulation experiments performed on the N^+ GaN and AlN-N^+ GaN sample, using the TT system and Zomega's system, shows no modulation.

THz spectroscopy experiments are performed on the sapphire sample and the GaN samples. The complex refractive index of sapphire and SI GaN agrees with literature; however, the complex refractive index of N^- and N^+ GaN does not agree with literature. The relative permittivity of SI GaN is accurately described by the Drude model; however, the Drude model cannot be properly fit to N^- and N^+ GaN.

Chapter 5

Conclusions and Future Work

In chapter 2, COMSOL Multiphysiscs software is used to study the amplification of THz radiation sustained by an amplifier and oscillator. The active component consists of a planar device that has a 2DEG at a GaN/AlN interface. The free electrons in the 2DEG are assumed to produce a static NDR, since a static NDR was measured from a GaN-based device in [58]. The amplifier and oscillator both amplify THz radiation over a frequency range of 0.5-2 THz and the amplification can be improved by increasing the number of contacts on the active device. However, the THz amplification is significantly limited by the 2DEG thickness (~ 1 nm) and using doped GaN (without a 2DEG) may actually increase the amplification.

In chapter 3, Crosslight APSYS software is used to study the electrical properties of the active device. Three planar GaN-devices (having a 2DEG) are simulated: (1) with ohmic contacts and no gate, (2) with ohmic contacts and a gate, and (3) with MIS contacts and no gate. Those devices having ohmic contacts exhibit

SPCT, while the device having MIS contacts is shown to exhibit a cathode domain. Therefore, a static NDR cannot be obtained from the studied devices. In light of this setback, Crosslight APSYS software is used to simulate a non-planar GaN-device having ohmic contacts, as well as a 2DEG planar device having no gate and ohmic contacts. The simulations determine the GaN resistivity in the non-planar device and confirm that the planar device is able to operate in the SA mode. Future work should determine if the planar device (operating in the SA mode) is able to amplify THz radiation. This requires the AC complex conductivity of the 2DEG to be obtained. However, a concern is that it may be difficult for the device to overcome losses inherent in the amplification devices, since only a portion of the GaN exhibits a negative resistivity.

In chapter 4, THz radiation is transmitted through (and reflected from) GaN samples in the presence and absence of 2DEG. One measurement shows a resonance at ~ 0.55 THz; however, this measurement is believed to be spurious or due to a defect located on the back surface of the sapphire substrate. It is clear from the remaining measurements that free electron absorption from the 2DEG does not modulate the THz radiation. However, it is expected that THz radiation scattered from a grating will excited surface plasmons on the 2DEG [81]. In turn, this would result in the absorption of THz radiation at specific frequencies [81]. A grating structure could be deposited on the AlN-GaN samples (that is, the samples with a 2DEG) and measurements could be performed to determine if THz radiation is absorbed.

THz time-domain spectroscopy experiments performed on sapphire and thin film GaN (having various doping densities) is also discussed in chapter 4. The complex refractive index of sapphire and GaN is determined from the measurements. The complex refractive index of GaN having an estimated doping density $< 10^{12}$ cm^{-3}, as well as sapphire, agrees with literature values. However, GaN having an estimated doping density of $\sim 10^{14}$ cm^{-3} and 7×10^{17} cm^{-3} does not agree with literature values. The GaN is further studied by comparing the GaN relative permittivity (determined from the experimental data) to the Drude model. The Drude model is fit to the relative permittivity of GaN having an estimated doping density of $< 10^{12}$ cm^{-3}. However, the Drude model cannot be properly fit to the relative permittivity of GaN having estimated doping densities of $\sim 10^{14}$ cm^{-3} and 7×10^{17} cm^{-3}. The disagreement with the Drude model suggests that impurities, defects, or traps influences the THz radiation transmitted through the GaN (in addition to free electron absorption of the radiation). Future work could attempt to deduce the exact cause of the disagreement.

References

[1] S. Perez, T. González, D. Pardo and J. Mateos, "Terahertz Gunn-like oscillations in InGaAs/InAlAs planar diodes," *J. Appl. Phys.,* vol. 103, pp. 094516, 2008.

[2] Y. Hao, L. Yang and J. Zhang, "GaN-based semiconductor devices for terahertz technology," *Terahertz Science and Technology,* vol. 1, pp. 51-64, 2008.

[3] A. Y. Pawar, D. D. Sonawane, K. B. Erande and D. V. Derle, "Terahertz technology and its applications." *Drug Invention Today,* vol. 5, pp. 157-163, 2013.

[4] P. Dean, A. Valavanis, J. Keeley, K. Bertling, Y. Lim, R. Alhathlool, A. Burnett, L. Li, S. Khanna and D. Indjin, "Terahertz imaging using quantum cascade lasers—a review of systems and applications," *J. Phys. D,* vol. 47, pp. 374008, 2014.

[5] T. Kleine-Ostmann, M. Koch and P. Dawson, "Modulation of THz radiation by semiconductor nanostructures," *Microw. Opt. Techn. Let.,* vol. 35, pp. 343-345, 2002.

[6] W. Zhang, A. K. Azad and D. Grischkowsky, "Terahertz studies of carrier dynamics and dielectric response of n-type, freestanding epitaxial GaN," *Appl. Phys. Lett.,* vol. 82, pp. 2841-2843, 2003.

[7] S. R. Tripathi, Y. Taira, S. Hayashi, K. Nawata, K. Murate, H. Minamide and K. Kawase, "Terahertz wave parametric amplifier," *Opt. Lett.,* vol. 39, pp. 1649-1652, 2014.

[8] Y. Wang, L. Yang, W. Mao, S. Long and Y. Hao, "Modulation of multidomain in AlGaN/GaN HEMT-like planar Gunn diode," *IEEE T. Electron Dev.,* vol. 60, pp. 1600-1606, 2013.

[9] E. Barry, V. Sokolov, K. Kim and R. Trew, "Large-signal analysis of terahertz generation in submicrometer GaN diodes," *IEEE Sens. J.,* vol. 10, pp. 765-771, 2010.

[10] T. Tsai, S. Chen, C. Chang, S. Hsu, T. Lin and C. Chi, "Terahertz response of GaN thin films," *Opt. Express,* vol. 14, pp. 4898-4907, 2006.

[11] T. Kleine-Ostmann, P. Dawson, K. Pierz, G. Hein and M. Koch, "Room-temperature operation of an electrically driven terahertz modulator," *Appl. Phys. Lett.,* vol. 84, pp. 3555-3557, 2004.

[12] T. Kleine-Ostmann, K. Pierz, G. Hein, P. Dawson, M. Marso and M. Koch, "Spatially resolved measurements of depletion properties of large gate two-

dimensional electron gas semiconductor terahertz modulators," *J. Appl. Phys.,* vol. 105, pp. 093707, 2009.

[13] T. Kleine-Ostmann, K. Pierz, G. Hein, P. Dawson and M. Koch, "Audio signal transmission over THz communication channel using semiconductor modulator," *Electron. Lett.,* vol. 40, pp. 124-126, 2004.

[14] T. Kleine-Ostmann, K. Pierz, G. Hein, P. Dawson and M. Koch, "Room-temperature semiconductor modulators for free-space signal transmission with THz waves," *SPIE Proc.,* vol. 5593, pp. 521-532, 2004.

[15] T. Kleine-Ostmann, M. Koch, G. Hein, K. Pierz and P. Dawson, "Electrically driven room temperature THz modulators," in *Conference on Lasers and Electro-Optics,* San Francisco, CA, 2004, pp. 1-3.

[16] T. Nagashima, K. Takata, S. Nashima, H. Harima and M. Hangyo, "Measurement of electrical properties of gan thin films using terahertz-time domain spectroscopy," *Jpn. J. Appl. Phys.,* vol. 44, pp. 926-931, 2005.

[17] H. Fang, R. Zhang, B. Liu, H. Lu, J. Ding, Z. Xie, X. Xiu, Y. Zheng, M. Xiao, C. Zhang, J. Chen and P. Wu, "Dielectric properties of GaN in THz frequencies," *Chinese Phys. Lett.,* vol. 27, pp. 017802, 2010.

[18] H. Guo, X. Zhang, W. Liu, A. Yong and S. Tang, "Terahertz carrier dynamics and dielectric properties of GaN epilayers with different carrier concentrations," *J. Appl. Phys.,* vol. 106, pp. 063104, 2009.

[19] S. Balci, W. Baughman, D. S. Wilbert, G. Shen, P. Kung and S. M. Kim, "Characteristics of THz carrier dynamics in GaN thin film and ZnO nanowires by temperature dependent terahertz time domain spectroscopy measurement," *Solid State Electron.,* vol. 78, pp. 68-74, 2012.

[20] H. Fang, R. Zhang, B. Liu, Y. Li, D. Fu, Y. Li, Z. Xie, Z. Zhuang, Y. Zheng and J. Wu, "Temperature dependence of the point defect properties of GaN thin films studied by terahertz time-domain spectroscopy," *Sci. China Phys. Mech. Astron.,* vol. 56, pp. 2059-2064, 2013.

[21] E. Yu, X. Dang, P. Asbeck, S. Lau and G. Sullivan, "Spontaneous and piezoelectric polarization effects in III–V nitride heterostructures," *Journal of Vacuum Science & Technology B,* vol. 17, pp. 1742-1749, 1999.

[22] O. Ambacher, J. Smart, J. Shealy, N. Weimann, K. Chu, M. Murphy, W. Schaff, L. Eastman, R. Dimitrov and L. Wittmer, "Two-dimensional electron gases induced by spontaneous and piezoelectric polarization charges in N-and Ga-face AlGaN/GaN heterostructures," *J. Appl. Phys.,* vol. 85, pp. 3222-3233, 1999.

[23] M. Stutzmann, O. Ambacher, M. Eickhoff, U. Karrer, A. Lima Pimenta, R. Neuberger, J. Schalwig, R. Dimitrov, P. Schuck and R. Grober, "Playing with polarity," *Physica Status Solidi (B),* vol. 228, pp. 505-512, 2001.

[24] J. Ibbetson, P. Fini, K. Ness, S. DenBaars, J. Speck and U. Mishra, "Polarization effects, surface states, and the source of electrons in AlGaN/GaN heterostructure field effect transistors," *Appl. Phys. Lett.,* vol. 77, pp. 250-252, 2000.

[25] S. Wu, P. Geiser, J. Jun, J. Karpinski, D. Wang and R. Sobolewski, "Time-resolved intervalley transitions in GaN single crystals," *J. Appl. Phys.,* vol. 101, pp. 043701, 2007.

[26] M. Piccardo, L. Martinelli, J. Iveland, N. Young, S. P. DenBaars, S. Nakamura, J. S. Speck, C. Weisbuch and J. Peretti, "Determination of the first satellite valley energy in the conduction band of wurtzite GaN by near-band-gapphotoemission spectroscopy," *Phys. Rev. B,* vol. 89, pp. 235124, 2014.

[27] D. McCumber and A. Chynoweth, "Theory of negative-conductance amplification and of Gunn instabilities in" two-valley" semiconductors," *IEEE T. Electron Dev.,* vol. 13, pp. 4-21, 1966.

[28] H. Thim, "Stability and switching in overcritically doped Gunn diodes," *P. IEEE,* vol. 59, pp. 1285-1286, 1971.

[29] H. W. Thim, "Active microwave semiconductor devices," in *4th European Microwave Conference,* Montreux, Switzerland, 1974, pp. 1-15.

[30] K. Hofmann, "Stability theory for thin Gunn diodes with dielectric surface loading," *Electron. Lett.,* vol. 8, pp. 124-125, 1972.

[31] T. W. Tucker, "Planar GaAs Gunn and field effect devices," Ph.D dissertation, Dept. of Electrical Engineering, University of British Columbia, Vancouver, BC, 1972.

[32] L. A. Yang, S. Long, X. Guo and Y. Hao, "A comparative investigation on sub-micrometer InN and GaN Gunn diodes working at terahertz frequency," *J. Appl. Phys.,* vol. 111, pp. 104514, 2012.

[33] E. Alekseev and D. Pavlidis, "GaN gunn diodes for THz signal generation," in *IEEE MTT-S International Microwave Symposium Digest,* Boston, Ma, 2000, pp. 1905-1908.

[34] A. Íñiguez-de-la-Torre, J. Mateos, I. Íñiguez-de-la-Torre and T. González, "Toward THz gunn oscillations in planar GaN nanodiodes," in *2011 Spanish*

Conference on Electron Devices (CDE), Palma de Mallorca, Illes Balears, 2011, pp. 1-4.

[35] B. Aslan and L. F. Eastman, "A THz-range planar NDR device utilizing ballistic electron acceleration in GaN," *Solid-State Electronics,* vol. 64, pp. 57-62, 2011.

[36] W. Shockley, "Negative resistance arising from transit time in semiconductor diodes," *Bell Syst. Tech. J.,* vol. 33, pp. 799-826, 1954.

[37] H. Kroemer, "Generalized proof of Shockley's positive conductance theorem," *Proc IEEE,* vol. 58, pp. 1844-1845, 1970.

[38] Z. Huang, R. Goldberg, J. Chen, Y. Zheng, D. B. Mott and P. Shu, "Direct observation of transferred-electron effect in GaN," *Appl. Phys. Lett.,* vol. 67, pp. 2825-2826, 1995.

[39] P. Hauge, "Static negative resistance in Gunn effect materials with field-dependent carrier diffusion," *IEEE T. Electron Dev.,* vol. 18, pp. 390-391, 1971.

[40] G. Dohler, "Shockley's positive conductance theorem for Gunn materials with field-dependent diffusion," *IEEE T. Electron Dev.,* vol. 18, pp. 1190-1192, 1971.

[41] H. Thim, "Temperature effects in bulk GaAs amplifiers," *IEEE T. Electron Dev.,* vol. 14, pp. 59-62, 1967.

[42] H. Thim and M. Barber, "Microwave amplification in a GaAs bulk semiconductor," *IEEE T. Electron Dev.,* vol. 13, pp. 110-114, 1966.

[43] A. Baynham and D. Colliver, "New mode of microwave emission from GaAs," *Electron. Lett.,* vol. 6, pp. 498-500, 1970.

[44] A. Baynham, "Emission of TEM waves generated within an n type Ge cavity," *Electron. Lett.,* vol. 6, pp. 306-307, 1970.

[45] P. Fleming, "The active medium propagation device," *P. IEEE,* vol. 63, pp. 1253-1254, 1975.

[46] P. Fleming, T. Smith, H. Carlson and W. Cox, "Continuous wave operation of AMP devices," *IEEE T. Electron Dev.,* vol. 26, pp. 1267-1272, 1979.

[47] A. Baynham, "Negative Conductivity Amplifiers and Oscillators," U.S. Patent 3 796 964, Mar 12, 1974.

[48] J. Copeland, "A new mode of operation for bulk negative resistance oscillators," *P. IEEE,* vol. 54, pp. 1479-1480, 1966.

[49] M. Xiangrong, S. Wei and X. Mei, "Experimental investigation of limit space charge accumulation mode operation in a semi-insulating GaAs photoconductive semiconductor switch," *J. Semicond.,* vol. 34, pp. 074011, 2013.

[50] G. P. Srivastava and V. L. Gupta, "Solid state microwave devices," in *Microwave Devices and Circuit Design*, Eastern Economy ed. Delhi, India: PHI Learning Pvt. Ltd., 2006, pp. 312.

[51] V. Sokolov, K. Kim, V. Kochelap and D. Woolard, "Terahertz generation in submicron GaN diodes within the limited space-charge accumulation regime," *J. Appl. Phys.,* vol. 98, pp. 064507, 2005.

[52] E. Barry, V. Sokolov, K. Kim and R. Trew, "Terahertz generation in GaN diodes in the limited space-charge accumulation mode," *J. Appl. Phys.,* vol. 103, pp. 126101, 2008.

[53] E. Barry, V. Sokolov, K. Kim and R. Trew, "Large-signal analysis of terahertz generation in submicrometer GaN diodes," *IEEE Sens. J.,* vol. 10, pp. 765-771, 2010.

[54] K. Böer and G. Döhler, "Influence of boundary conditions on high-field domains in Gunn diodes," *Phys. Rev.,* vol. 186, pp. 793-800, 1969.

[55] H. Kroemer, "The Gunn effect under imperfect cathode boundary conditions," *IEEE T. Electron Dev.,* vol. 15, pp. 819-837, 1968.

[56] J. Gunn, "Properties of a free, steadily travelling electrical domain in GaAs," *IBM J. Res. Dev.,* vol. 10, pp. 300-309, 1966.

[57] O. Yilmazoglu, K. Mutamba, D. Pavlidis and T. Karaduman, "Measured negative differential resistivity for GaN Gunn diodes on GaN substrate," *Electron. Lett.,* vol. 43, pp. 480-482, 2007.

[58] C. Ceroici, M. A. L. Johnson and D. Barlage, "Lateral GaN device displaying NDR at minimal current densities," *Unpublished,* 2012.

[59] B. P. Lathi and Z. Ding, *Modern Digital and Analog Communication Systems.* Oxford, NY: Oxford University Press, 2009.

[60] K. Voon, K. Bothe, P. Motamedi, K. Cadien and D. Barlage, "Polarization charge properties of low-temperature atomic layer deposition of AlN on GaN," *J. Phys. D,* vol. 47, pp. 345104, 2014.

[61] M. Pokorný, "Modeling of Microwave Semiconductor Structures," Doctoral thesis, Dept. of Radio Electronics, Brno University of Technology, Brno, Czech Republic, 2011.

[62] A. Baynham, "Wave propagation in negative differential conductivity media: n-Ge," *IBM J. Res. Dev.,* vol. 13, pp. 568-572, 1969.

[63] D. Grischkowsky, S. Keiding, M. v. Exter and C. Fattinger, "Far-infrared time-domain spectroscopy with terahertz beams of dielectrics and semiconductors," *J. Opt. Soc. Am.,* vol. 7, pp. 2006-2015, 1990.

[64] H. Yasuda and I. Hosako, "Measurement of terahertz refractive index of metal with terahertz time-domain spectroscopy," *Jpn. J. Appl. Phys.,* vol. 47, pp. 1632-1634, 2008.

[65] J. S. Ward, "Terahertz waveguide standards," in *IEEE MTT-S International Microwave Symposium Workshop,* San Francisco, CA, 2006, pp. 1-28.

[66] D. M. Pozar, "Microwave resonators," in *Microwave Engineering*, 4th ed. Hoboken, NJ: Wiley, 2011, pp. 285.

[67] V. O. Turin, "A modified transferred-electron high-field mobility model for GaN devices simulation," *Solid State Electron.,* vol. 49, pp. 1678-1682, 2005.

[68] K. Voon, K. Bothe, P. Motamedi, K. Cadien and D. Barlage, "Engineered Tunneling Contacts with Low-Temperature Atomic Layer Deposition of AlN on GaN," *IEEE T. Electron Dev.,* vol. 59, pp. 175-178, 2012.

[69] A. A. Grinberg, M. S. Shur, R. J. Fischer and H. Morkoc, "An investigation of the effect of graded layers and tunneling on the performance of AlGaAs/GaAs heterojunction bipolar transistors," *IEEE T. Electron Dev.,* vol. 31, pp. 1758-1765, 1984.

[70] X. Wang, W. Hu, X. Chen and W. Lu, "The study of self-heating and hot-electron effects for AlGaN/GaN double-channel HEMTs," *IEEE T. Electron Dev.,* vol. 59, pp. 1393-1401, 2012.

[71] J. Kuzmik, P. Javorka, A. Alam, M. Marso, M. Heuken and P. Kordos, "Determination of channel temperature in AlGaN/GaN HEMTs grown on sapphire and silicon substrates using DC characterization method," *IEEE T. Electron Dev.,* vol. 49, pp. 1496-1498, 2002.

[72] N. Braga, R. Mickevicius, R. Gaska, X. Hu, M. Shur, M. A. Khan, G. Simin and J. Yang, "Simulation of hot electron and quantum effects in AlGaN/GaN heterostructure field effect transistors," *J. Appl. Phys.,* vol. 95, pp. 6409-6413, 2004.

[73] R. Borges, N. Braga, B. Wu and V. Mickevicius, "Simulations provide additional insights into GaN HFET reliability," *Technology Transistor Modeling,* 2006.

[74] D. Marcon, "Reliability Study of Power Gallium Nitride Based Transistors," Ph.D. dissertation, Dept. of Electrical Engineering, University of Leuven, Leuven, Flanders, Belgium, 2011, pp. 51.

[75] X. Yang, "Simulation of MOSFETs, BJTs and JFETs At and Near the Pinch-off Region," M.S. thesis, Arizona State University, Tempe, AZ, 2011.

[76] S. Bharadwaj, "Investigation of oxide thickness dependence of Fowler-Nordheim parameter B," M.S. thesis, Dept. of Electrical Engineering, University of South Florida, Tampa, FL, 2004.

[77] P. L. Fleming, "Planar transmission line comprising a material having negative differential conductivity," U.S. Patent 3 975 690, Aug 17, 1976.

[78] E. M. Conwell, "Boundary conditions and high-field domains in GaAs," *IEEE T. Electron Dev.,* vol. 17, pp. 262-270, 1970.

[79] C. Baron and A. Elezzabi, "A 360 angularly ranging time-domain terahertz spectroscopy system," *Meas. Sci. Technol.,* vol. 19, pp. 065602, 2008.

[80] A. Gauthier-Brun, J. Teng, E. Dogheche, W. Liu, A. Gokarna, M. Tonouchi, S. Chua and D. Decoster, "Properties of InxGa1− xN films in terahertz range," *Appl. Phys. Lett.,* vol. 100, pp. 071913, 2012.

[81] N. Pala, D. Veksler, A. Muravjov, W. Stillman, R. Gaska and M. Shur, "Resonant detection and modulation of terahertz radiation by 2DEG plasmons in GaN grating-gate structures," in *IEEE Sensors 2007 Conference,* Atlanta, GA, 2007, pp. 570-572.

Appendices

Appendix A: MATLAB Analysis of THz-TDS Modulation Measurements

The MATLAB script files used to analyse modulation in the GaN and the AlN-GaN samples (discussed in section 4.3) are displayed below.

TT_system_Nminus_GaN.m

```
%%%%%%%%%%%%%%%%%%%%%%%%%%%%%%%%%%%%%%%%%%%%%%%%%%%%
%%%%%%%%%%%%%%%%---TT system---%%%%%%%%%%%%%%%%
%%%%%%%%%%%%%%%%---N- GaN---%%%%%%%%%%%%%%%%
%%%%%%%%%%%%%%%%%%%%%%%%%%%%%%%%%%%%%%%%%%%%%%%%%%%%

%%%-----------------------------------------------------------%%%
% The following script compares THz time-domain
% spectroscopy measurements performed on an N- GaN sample
% without a 2DEG and on an N- GaN/AlN sample with a 2DEG.
% Measurements are performed using the TT system.
%%%-----------------------------------------------------------%%%

%%%%%%%%-----Clear environment-----%%%%%%
clear
clc
close all
%%%%%%%%-----End sub-----%%%%%%

%%%%%%%%-----Define parameters-----%%%%%%
L = 281;   %Number of data points
NFFT = 2^nextpow2(1000);   %length of Fourier Transform
dt=0.042;   %time step in picoseconds
f = 1/2/dt*linspace(0,1,NFFT/2+1);   %frequency
file1='modulation.xlsx';   %Excel file name
sheet_name_td='td_TT_system_N-_GaN';   %time domain sheet name
sheet_name_fd='fd_TT_system_N-_GaN';   %frequency domain sheet name
%%%%%%%%-----End sub-----%%%%%%

%%%%%%%%-----Import text files-----%%%%%%
s1 = 'TT_system_N-_GaN_with_2DEG_march_20.txt';
s2 = 'TT_system_N-_GaN_without_2DEG_march_20.txt';
%%%%%%%%-----End sub-----%%%%%%
```

```
%%%%%%%%-----time domain signals-----%%%%%%
y1=dlmread(s1, '\t', 'A1..J281');
y2=dlmread(s2, '\t', 'A1..J281');
%%%%%%%%-----End sub-----%%%%%%

%%%%%%%%-----Export time domain signals-----%%%%%%
warning('off','MATLAB:xlswrite:AddSheet')

xlswrite(file1,{'time'},sheet_name_td,'A1');
xlswrite(file1,{'N- GaN with 2DEG'},sheet_name_td,'B1');
xlswrite(file1,y1,sheet_name_td,'A2');

xlswrite(file1,{'time'},sheet_name_td,'K1');
xlswrite(file1,{'N- GaN without 2DEG'},sheet_name_td,'L1');
xlswrite(file1,y2,sheet_name_td,'K2');
%%%%%%%%-----End sub-----%%%%%%

%%%%%%%%-----Fourier Transform signals-----%%%%%%
aa=9;   %number of measurements (for N- GaN with 2DEG)
Y1=zeros(NFFT,aa);
for ii=1:aa
    Y1(:,ii) = fft(y1(:,ii+1),NFFT);   %N- GaN with 2DEG
end

aa=9;   %number of measurements (for N- GaN without 2DEG)
Y2=zeros(NFFT,aa);
for ii=1:aa
    Y2(:,ii) = fft(y2(:,ii+1),NFFT);   %N- GaN without 2DEG
end
%%%%%%%%-----End sub-----%%%%%%

%%%%%%%%-----Export Fourier Transform amplitude-----%%%%%%
xlswrite(file1,{'frequency'},sheet_name_fd,'A1');
xlswrite(file1,f(:),sheet_name_fd,'A2');
xlswrite(file1,{'N- GaN with 2DEG'},sheet_name_fd,'B1');
xlswrite(file1,abs(Y1(1:NFFT/2+1,:)),sheet_name_fd,'B2');

xlswrite(file1,{'frequency'},sheet_name_fd,'K1');
xlswrite(file1,f(:),sheet_name_fd,'K2');
xlswrite(file1,{'N- GaN without 2DEG'},sheet_name_fd,'L1');
xlswrite(file1,abs(Y2(1:NFFT/2+1,:)),sheet_name_fd,'L2');
%%%%%%%%-----End sub-----%%%%%%
```

TT_system_Nplus_GaN.m

```
%%%%%%%%%%%%%%%%%%%%%%%%%%%%%%%%%%%%%%%%%%%%%%%%
%%%%%%%%%%%%%%%---TT system---%%%%%%%%%%%%%%%%%
%%%%%%%%%%%%%%%---N+ GaN---%%%%%%%%%%%%%%%%%%%%
%%%%%%%%%%%%%%%%%%%%%%%%%%%%%%%%%%%%%%%%%%%%%%%%

%%%-------------------------------------------------------%%%
% The following script compares THz time-domain
```

```
% spectroscopy measurements performed on an N+ GaN sample
% without a 2DEG and on an N+ GaN/AlN sample with a 2DEG.
% Measurements are performed using the TT system.
%%%-------------------------------------------------------%%%

%%%%%%%%-----Clear environment-----%%%%%%
clear
clc
close all
%%%%%%%%-----End sub-----%%%%%%

%%%%%%%%-----Define parameters-----%%%%%%
L = 281;   %Number of data points
NFFT = 2^nextpow2(1000);   %length of Fourier Transform
dt=0.042;   %time step in picoseconds
f = 1/2/dt*linspace(0,1,NFFT/2+1);   %frequency
file1='modulation.xlsx';   %Excel file name
sheet_name_td='td_TT_system_N+_GaN';   %time domain sheet name
sheet_name_fd='fd_TT_system_N+_GaN';   %frequency domain sheet name
%%%%%%%%-----End sub-----%%%%%%

%%%%%%%%-----Import text files-----%%%%%%
s1 = 'TT_system_N+_GaN_with_2DEG_march_20.txt';
s2 = 'TT_system_N+_GaN_without_2DEG_march_20.txt';
%%%%%%%%-----End sub-----%%%%%%

%%%%%%%%-----time domain signals-----%%%%%%
y1=dlmread(s1, '\t', 'A1..I281');
y2=dlmread(s2, '\t', 'A1..J281');
%%%%%%%%-----End sub-----%%%%%%

%%%%%%%%-----Export time domain signals-----%%%%%%
warning('off','MATLAB:xlswrite:AddSheet')

xlswrite(file1,{'time'},sheet_name_td,'A1');
xlswrite(file1,{'N+ GaN with 2DEG'},sheet_name_td,'B1');
xlswrite(file1,y1,sheet_name_td,'A2');

xlswrite(file1,{'time'},sheet_name_td,'J1');
xlswrite(file1,{'N+ GaN without 2DEG'},sheet_name_td,'K1');
xlswrite(file1,y2,sheet_name_td,'J2');
%%%%%%%%-----End sub-----%%%%%%

%%%%%%%%-----FT of signals-----%%%%%%
aa=8;   %number of measurements (for N+ GaN with 2DEG)
Y1=zeros(NFFT,aa);
for ii=1:aa
    Y1(:,ii) = fft(y1(:,ii+1),NFFT);   %N+ GaN with 2DEG
end

aa=9;   %number of measurements (for N+ GaN without 2DEG)
Y2=zeros(NFFT,aa);
for ii=1:aa
    Y2(:,ii) = fft(y2(:,ii+1),NFFT);   %N+ GaN without 2DEG
end
```

```
%%%%%%%%-----End sub-----%%%%%%

%%%%%%%%-----Export Fourier Transform signal amplitude-----%%%%%%
xlswrite(file1,{'frequency'},sheet_name_fd,'A1');
xlswrite(file1,f(:),sheet_name_fd,'A2');
xlswrite(file1,{'N+ GaN with 2DEG'},sheet_name_fd,'B1');
xlswrite(file1,abs(Y1(1:NFFT/2+1,:)),sheet_name_fd,'B2');

xlswrite(file1,{'frequency'},sheet_name_fd,'J1');
xlswrite(file1,f(:),sheet_name_fd,'J2');
xlswrite(file1,{'N+ GaN without 2DEG'},sheet_name_fd,'K1');
xlswrite(file1,abs(Y2(1:NFFT/2+1,:)),sheet_name_fd,'K2');
%%%%%%%%-----End sub-----%%%%%%
```

Zomega.m

```
%%%%%%%%%%%%%%%%%%%%%%%%%%%%%%%%%%%%%%%%%%%%%%%%%%%%
%%%%%%%%%%%%%%%%---Zomega---%%%%%%%%%%%%%%%%%
%%%%%%%%%%%%%%%%%%%%%%%%%%%%%%%%%%%%%%%%%%%%%%%%%%%%

%%%-----------------------------------------------------------%%%
% The following script compares THz time-domain
% spectroscopy measurements performed on an N- GaN sample
% without a 2DEG and on an N- GaN/AlN sample with a 2DEG.
% This script also compares THz time-domain spectroscopy
% measurements performed on an N+ GaN sample without a 2DEG
% and on an N+ GaN/AlN sample with a 2DEG. Measurements
% are performed using Zomega's system.
%%%-----------------------------------------------------------%%%

%%%%%%%%-----Clear environment-----%%%%%%
clear
clc
close all
%%%%%%%%-----End sub-----%%%%%%

%%%%%%%%-----Define parameters-----%%%%%%
L = 1939;   %Number of data points
NFFT = 2^nextpow2(L);   %length of Fourier Transform
dt=0.05524655;   %time step in picoseconds
f = 1/2/dt*linspace(0,1,NFFT/2+1);    %frequency
file1='modulation.xlsx';   %Excel file name
%%%%%%%%-----End sub-----%%%%%%

%%%%%%%%-----Import text files-----%%%%%%
s1 = 'Zomega_N-_GaN_with_2DEG.txt';
s2 = 'Zomega_N-_GaN_without_2DEG.txt';
s3 = 'Zomega_N+_GaN_with_2DEG.txt';
s4 = 'Zomega_N+_GaN_without_2DEG.txt';
s5 = 'Zomega_free_space.txt';
%%%%%%%%-----End sub-----%%%%%%

%%%%%%%%-----time domain signals-----%%%%%%
y1=dlmread(s1, '\t', 'B1..C1939');
```

```
y2=dlmread(s2, '\t', 'B1..C1939');
y3=dlmread(s3, '\t', 'B1..C1939');
y4=dlmread(s4, '\t', 'B1..C1939');
y5=dlmread(s5, '\t', 'B1..C1939');
%%%%%%%%-----End sub-----%%%%%%

%%%%%%%%-----Export time domain signals-----%%%%%%
warning('off','MATLAB:xlswrite:AddSheet')
xlswrite(file1,{'time'},'td_Zomega','A1');
xlswrite(file1,y1(:,1),'td_Zomega','A2');
xlswrite(file1,{'N- GaN with 2DEG'},'td_Zomega','B1');
xlswrite(file1,y1(:,2),'td_Zomega','B2');
xlswrite(file1,{'N- GaN without 2DEG'},'td_Zomega','C1');
xlswrite(file1,y2(:,2),'td_Zomega','C2');
xlswrite(file1,{'N+ GaN with 2DEG'},'td_Zomega','D1');
xlswrite(file1,y3(:,2),'td_Zomega','D2');
xlswrite(file1,{'N+ GaN without 2DEG'},'td_Zomega','E1');
xlswrite(file1,y4(:,2),'td_Zomega','E2');
%%%%%%%%-----End sub-----%%%%%%

%%%%%%%%-----cut-off time domain signals-----%%%%%%
y1(1075:L,2)=0;
y2(1075:L,2)=0;
y3(1075:L,2)=0;
y4(1075:L,2)=0;
y5(1080:L,2)=0;
%%%%%%%%----- End sub-----%%%%%%

%%%%%%%%-----FT of signals-----%%%%%%
Y1 = fft(y1(1:L,2),NFFT);   %N- GaN with 2DEG
Y2 = fft(y2(1:L,2),NFFT);   %N- GaN without 2DEG
Y3 = fft(y3(1:L,2),NFFT);   %N+ GaN with 2DEG
Y4 = fft(y4(1:L,2),NFFT);   %N+ GaN without 2DEG
Y5 = fft(y5(1:L,2),NFFT);   %free space
%%%%%%%%-----End sub-----%%%%%%

%%%%%%%%-----Relative signals-----%%%%%%
Yrel_1=Y1(:)./Y5(:);
Yrel_1(:,1)=real(Yrel_1(:,1))-i*imag(Yrel_1(:,1));
Yrel_2=Y2(:)./Y5(:);
Yrel_2(:,1)=real(Yrel_2(:,1))-i*imag(Yrel_2(:,1));
Yrel_3=Y3(:)./Y5(:);
Yrel_3(:,1)=real(Yrel_3(:,1))-i*imag(Yrel_3(:,1));
Yrel_4=Y4(:)./Y5(:);
Yrel_4(:,1)=real(Yrel_4(:,1))-i*imag(Yrel_4(:,1));
%%%%%%%%-----End sub-----%%%%%%

%%%%%%%%-----Export FT signal amplitude-----%%%%%%
xlswrite(file1,{'frequency'},'fd_Zomega','A1');
xlswrite(file1,f(:),'fd_Zomega','A2');
xlswrite(file1,{'N- GaN with 2DEG'},'fd_Zomega','B1');
xlswrite(file1,abs(Yrel_1(1:NFFT/2+1)),'fd_Zomega','B2');
xlswrite(file1,{'N- GaN without 2DEG'},'fd_Zomega','C1');
xlswrite(file1,abs(Yrel_2(1:NFFT/2+1)),'fd_Zomega','C2');
xlswrite(file1,{'N+ GaN with 2DEG'},'fd_Zomega','D1');
xlswrite(file1,abs(Yrel_3(1:NFFT/2+1)),'fd_Zomega','D2');
```

```
xlswrite(file1,{'N+ GaN without 2DEG'},'fd_Zomega','E1');
xlswrite(file1,abs(Yrel_4(1:NFFT/2+1)),'fd_Zomega','E2');
%%%%%%%%-----End sub-----%%%%%%

%%%%%%%%-----Export FT signal phase-----%%%%%%
xlswrite(file1, ...
{'phase(N- GaN with 2DEG)-phase(N- GaN without 2DEG)'}, ...
'fd_Zomega', 'F1');
xlswrite(file1, ...
phase(Yrel_1(1:NFFT/2+1))-phase(Yrel_2(1:NFFT/2+1)), ...
'fd_Zomega', 'F2');
%%%%%%%%-----End sub-----%%%%%%
```

TA_system_transmission.m

```
%%%%%%%%%%%%%%%%%%%%%%%%%%%%%%%%%%%%%%%%%%%%%%%%%%%%
%%%%%%%%%%%%%%%---TA system---%%%%%%%%%%%%%%%
%%%%%%%%%%%%%%%---transmission---%%%%%%%%%%%
%%%%%%%%%%%%%%%%%%%%%%%%%%%%%%%%%%%%%%%%%%%%%%%%%%%%

%%%-----------------------------------------------------------%%%
% The following script compares THz time-domain
% spectroscopy measurements performed on an N- GaN sample
% without a 2DEG and on an N- GaN/AlN sample with a 2DEG.
% Transmission experiments are performed (at normal
% incidence) using the TA system.
%%%-----------------------------------------------------------%%%

%%%%%%%%-----Clear environment-----%%%%%%
clear
clc
close all
%%%%%%%%-----End sub-----%%%%%%

%%%%%%%%-----Define parameters-----%%%%%%
L = 200;   %Number of data points
NFFT = 2^nextpow2(1000);   %length of Fourier Transform
dt=0.08;   %time step in picoseconds
f = 1/2/dt*linspace(0,1,NFFT/2+1);   %frequency
file1='modulation.xlsx';   %Excel file name
sheet_name_td='td_TA_system_transmission';  %time domain sheet name
%%%%%%%%-----End sub-----%%%%%%

%%%%%%%%-----Import text files-----%%%%%%
s1 = 'TA_system_N-_GaN_with_2DEG_transmission.txt';
s2 = 'TA_system_N-_GaN_without_2DEG_transmission.txt';
%%%%%%%%-----End sub-----%%%%%%

%%%%%%%%-----time domain signals-----%%%%%%
y1=dlmread(s1, '\t', 'A1..AE200');
y2=dlmread(s2, '\t', 'A1..AE200');
%%%%%%%%-----End-----%%%%%%

%%%%%%%%-----Export time domain signals-----%%%%%%
```

```
warning('off','MATLAB:xlswrite:AddSheet')

xlswrite(file1,{'time'},sheet_name_td,'A1');
xlswrite(file1,{'N- GaN with 2DEG_transmission'}, ...
sheet_name_td,'B1');
xlswrite(file1,y1,sheet_name_td,'A2');

xlswrite(file1,{'time'},sheet_name_td,'AF1');
xlswrite(file1,{'N- GaN without 2DEG_transmission'}, ...
sheet_name_td,'AG1');
xlswrite(file1,y2,sheet_name_td,'AF2');
%%%%%%%%-----End-----%%%%%%
```

TA_system_reflection.m

```
%%%%%%%%%%%%%%%%%%%%%%%%%%%%%%%%%%%%%%%%%%%%%%%%%%%%
%%%%%%%%%%%%%%%%---TA system---%%%%%%%%%%%%%%%%
%%%%%%%%%%%%%%%%---reflection---%%%%%%%%%%%%
%%%%%%%%%%%%%%%%%%%%%%%%%%%%%%%%%%%%%%%%%%%%%%%%%%%%

%%%-----------------------------------------------------------%%%
% The following script compares THz time-domain
% spectroscopy measurements performed on an N- GaN sample
% without a 2DEG and on an N- GaN/AlN sample with a 2DEG.
% Reflection experiments are performed (at 45 degrees)
% using the TA system.
%%%-----------------------------------------------------------%%%

%%%%%%%%-----Clear environment-----%%%%%%
clear
clc
close all
%%%%%%%%-----End sub-----%%%%%%

%%%%%%%%-----Define parameters-----%%%%%%
L = 120;    %Number of data points
NFFT = 2^nextpow2(1000);    %length of Fourier Transform
dt=0.08;    %time step in picoseconds
f = 1/2/dt*linspace(0,1,NFFT/2+1);    %frequency
file1='modulation.xlsx';    %Excel file name
sheet_name_td='td_TA_system_reflection';    %time domain sheet name
%%%%%%%%-----End sub-----%%%%%%

%%%%%%%%-----Import text files-----%%%%%%
s1 = 'TA_system_N-_GaN_with_2DEG_reflection.txt';
s2 = 'TA_system_N-_GaN_without_2DEG_reflection.txt';
%%%%%%%%-----End sub-----%%%%%%

%%%%%%%%-----time domain signals-----%%%%%%
y1=dlmread(s1, '\t', 'A1..AE120');
y2=dlmread(s2, '\t', 'A1..AE120');
%%%%%%%%-----End sub-----%%%%%%
```

```
%%%%%%%%-----Export time domain signals-----%%%%%%
warning('off','MATLAB:xlswrite:AddSheet')

xlswrite(file1,{'time'},sheet_name_td,'A1');
xlswrite(file1,{'N- GaN with 2DEG_reflection'},sheet_name_td,'B1');
xlswrite(file1,y1,sheet_name_td,'A2');

xlswrite(file1,{'time'},sheet_name_td,'AF1');
xlswrite(file1,{'N- GaN without 2DEG_reflection'}, ...
sheet_name_td,'AG1');
xlswrite(file1,y2,sheet_name_td,'AF2');
%%%%%%%%-----End sub-----%%%%%%
```

Appendix B: MATLAB Analysis of the Sapphire THz-TDS Measurements

The MATLAB files used to analyse the measurements performed on the bare sapphire wafer (discussed in section 4.4.1) are displayed below. The three script files use the function called SAPPHIRE_REFRACTIVE_INDEX.m to determine the sapphire complex refractive index.

TT_system_sapphire.m

```
%%%%%%%%%%%%%%%%%%%%%%%%%%%%%%%%%%%%%%%%%%%%%%%%%%%%
%%%%%%%%%%%%%%%---TT system---%%%%%%%%%%%%%%%
%%%%%%%%%%%%%%%---Sapphire---%%%%%%%%%%%%%%%
%%%%%%%%%%%%%%%%%%%%%%%%%%%%%%%%%%%%%%%%%%%%%%%%%%%%

%%%-----------------------------------------------------------%%%
% The following script outputs the THz time-domain traces
% obtained by performing THz time-domain spectroscopy
% measurements on sapphire. The Fourier Transform of the
% time-domain traces are obtained and used to determine the
% sapphire refractive index. The experimental data is
% obtained using the TT system.
%%%-----------------------------------------------------------%%%

%%%%%%%%-----Clear environment-----%%%%%%
clear
clc
close all
%%%%%%%%-----End sub-----%%%%%%

%%%%%%%%-----Define parameters-----%%%%%%
```

```
L = 281;   %Number of data points
NFFT = 2^nextpow2(1000);   %length of Fourier Transform
dt=0.042;   %time step in picoseconds
f = 1/2/dt*linspace(0,1,NFFT/2+1);   %frequency
file1='refractive_index.xlsx';   %Excel file name
%%%%%%%%-----End sub-----%%%%%%

%%%%%%%%-----Import text files-----%%%%%%
s1 = 'TT_system_sapphire_one.txt';
s2 = 'TT_system_free_space_one.txt';
%%%%%%%%-----End sub-----%%%%%%

%%%%%%%%-----time domain signals-----%%%%%%
y1=dlmread(s1, '\t', 'A1..B281');
y2=dlmread(s2, '\t', 'A1..B281');
%%%%%%%%-----End sub-----%%%%%%

%%%%%%%%-----Export FULL time domain signals-----%%%%%%
warning('off','MATLAB:xlswrite:AddSheet')
aa=0.04;   %vertical shift in sapphire trace
xlswrite(file1,{'time'},'sap_td_full','A1');
xlswrite(file1,y1(:,1),'sap_td_full','A2');
xlswrite(file1,{'TT_system_sapphire'},'sap_td_full','B1');
xlswrite(file1,y1(:,2)+aa,'sap_td_full','B2');
xlswrite(file1,{'TT_system_free space'},'sap_td_full','C1');
xlswrite(file1,y2(:,2),'sap_td_full','C2');
%%%%%%%%-----End sub-----%%%%%%

%%%%%%%%-----cut-off time domain signals-----%%%%%%
y1(281:L,2)=0;
y2(211:L,2)=0;
%%%%%%%%-----End-----%%%%%%

%%%%%%%%-----Export CUT-OFF time domain signals-----%%%%%%
xlswrite(file1,{'time'},'sap_td_co','A1');
xlswrite(file1,y1(:,1),'sap_td_co','A2');
xlswrite(file1,{'TT_system_sapphire'},'sap_td_co','B1');
xlswrite(file1,y1(:,2)+aa,'sap_td_co','B2');
xlswrite(file1,{'TT_system_free space'},'sap_td_co','C1');
xlswrite(file1,y2(:,2),'sap_td_co','C2');
%%%%%%%%-----End-----%%%%%%

%%%%%%%%-----FT of signals-----%%%%%%
Y1 = fft(y1(1:L,2),NFFT);   %sapphire
Y2 = fft(y2(1:L,2),NFFT);   %free space
%%%%%%%%-----End sub-----%%%%%%

%%%%%%%%-----Relative signal-----%%%%%%
Yrel=Y1(1:NFFT/2+1)./Y2(1:NFFT/2+1);
Yrel(:,1)=real(Yrel(:,1))-i*imag(Yrel(:,1));
%%%%%%%%-----End sub-----%%%%%%

%%%%%%%%-----Export FT-----%%%%%%
xlswrite(file1,{'frequency'},'sap_fd','A1');
xlswrite(file1,f(:),'sap_fd','A2');
```

```
xlswrite(file1,{'TT_system_amplitude'},'sap_fd','B1');
xlswrite(file1,abs(Yrel(:)),'sap_fd','B2');
xlswrite(file1,{'TT_system_phase'},'sap_fd','C1');
xlswrite(file1,unwrap(angle(Yrel(:))),'sap_fd','C2')
%%%%%%%%-----End-----%%%%%%

%%%%%%%%-----Find refractive index-----%%%%%%
V=90;   %number of points that are solved for
d2=435e-6;   %thickness of sapphire
lower_limit=3-0.1*i;   %lower limit of solver
upper_limit=3.3+0.1*i;   %upper limit of solver

Nf=SAPPHIRE_REFRACTIVE_INDEX(V, d2, lower_limit, upper_limit, ...
f, Yrel);
%%%%%%%%-----End sub-----%%%%%%

%%%%%%%%-----Export refractive index-----%%%%%%
xlswrite(file1,{'frequency'},'sap_RI','A1');
xlswrite(file1,f(1:V)','sap_RI','A2');
xlswrite(file1,{'n_TT_system'},'sap_RI','B1');
xlswrite(file1,real(Nf(1:V)),'sap_RI','B2');
xlswrite(file1,{'K_TT_system'},'sap_RI','C1');
xlswrite(file1,imag(Nf(1:V)),'sap_RI','C2');
%%%%%%%%-----End-----%%%%%%
```

Zomega_system_sapphire.m

```
%%%%%%%%%%%%%%%%%%%%%%%%%%%%%%%%%%%%%%%%%%%%%%%%%%%%
%%%%%%%%%%%%%%%---Zomega---%%%%%%%%%%%%%%%
%%%%%%%%%%%%%%%---Sapphire---%%%%%%%%%%%%%%%
%%%%%%%%%%%%%%%%%%%%%%%%%%%%%%%%%%%%%%%%%%%%%%%%%%%%

%%%-----------------------------------------------------------%%%
% The following script outputs the THz time-domain traces
% obtained by performing THz time-domain spectroscopy
% measurements on sapphire. The Fourier Transform of the
% time-domain traces are obtained and used to determine
% the sapphire refractive index. The experimental data is
% obtained using Zomega's system.
%%%-----------------------------------------------------------%%%

%%%%%%%%-----Clear environment-----%%%%%%
clear
clc
close all
%%%%%%%%-----End sub-----%%%%%%

%%%%%%%%-----Define parameters-----%%%%%%
L = 1939;   %Number of data points
NFFT = 2^nextpow2(L);   %length of Fourier Transform
dt=0.05524655;   %time step in picoseconds
f = 1/2/dt*linspace(0,1,NFFT/2+1);   %frequency
file1='refractive_index.xlsx';   %Excel file name
```

```
%%%%%%%%-----End sub-----%%%%%%

%%%%%%%%-----Import text files-----%%%%%%
s1 = 'Zomega_sapphire.txt';
s2 = 'Zomega_free_space.txt';
%%%%%%%%-----End sub-----%%%%%%

%%%%%%%%-----time domain signals-----%%%%%%
y1=dlmread(s1, '\t', 'B1..C1939');
y2=dlmread(s2, '\t', 'B1..C1939');
%%%%%%%%-----End sub-----%%%%%%

%%%%%%%%-----Export FULL time domain signals-----%%%%%%
warning('off','MATLAB:xlswrite:AddSheet')
aa=500;   %vertical shift in sapphire trace
xlswrite(file1,{'time'},'sap_td_full','D1');
xlswrite(file1,y1(:,1),'sap_td_full','D2');
xlswrite(file1,{'Zomega_sapphire'},'sap_td_full','E1');
xlswrite(file1,y1(:,2)+aa,'sap_td_full','E2');
xlswrite(file1,{'Zomega_free space'},'sap_td_full','F1');
xlswrite(file1,y2(:,2),'sap_td_full','F2');
%%%%%%%%-----End sub-----%%%%%%

%%%%%%%%-----cutt-off time domain signals-----%%%%%%
y1(1080:L,2)=0;
y2(1080:L,2)=0;
%%%%%%%%-----End sub-----%%%%%%

%%%%%%%%-----Export CUT-OFF time domain signals-----%%%%%%
xlswrite(file1,{'time'},'sap_td_co','D1');
xlswrite(file1,y1(:,1),'sap_td_co','D2');
xlswrite(file1,{'Zomega_sapphire'},'sap_td_co','E1');
xlswrite(file1,y1(:,2)+aa,'sap_td_co','E2');
xlswrite(file1,{'Zomega_free space'},'sap_td_co','F1');
xlswrite(file1,y2(:,2),'sap_td_co','F2');
%%%%%%%%-----End-----%%%%%%

%%%%%%%%-----FT of signals-----%%%%%%
Y1 = fft(y1(1:L,2),NFFT);      %sapphire
Y2 = fft(y2(1:L,2),NFFT);      %free space
%%%%%%%%-----End-----%%%%%%

%%%%%%%%-----Relative signal-----%%%%%%
Yrel=Y1(1:NFFT/2+1)./Y2(1:NFFT/2+1);
Yrel(:,1)=real(Yrel(:,1))-i*imag(Yrel(:,1));
%%%%%%%%-----End-----%%%%%%

%%%%%%%%-----Export FT-----%%%%%%
xlswrite(file1,{'frequency'},'sap_fd','D1');
xlswrite(file1,f(:),'sap_fd','D2');
xlswrite(file1,{'Zomega_amplitude'},'sap_fd','E1');
xlswrite(file1,abs(Yrel(:)),'sap_fd','E2');
xlswrite(file1,{'Zomega_phase'},'sap_fd','F1');
xlswrite(file1,unwrap(angle(Yrel(:))),'sap_fd','F2')
%%%%%%%%-----End-----%%%%%%
```

```
%%%%%%%%-----Find refractive index-----%%%%%%
V=230;   %number of points that are solved for
d2=435e-6;   %thickness of sapphire
lower_limit=2.8-0.1*i;   %lower limit of solver
upper_limit=3.3+1*i;   %upper limit of solver

Nf=SAPPHIRE_REFRACTIVE_INDEX(V, d2, lower_limit, upper_limit, ...
f, Yrel);
%%%%%%%%-----End sub-----%%%%%%

%%%%%%%%-----Export refractive index-----%%%%%%
xlswrite(file1,{'frequency'},'sap_RI','D1');
xlswrite(file1,f(1:V)','sap_RI','D2');
xlswrite(file1,{'n_Zomega'},'sap_RI','E1');
xlswrite(file1,real(Nf(1:V)),'sap_RI','E2');
xlswrite(file1,{'K_Zomega'},'sap_RI','F1');
xlswrite(file1,imag(Nf(1:V)),'sap_RI','F2');
%%%%%%%%-----End sub-----%%%%%%
```

TA_system_sapphire.m

```
%%%%%%%%%%%%%%%%%%%%%%%%%%%%%%%%%%%%%%%%%%%%%%%%%%%%%%%%
%%%%%%%%%%%%%%%---TA system---%%%%%%%%%%%%%%%
%%%%%%%%%%%%%%%---Sapphire---%%%%%%%%%%%%%%%
%%%%%%%%%%%%%%%%%%%%%%%%%%%%%%%%%%%%%%%%%%%%%%%%%%%%%%%%

%%%-----------------------------------------------------------%%%
% The following script outputs the THz time-domain traces
% obtained by performing THz time-domain spectroscopy
% measurements on sapphire. The Fourier Transform of the
% time-domain traces are obtained and used to determine the
% sapphire refractive index. The experimental data is
% obtained using the TA system.
%%%-----------------------------------------------------------%%%

%%%%%%%%-----Clear environment-----%%%%%%
clear
clc
close all
%%%%%%%%-----End sub-----%%%%%%

%%%%%%%%-----Define parameters-----%%%%%%
L = 150;   %Number of data points
NFFT = 2^nextpow2(1000);   %length of Fourier Transform
dt=0.08;   %time step in picoseconds
f = 1/2/dt*linspace(0,1,NFFT/2+1);   %frequency
file1='refractive_index.xlsx';   %Excel file name
%%%%%%%%-----End sub-----%%%%%%

%%%%%%%%-----Import text files-----%%%%%%
s1 = 'TA_system_sapphire.txt';
s2 = 'TA_system_free_space_sapphire.txt';
```

```
%%%%%%%%-----End sub-----%%%%%%

%%%%%%%%-----time domain signals-----%%%%%%
y1=dlmread(s1, '\t', 'A1..B150');
y2=dlmread(s2, '\t', 'A1..B150');
%%%%%%%%-----End sub-----%%%%%%

%%%%%%%%-----Export FULL time domain signals-----%%%%%%
warning('off','MATLAB:xlswrite:AddSheet')
aa=0.012;   %vertical shift in sapphire trace
xlswrite(file1,{'time'},'sap_td_full','G1');
xlswrite(file1,y1(:,1),'sap_td_full','G2');
xlswrite(file1,{'TA_system_sapphire'},'sap_td_full','H1');
xlswrite(file1,y1(:,2)+aa,'sap_td_full','H2');
xlswrite(file1,{'TA_system_free space'},'sap_td_full','I1');
xlswrite(file1,y2(:,2),'sap_td_full','I2');
%%%%%%%%-----End sub-----%%%%%%

%%%%%%%%-----cut-off time domain signals-----%%%%%%
y1(1:40,2)=0;
y2(1:1,2)=0;
y1(150:L,2)=0;
y2(110:L,2)=0;
%%%%%%%%-----End sub-----%%%%%%

%%%%%%%%-----Export CUT-OFF time domain signals-----%%%%%%
xlswrite(file1,{'time'},'sap_td_co','G1');
xlswrite(file1,y1(:,1),'sap_td_co','G2');
xlswrite(file1,{'TA_system_sapphire'},'sap_td_co','H1');
xlswrite(file1,y1(:,2)+aa,'sap_td_co','H2');
xlswrite(file1,{'TA_system_free space'},'sap_td_co','I1');
xlswrite(file1,y2(:,2),'sap_td_co','I2');
%%%%%%%%-----End-----%%%%%%

%%%%%%%%-----FT of signals-----%%%%%%
Y1 = fft(y1(1:L,2),NFFT);      %sapphire
Y2 = fft(y2(1:L,2),NFFT);      %free space
%%%%%%%%-----End-----%%%%%%

%%%%%%%%-----Relative signal-----%%%%%%
Yrel=Y1(1:NFFT/2+1)./Y2(1:NFFT/2+1);
Yrel(:,1)=real(Yrel(:,1))-i*imag(Yrel(:,1));
%%%%%%%%-----End sub-----%%%%%%

%%%%%%%%-----Export FT-----%%%%%%
xlswrite(file1,{'frequency'},'sap_fd','G1');
xlswrite(file1,f(:),'sap_fd','G2');
xlswrite(file1,{'TA_system_amplitude'},'sap_fd','H1');
xlswrite(file1,abs(Yrel(:)),'sap_fd','H2');
xlswrite(file1,{'TA_system_phase'},'sap_fd','I1');
xlswrite(file1,unwrap(angle(Yrel(:)))-2*pi,'sap_fd','I2')
%%%%%%%%-----End sub-----%%%%%%

%%%%%%%%-----Find refractive index-----%%%%%%
V=85;   %number of points that are solved for
```

```
d2=435e-6;   %thickness of sapphire
lower_limit=2.8-0.1*i;   %lower limit of solver
upper_limit=3.3+1*i;   %upper limit of solver

Nf=SAPPHIRE_REFRACTIVE_INDEX(V, d2, lower_limit, upper_limit, ...
f, Yrel);
%%%%%%%%-----End sub-----%%%%%%

%%%%%%%%-----Export refractive index-----%%%%%%
xlswrite(file1,{'frequency'},'sap_RI','G1');
xlswrite(file1,f(1:V)','sap_RI','G2');
xlswrite(file1,{'n_TA_system'},'sap_RI','H1');
xlswrite(file1,real(Nf(1:V)),'sap_RI','H2');
xlswrite(file1,{'K_TA_system'},'sap_RI','I1');
xlswrite(file1,imag(Nf(1:V)),'sap_RI','I2');
%%%%%%%%-----End-----%%%%%%
```

SAPPHIRE_REFRACTIVE_INDEX.m

```
function Nf = SAPPHIRE_REFRACTIVE_INDEX(V, d2, lower_limit, ...
upper_limit, f, Yrel)
%%%------------------------------------------------------------%%%
% The following code uses experimental data obtained by THz
% time-domain spectroscopy experiments (performed on a
% bare sapphire substrate) to determine the sapphire
% refractive index.
%
% Input parameters:
% -V is  the number of points that are solved for
% -d2 is the thickness of the sapphire wafer
% -lower limit is the minimum sapphire refractive index the
%  solver considers
% -upper limit is the maximum sapphire refractive index the
%  solver considers
% -f is the frequency of the radiation
% -Yrel is the experimental measurements
%
% Output parameter:
% -Nf is the vector containing the sapphire refractive index
%%%------------------------------------------------------------%%%

%%%%%%%%-----Define parameters-----%%%%%%
n1p=1;   %refractive index of air
syms n2p;
n3p=1;   %refractive index of air
c=299792458;   %speed of light in a vacuum
%%%%%%%%-----End sub-----%%%%%%

%%%%%%%%-----Find refractive index of SI GaN-----%%%%%%
Nf=zeros(V,1);
for ii=1:V
    fi=f(ii)*10^12;   %frequency
    w=2*pi*fi;   %angular frequency
    k0=w/c;   %free space wavevector
```

```
    k2=w/c*n2p;   %sapphire wavevector
    t12=2*n1p/(n1p+n2p);   %transmission from air to sapphire
    t23=2*n2p/(n2p+n3p);   %transmission from sapphire to air
    t=t12*t23*exp(i*k2*d2)/exp(i*k0*d2);   %trans. through sapphire

    n_temp=vpasolve(Yrel(ii)==t,n2p,[lower_limit upper_limit]);
    if length(n_temp)>0
        Nf(ii)=n_temp;
    end

end
%%%%%%%-----End sub-----%%%%%%

end
```

Appendix C: MATLAB Analysis of the GaN THz-TDS Measurements

The MATLAB files used to analyse the measurements performed on the GaN thin film samples (discussed in section 4.4.2) are displayed below. The three script files use the function called GAN_REFRACTIVE_INDEX.m to determine the GaN complex refractive index.

TT_system_GaN.m

```
%%%%%%%%%%%%%%%%%%%%%%%%%%%%%%%%%%%%%%%%%%%%%%%%%%%%
%%%%%%%%%%%%%%%%---TT system---%%%%%%%%%%%%%%%%
%%%%%%%%%%%%%%%%---GaN---%%%%%%%%%%%%%%%%%%%%%%
%%%%%%%%%%%%%%%%%%%%%%%%%%%%%%%%%%%%%%%%%%%%%%%%

%%%-----------------------------------------------------------%%%
% The following script outputs the THz time-domain traces
% obtained by performing THz time-domain spectroscopy
% measurements on GaN. The Fourier Transform of the
% time-domain traces are obtained and used to
% determine the GaN refractive index. Furthermore,
% the GaN relative% permittivity is determined and
% compared to the Drude model. The experimental data is
% obtained using the TT system.
%%%-----------------------------------------------------------%%%

%%%%%%%-----Clear environment-----%%%%%%
```

```
clear
clc
close all
%%%%%%%%-----End sub-----%%%%%%

%%%%%%%%-----Define parameters-----%%%%%%
L = 281;   %Number of data points
NFFT = 2^nextpow2(1000);   %length of Fourier Transform
dt=0.042;   %time step in picoseconds
f = 1/2/dt*linspace(0,1,NFFT/2+1);   %frequency
file1='refractive_index.xlsx';   %Excel file name
%%%%%%%%-----End sub-----%%%%%%

%%%%%%%%-----Import text files-----%%%%%%
s1 = 'TT_system_SI_GaN_two.txt';
s2 = 'TT_system_N-_GaN_two.txt';
s3 = 'TT_system_N+_GaN_two.txt';
s4 = 'TT_system_sapphire_two.txt';
%%%%%%%%-----End sub-----%%%%%%

%%%%%%%%-----time domain signals-----%%%%%%
y1=dlmread(s1, '\t', 'A1..B281');
y2=dlmread(s2, '\t', 'A1..B281');
y3=dlmread(s3, '\t', 'A1..B281');
y4=dlmread(s4, '\t', 'A1..B281');
%%%%%%%%-----End sub-----%%%%%%

%%%%%%%%-----Export FULL time domain signals-----%%%%%%
warning('off','MATLAB:xlswrite:AddSheet')
aa=0.045;   %vertical shift in SI GaN trace
bb=0.075;   %vertical shift in N- GaN trace
cc=0.1;   %vertical shift in N+ GaN trace
xlswrite(file1,{'time'},'GaN_td_full','A1');
xlswrite(file1,y1(:,1),'GaN_td_full','A2');
xlswrite(file1,{'TT_system_SI GaN'},'GaN_td_full','B1');
xlswrite(file1,y1(:,2)+aa,'GaN_td_full','B2');
xlswrite(file1,{'TT_system_n- GaN'},'GaN_td_full','C1');
xlswrite(file1,y2(:,2)+bb,'GaN_td_full','C2');
xlswrite(file1,{'TT_system_n+ GaN'},'GaN_td_full','D1');
xlswrite(file1,y3(:,2)+cc,'GaN_td_full','D2');
xlswrite(file1,{'TT_system_sapphire'},'GaN_td_full','E1');
xlswrite(file1,y4(:,2),'GaN_td_full','E2');
%%%%%%%%-----End-----%%%%%%

%%%%%%%%-----cut-off time domain signals-----%%%%%%
y1(281:L,2)=0;
y2(281:L,2)=0;
y3(281:L,2)=0;
y4(281:L,2)=0;
%%%%%%%%-----End-----%%%%%%

%%%%%%%%-----Export CUT-OFF time domain signals-----%%%%%%
warning('off','MATLAB:xlswrite:AddSheet')
xlswrite(file1,{'time'},'GaN_td_co','A1');
xlswrite(file1,y1(:,1),'GaN_td_co','A2');
xlswrite(file1,{'TT_system_SI GaN'},'GaN_td_co','B1');
```

```
xlswrite(file1,y1(:,2)+aa,'GaN_td_co','B2');
xlswrite(file1,{'TT_system_n- GaN'},'GaN_td_co','C1');
xlswrite(file1,y2(:,2)+bb,'GaN_td_co','C2');
xlswrite(file1,{'TT_system_n+ GaN'},'GaN_td_co','D1');
xlswrite(file1,y3(:,2)+cc,'GaN_td_co','D2');
xlswrite(file1,{'TT_system_sapphire'},'GaN_td_co','E1');
xlswrite(file1,y4(:,2),'GaN_td_co','E2');
%%%%%%%%-----End-----%%%%%%

%%%%%%%%-----FT of signals-----%%%%%%
Y1 = fft(y1(1:L,2),NFFT);    %SI GaN
Y2 = fft(y2(1:L,2),NFFT);    %N- GaN
Y3 = fft(y3(1:L,2),NFFT);    %N+ GaN
Y4 = fft(y4(1:L,2),NFFT);    %sapphire
%%%%%%%%-----End-----%%%%%%

%%%%%%%%-----Relative signals-----%%%%%%
Yrel_1=Y1(1:NFFT/2+1)./Y4(1:NFFT/2+1);
Yrel_1(:,1)=real(Yrel_1(:,1))-i*imag(Yrel_1(:,1));
Yrel_2=Y2(1:NFFT/2+1)./Y4(1:NFFT/2+1);
Yrel_2(:,1)=real(Yrel_2(:,1))-i*imag(Yrel_2(:,1));
Yrel_3=Y3(1:NFFT/2+1)./Y4(1:NFFT/2+1);
Yrel_3(:,1)=real(Yrel_3(:,1))-i*imag(Yrel_3(:,1));
%%%%%%%%-----End-----%%%%%%

%%%%%%%%-----Export FT amplitude-----%%%%%%
xlswrite(file1,{'frequency'},'GaN_fd_amp','A1');
xlswrite(file1,f(:),'GaN_fd_amp','A2');
xlswrite(file1,{'TT_system_amp_SI'},'GaN_fd_amp','B1');
xlswrite(file1,abs(Yrel_1(:)),'GaN_fd_amp','B2');
xlswrite(file1,{'TT_system_amp_n-'},'GaN_fd_amp','C1');
xlswrite(file1,abs(Yrel_2(:)),'GaN_fd_amp','C2');
xlswrite(file1,{'TT_system_amp_n+'},'GaN_fd_amp','D1');
xlswrite(file1,abs(Yrel_3(:)),'GaN_fd_amp','D2');
%%%%%%%%-----End-----%%%%%%

%%%%%%%%-----Export FT phase-----%%%%%%
xlswrite(file1,{'frequency'},'GaN_fd_phase','A1');
xlswrite(file1,f(:),'GaN_fd_phase','A2');
xlswrite(file1,{'TT_system_phase_SI'},'GaN_fd_phase','B1');
xlswrite(file1,unwrap(angle(Yrel_1(:))),'GaN_fd_phase','B2');
xlswrite(file1,{'TT_system_phase_n-'},'GaN_fd_phase','C1');
xlswrite(file1,unwrap(angle(Yrel_2(:))),'GaN_fd_phase','C2');
xlswrite(file1,{'TT_system_phase_n+'},'GaN_fd_phase','D1');
xlswrite(file1,unwrap(angle(Yrel_3(:))),'GaN_fd_phase','D2');
%%%%%%%%-----End-----%%%%%%

%%%%%%%%%%%
%%-SI GaN-%%
%%%%%%%%%%%

%%%%%%%%-----Find refractive index-----%%%%%%
V=90;       %number of points that are solved for
n3p=3.10;    %refractive index of sapphire
d2=5e-6;    %thickness of GaN
d3=419e-6;    %thickness of sapphire substrate on GaN sample
```

```
d3_ref=435e-6;   %thickness of bare sapphire wafer
lower_limit=zeros(V,1);
lower_limit(:)=1-1*i;   %lower limit of solver
upper_limit=zeros(V,1);
upper_limit(:)=10+10*i;   %upper limit of solver

Nf=GAN_REFRACTIVE_INDEX(V, n3p, d2, d3, d3_ref, ...
lower_limit, upper_limit, f, Yrel_1);
%%%%%%%%-----End sub-----%%%%%%

%%%%%%%%-----Export refractive index-----%%%%%%
xlswrite(file1,{'frequency'},'SI_GaN_RI','A1');
xlswrite(file1,f(1:V)','SI_GaN_RI','A2');
xlswrite(file1,{'n_TT_system'},'SI_GaN_RI','B1');
xlswrite(file1,real(Nf(1:V)),'SI_GaN_RI','B2');
xlswrite(file1,{'K_TT_system'},'SI_GaN_RI','C1');
xlswrite(file1,imag(Nf(1:V)),'SI_GaN_RI','C2');
%%%%%%%%-----End-----%%%%%%

%%%%%-----find relative permittivity-----%%%%%%
ERf=zeros(V,1);
for ii=1:V
    fi=f(ii)*10^12;   %frequency
    w=2*pi*fi;   %angular frequency
    ERf(ii) = Nf(ii)^2;   %GaN relative permittivity
end
%%%%%End sub%%%%%%

%%%%%%%%-----Export relative permittivity-----%%%%%%
xlswrite(file1,{'frequency'},'SI_GaN_RP','A1');
xlswrite(file1,f(1:V)','SI_GaN_RP','A2');
xlswrite(file1,{'eps_real_TT_system'},'SI_GaN_RP','B1');
xlswrite(file1,real(ERf(1:V)),'SI_GaN_RP','B2');
xlswrite(file1,{'eps_imag_TT_system'},'SI_GaN_RP','C1');
xlswrite(file1,imag(ERf(1:V)),'SI_GaN_RP','C2');
%%%%%%%%-----End sub-----%%%%%%

%%%%%-----find drude relative permittivity-----%%%%%%
eps_b=9.4+0*i;   %background relative permittivity
N_doping=10^21;   %GaN doping density
mobility=0.2;   %GaN electron mobility
eps0=8.854e-12;   %permittivity of free space
wp=sqrt(N_doping*(1.602e-19)^2/eps0/0.22/9.11e-31);   %plasma freq
tau=mobility*0.22*9.11e-31/1.602e-19;   %GaN time constant
DRUDE=zeros(V,1);

for ii=1:V
    fi=f(ii)*10^12;
    w=2*pi*fi;
    DRUDE(ii)=eps_b+i*wp^2*tau/w/(1-i*w*tau);
end
%%%%%-----End sub-----%%%%%%

%%%%%%%%-----Export drude relative permittivity----%%%%%%
xlswrite(file1,{'drude_real_TT_system'},'SI_GaN_RP','D1');
```

```
xlswrite(file1,real(DRUDE(1:V)),'SI_GaN_RP','D2');
xlswrite(file1,{'drude_imag_system'},'SI_GaN_RP','E1');
xlswrite(file1,imag(DRUDE(1:V)),'SI_GaN_RP','E2');
%%%%%%%%-----End sub-----%%%%%%

%%%%%%%%%%%
%%-N- GaN-%%
%%%%%%%%%%%

%%%%%%%%-----Find refractive index-----%%%%%%
V=90;      %number of points that are solved for
n3p=3.10;   %refractive index of sapphire
d2=5e-6;   %thickness of GaN
d3=435e-6;   %thickness of sapphire substrate on GaN sample
d3_ref=435e-6;   %thickness of bare sapphire wafer
lower_limit=zeros(V,1);
lower_limit(:)=1-1*i;   %lower limit of solver
upper_limit=zeros(V,1);
upper_limit(:)=30+30*i;   %upper limit of solver

Nf=GAN_REFRACTIVE_INDEX(V, n3p, d2, d3, d3_ref, ...
lower_limit, upper_limit, f, Yrel_2);
%%%%%%%%-----End sub-----%%%%%%

%%%%%%%%-----Export refractive index-----%%%%%%
xlswrite(file1,{'frequency'},'N-_GaN_RI','A1');
xlswrite(file1,f(1:V)','N-_GaN_RI','A2');
xlswrite(file1,{'n_TT_system'},'N-_GaN_RI','B1');
xlswrite(file1,real(Nf(1:V)),'N-_GaN_RI','B2');
xlswrite(file1,{'K_TT_system'},'N-_GaN_RI','C1');
xlswrite(file1,imag(Nf(1:V)),'N-_GaN_RI','C2');
%%%%%%%%-----End-----%%%%%%

%%%%%-----find relative permittivity-----%%%%%%
ERf=zeros(V,1);
for ii=1:V
    fi=f(ii)*10^12;
    w=2*pi*fi;
    ERf(ii) = Nf(ii)^2;
end
%%%%%-----End sub-----%%%%%%

%%%%%%%%-----Export relative permittivity-----%%%%%%
file1='REFRACTIVE_INDEX.xlsx';
xlswrite(file1,{'frequency'},'N-_GaN_RP','A1');
xlswrite(file1,f(1:V)','N-_GaN_RP','A2');
xlswrite(file1,{'epsr_real_TT_system'},'N-_GaN_RP','B1');
xlswrite(file1,real(ERf(1:V)),'N-_GaN_RP','B2');
xlswrite(file1,{'epsr_imag_TT_system'},'N-_GaN_RP','C1');
xlswrite(file1,imag(ERf(1:V)),'N-_GaN_RP','C2');
%%%%%%%%-----End-----%%%%%%

%%%%%-----find drude relative permittivity-----%%%%%%
eps_b=23.5+0*i;
N_doping=2.4e23;
```

```
mobility=0.05;
wp=sqrt(N_doping*(1.602e-19)^2/eps0/0.22/9.11e-31);
tau=mobility*0.22*9.11e-31/1.602e-19;
DRUDE=zeros(V,1);
for ii=1:V
    fi=f(ii)*10^12;
    w=2*pi*fi;
    DRUDE(ii)=eps_b+i*wp^2*tau/w/(1-i*w*tau);
end
%%%%-----End sub-----%%%%%

%%%%%%%-----Export drude relative permittivity----%%%%%
xlswrite(file1,{'drude_real_TT_system'},'N-_GaN_RP','D1');
xlswrite(file1,real(DRUDE(1:V)),'N-_GaN_RP','D2');
xlswrite(file1,{'drude_imag_TT_system'},'N-_GaN_RP','E1');
xlswrite(file1,imag(DRUDE(1:V)),'N-_GaN_RP','E2');
%%%%%%%-----End sub-----%%%%%

%%%%%%%%%%%
%%-N+ GaN-%%
%%%%%%%%%%%

%%%%%%%-----Find refractive index-----%%%%%
V=90;      %number of points that are solved for
n3p=3.10;   %refractive index of sapphire
d2=5e-6;   %thickness of GaN
d3=435e-6;   %thickness of sapphire substrate on GaN sample
d3_ref=435e-6;   %thickness of bare sapphire wafer
lower_limit=zeros(V,1);
lower_limit(:)=1-1*i;   %lower limit of solver
upper_limit=zeros(V,1);
upper_limit(:)=50+50*i;   %upper limit of solver

Nf=GAN_REFRACTIVE_INDEX(V, n3p, d2, d3, d3_ref, ...
lower_limit, upper_limit, f, Yrel_3);
%%%%%%%-----End sub-----%%%%%

%%%%%%%-----Export refractive index-----%%%%%
xlswrite(file1,{'frequency'},'N+_GaN_RI','A1');
xlswrite(file1,f(1:V)','N+_GaN_RI','A2');
xlswrite(file1,{'n_TT_system'},'N+_GaN_RI','B1');
xlswrite(file1,real(Nf(1:V)),'N+_GaN_RI','B2');
xlswrite(file1,{'K_TT_system'},'N+_GaN_RI','C1');
xlswrite(file1,imag(Nf(1:V)),'N+_GaN_RI','C2');
%%%%%%%-----End-----%%%%%

%%%%%find relative permitivity%%%%%
ERf=zeros(V,1);
for ii=1:V
    fi=f(ii)*10^12;
    w=2*pi*fi;
    ERf(ii) = Nf(ii)^2;
end
%%%%%End%%%%%
```

```
%%%%%%%%-----Export relative permittivity-----%%%%%%
xlswrite(file1,{'frequency'},'N+_GaN_RP','A1');
xlswrite(file1,f(1:V)','N+_GaN_RP','A2');
xlswrite(file1,{'epsr_real_TT_system'},'N+_GaN_RP','B1');
xlswrite(file1,real(ERf(1:V)),'N+_GaN_RP','B2');
xlswrite(file1,{'epsr_imag_TT_system'},'N+_GaN_RP','C1');
xlswrite(file1,imag(ERf(1:V)),'N+_GaN_RP','C2');
%%%%%%%%-----End sub-----%%%%%%

%%%%%find drude relative permittivity%%%%%%
eps_b=45+0*i;
N_doping=1.5e24;
mobility=0.05;
wp=sqrt(N_doping*(1.602e-19)^2/eps0/0.22/9.11e-31);
tau=mobility*0.22*9.11e-31/1.602e-19;
DRUDE=zeros(V,1);
for ii=1:V
    fi=f(ii)*10^12;
    w=2*pi*fi;
    DRUDE(ii)=eps_b+i*wp^2*tau/w/(1-i*w*tau);
end
%%%%%-----End sub-----%%%%%%

%%%%%%%%-----Export drude relative permittivity----%%%%%%
xlswrite(file1,{'drude_real_TT_system'},'N+_GaN_RP','D1');
xlswrite(file1,real(DRUDE(1:V)),'N+_GaN_RP','D2');
xlswrite(file1,{'drude_imag_TT_system'},'N+_GaN_RP','E1');
xlswrite(file1,imag(DRUDE(1:V)),'N+_GaN_RP','E2');
%%%%%%%%-----End sub-----%%%%%%
```

Zomega_system_GaN.m

```
%%%%%%%%%%%%%%%%%%%%%%%%%%%%%%%%%%%%%%%%%%%%%%%%%%%
%%%%%%%%%%%%%%%%---Zomega---%%%%%%%%%%%%%%%%
%%%%%%%%%%%%%%%%---GaN---%%%%%%%%%%%%%%%%%%%%
%%%%%%%%%%%%%%%%%%%%%%%%%%%%%%%%%%%%%%%%%%%%%%%%%%%

%%%-----------------------------------------------------------%%%
% The following script outputs the THz time-domain traces
% obtained by performing THz time-domain spectroscopy
% measurements on GaN. The Fourier Transform of the
% time-domain traces are obtained and used to
% determine the GaN refractive index. Additionally, the
% GaN relative permittivity is determined. The experimental
% data is obtained using Zomega's system.
%%%-----------------------------------------------------------%%%

%%%%%%%%-----Clear environment-----%%%%%%
clear
clc
close all
%%%%%%%%-----End sub-----%%%%%%
```

```
%%%%%%%%-----Define parameters-----%%%%%%
L = 1939;  % Number of points
NFFT = 2^nextpow2(L); % Next power of 2 from length of y
dt=0.05524655;
f = 1/2/dt*linspace(0,1,NFFT/2+1);
file1='refractive_index.xlsx';
%%%%%%%%-----End sub-----%%%%%%

%%%%%%%%-----Import text files-----%%%%%%
s1 = 'Zomega_SI_GaN.txt';
s2 = 'Zomega_N-_GaN.txt';
s3 = 'Zomega_N+_GaN.txt';
s4 = 'Zomega_sapphire.txt';
%%%%%%%%-----End sub-----%%%%%%

%%%%%%%%-----time domain signals-----%%%%%%
y1=dlmread(s1, '\t', 'B1..C1939');
y2=dlmread(s2, '\t', 'B1..C1939');
y3=dlmread(s3, '\t', 'B1..C1939');
y4=dlmread(s4, '\t', 'B1..C1939');
%%%%%%%%-----End sub-----%%%%%%

%%%%%%%%-----Export FULL time domain signals-----%%%%%%
warning('off','MATLAB:xlswrite:AddSheet')
aa=500;
bb=900;
cc=1150;
xlswrite(file1,{'time'},'GaN_td_full','F1');
xlswrite(file1,y1(:,1),'GaN_td_full','F2');
xlswrite(file1,{'Zomega_SI GaN'},'GaN_td_full','G1');
xlswrite(file1,y1(:,2)+aa,'GaN_td_full','G2');
xlswrite(file1,{'Zomega_N- GaN'},'GaN_td_full','H1');
xlswrite(file1,y2(:,2)+bb,'GaN_td_full','H2');
xlswrite(file1,{'Zomega_N+ GaN'},'GaN_td_full','I1');
xlswrite(file1,y3(:,2)+cc,'GaN_td_full','I2');
xlswrite(file1,{'Zomega_sapphire'},'GaN_td_full','J1');
xlswrite(file1,y4(:,2),'GaN_td_full','J2');
%%%%%%%%-----End sub-----%%%%%%

%%%%%%%%-----cut-off time domain signals-----%%%%%%
y1(1075:L,2)=0;
y2(1075:L,2)=0;
y3(1075:L,2)=0;
y4(1080:L,2)=0;
%%%%%%%%-----End sub-----%%%%%%

%%%%%%%%-----Export CUT-OFF time domain signals-----%%%%%%
xlswrite(file1,{'time'},'GaN_td_co','F1');
xlswrite(file1,y1(:,1),'GaN_td_co','F2');
xlswrite(file1,{'Zomega_SI GaN'},'GaN_td_co','G1');
xlswrite(file1,y1(:,2)+aa,'GaN_td_co','G2');
xlswrite(file1,{'Zomega_N- GaN'},'GaN_td_co','H1');
xlswrite(file1,y2(:,2)+bb,'GaN_td_co','H2');
xlswrite(file1,{'Zomega_N+ GaN'},'GaN_td_co','I1');
xlswrite(file1,y3(:,2)+cc,'GaN_td_co','I2');
xlswrite(file1,{'Zomega_sapphire'},'GaN_td_co','J1');
```

```
xlswrite(file1,y4(:,2),'GaN_td_co','J2');
%%%%%%%%-----End sub-----%%%%%%

%%%%%%%%-----FT of signals-----%%%%%%
Y1 = fft(y1(1:L,2),NFFT);
Y2 = fft(y2(1:L,2),NFFT);
Y3 = fft(y3(1:L,2),NFFT);
Y4 = fft(y4(1:L,2),NFFT);
%%%%%%%%-----End sub-----%%%%%%

%%%%%%%%-----Relative signals-----%%%%%%
Yrel_1=Y1(1:NFFT/2+1)./Y4(1:NFFT/2+1);
Yrel_1(:,1)=real(Yrel_1(:,1))-i*imag(Yrel_1(:,1));
Yrel_2=Y2(1:NFFT/2+1)./Y4(1:NFFT/2+1);
Yrel_2(:,1)=real(Yrel_2(:,1))-i*imag(Yrel_2(:,1));
Yrel_3=Y3(1:NFFT/2+1)./Y4(1:NFFT/2+1);
Yrel_3(:,1)=real(Yrel_3(:,1))-i*imag(Yrel_3(:,1));
%%%%%%%%-----End-----%%%%%%

%%%%%%%%-----Export FT amplitude-----%%%%%%
xlswrite(file1,{'frequency'},'GaN_fd_amp','E1');
xlswrite(file1,f(:),'GaN_fd_amp','E2');
xlswrite(file1,{'Zomega_amp_SI'},'GaN_fd_amp','F1');
xlswrite(file1,abs(Yrel_1(:)),'GaN_fd_amp','F2');
xlswrite(file1,{'Zomega_amp_N-'},'GaN_fd_amp','G1');
xlswrite(file1,abs(Yrel_2(:)),'GaN_fd_amp','G2');
xlswrite(file1,{'Zomega_amp_N+'},'GaN_fd_amp','H1');
xlswrite(file1,abs(Yrel_3(:)),'GaN_fd_amp','H2');
%%%%%%%%-----End-----%%%%%%

%%%%%%%%-----Export FT phase-----%%%%%%
xlswrite(file1,{'frequency'},'GaN_fd_phase','E1');
xlswrite(file1,f(:),'GaN_fd_phase','E2');
xlswrite(file1,{'Zomega_phase_SI'},'GaN_fd_phase','F1');
xlswrite(file1,unwrap(angle(Yrel_1(:))),'GaN_fd_phase','F2');
xlswrite(file1,{'Zomega_phase_N-'},'GaN_fd_phase','G1');
xlswrite(file1,unwrap(angle(Yrel_2(:))),'GaN_fd_phase','G2');
xlswrite(file1,{'Zomega_phase_N+'},'GaN_fd_phase','H1');
xlswrite(file1,unwrap(angle(Yrel_3(:)))-2*pi,'GaN_fd_phase','H2');
%%%%%%%%-----End-----%%%%%%

%%%%%%%%%%%
%%-SI GaN-%%
%%%%%%%%%%%

%%%%%%%%-----Find refractive index-----%%%%%%
V=230;      %number of points that are solved for
n3p=3.03;   %refractive index of sapphire
d2=5e-6;   %thickness of GaN
d3=419e-6;   %thickness of sapphire substrate on GaN sample
d3_ref=435e-6;   %thickness of bare sapphire wafer
lower_limit=zeros(V,1);
lower_limit(:)=1-1*i;   %lower limit of solver
upper_limit=zeros(V,1);
upper_limit(:)=10+10*i;   %upper limit of solver
```

```
Nf=GAN_REFRACTIVE_INDEX(V, n3p, d2, d3, d3_ref, ...
lower_limit, upper_limit, f, Yrel_1);
%%%%%%%%-----End sub-----%%%%%%

%%%%%%%%-----Export refractive index-----%%%%%%
xlswrite(file1,{'frequency'},'SI_GaN_RI','D1');
xlswrite(file1,f(1:V)','SI_GaN_RI','D2');
xlswrite(file1,{'n_Zomega'},'SI_GaN_RI','E1');
xlswrite(file1,real(Nf(1:V)),'SI_GaN_RI','E2');
xlswrite(file1,{'K_Zomega'},'SI_GaN_RI','F1');
xlswrite(file1,imag(Nf(1:V)),'SI_GaN_RI','F2');
%%%%%%%%-----End sub-----%%%%%%

%%%%%-----find relative permittivity-----%%%%%%
ERf=zeros(V,1);
for ii=1:V
    fi=f(ii)*10^12;
    w=2*pi*fi;
    ERf(ii) = Nf(ii)^2;
end
%%%%%-----End sub-----%%%%%%

%%%%%%%%-----Export relative permittivity-----%%%%%%
xlswrite(file1,{'frequency'},'SI_GaN_RP','F1');
xlswrite(file1,f(1:V)','SI_GaN_RP','F2');
xlswrite(file1,{'epsr_real_Zomega'},'SI_GaN_RP','G1');
xlswrite(file1,real(ERf(1:V)),'SI_GaN_RP','G2');
xlswrite(file1,{'epsr_imag_Zomega'},'SI_GaN_RP','H1');
xlswrite(file1,imag(ERf(1:V)),'SI_GaN_RP','H2');
%%%%%%%%-----End-----%%%%%%

%%%%%%%%%%%
%%-N- GaN-%%
%%%%%%%%%%%

%%%%%%%%-----Find refractive index-----%%%%%%
V=230;      %number of points that are solved for
n3p=3.03;   %refractive index of sapphire
d2=5e-6;   %thickness of GaN
d3=435e-6;   %thickness of sapphire substrate on GaN sample
d3_ref=435e-6;   %thickness of bare sapphire wafer
lower_limit=zeros(V,1);
lower_limit(:)=1-1*i;   %lower limit of solver
upper_limit=zeros(V,1);
upper_limit(1:V/2)=50+55*i;   %upper limit of solver
upper_limit(V/2+1:V)=20+20*i;   %upper limit of solver

Nf=GAN_REFRACTIVE_INDEX(V, n3p, d2, d3, d3_ref, ...
lower_limit, upper_limit, f, Yrel_2);
%%%%%%%%-----End sub-----%%%%%%

%%%%%%%%-----Export refractive index-----%%%%%%
xlswrite(file1,{'frequency'},'N-_GaN_RI','D1');
xlswrite(file1,f(1:V)','N-_GaN_RI','D2');
```

```
xlswrite(file1,{'n_Zomega'},'N-_GaN_RI','E1');
xlswrite(file1,real(Nf(1:V)),'N-_GaN_RI','E2');
xlswrite(file1,{'K_Zomega'},'N-_GaN_RI','F1');
xlswrite(file1,imag(Nf(1:V)),'N-_GaN_RI','F2');
%%%%%%%%-----End-----%%%%%%

%%%%%-----find relative permittivity-----%%%%%%
ERf=zeros(V,1);
for ii=1:V
    fi=f(ii)*10^12;
    w=2*pi*fi;
    ERf(ii) = Nf(ii)^2;
end
%%%%%-----End-----%%%%%%

%%%%%%%%-----Export relative permittivity-----%%%%%%
xlswrite(file1,{'frequency'},'N-_GaN_RP','F1');
xlswrite(file1,f(1:V)','N-_GaN_RP','F2');
xlswrite(file1,{'epsr_real_Zomega'},'N-_GaN_RP','G1');
xlswrite(file1,real(ERf(1:V)),'N-_GaN_RP','G2');
xlswrite(file1,{'epsr_imag_Zomega'},'N-_GaN_RP','H1');
xlswrite(file1,imag(ERf(1:V)),'N-_GaN_RP','H2');
%%%%%%%%-----End-----%%%%%%

%%%%%%%%%%%%
%%-N+ GaN-%%
%%%%%%%%%%%%

%%%%%%%%-----Find refractive index-----%%%%%%
V=230;      %number of points that are solved for
n3p=3.03;   %refractive index of sapphire
d2=5e-6;   %thickness of GaN
d3=435e-6;   %thickness of sapphire substrate on GaN sample
d3_ref=435e-6;   %thickness of bare sapphire wafer
lower_limit=zeros(V,1);
lower_limit(:)=1-1*i;   %lower limit of solver
upper_limit=zeros(V,1);
upper_limit(1:20)=90+90*i;   %upper limit of solver
upper_limit(21:V)=40+40*i;   %upper limit of solver

Nf=GAN_REFRACTIVE_INDEX(V, n3p, d2, d3, d3_ref, ...
lower_limit, upper_limit, f, Yrel_3);
%%%%%%%%-----End sub-----%%%%%%

%%%%%%%%-----Export refractive index-----%%%%%%
xlswrite(file1,{'frequency'},'N+_GaN_RI','D1');
xlswrite(file1,f(1:V)','N+_GaN_RI','D2');
xlswrite(file1,{'n_Zomega'},'N+_GaN_RI','E1');
xlswrite(file1,real(Nf(1:V)),'N+_GaN_RI','E2');
xlswrite(file1,{'K_Zomega'},'N+_GaN_RI','F1');
xlswrite(file1,imag(Nf(1:V)),'N+_GaN_RI','F2');
%%%%%%%%-----End sub-----%%%%%%

%%%%%-----find relative permittivity-----%%%%%%
ERf=zeros(V,1);
```

```
for ii=1:V
    fi=f(ii)*10^12;
    w=2*pi*fi;
    ERf(ii) = Nf(ii)^2;
end
%%%%-----End sub-----%%%%%%

%%%%%%%-----Export relative permittivity-----%%%%%%
xlswrite(file1,{'frequency'},'N+_GaN_RP','F1');
xlswrite(file1,f(1:V)','N+_GaN_RP','F2');
xlswrite(file1,{'epsr_real_Zomega'},'N+_GaN_RP','G1');
xlswrite(file1,real(ERf(1:V)),'N+_GaN_RP','G2');
xlswrite(file1,{'imag_real_Zomega'},'N+_GaN_RP','H1');
xlswrite(file1,imag(ERf(1:V)),'N+_GaN_RP','H2');
%%%%%%%-----End sub-----%%%%%%
```

TA_system_GaN.m

```
%%%%%%%%%%%%%%%%%%%%%%%%%%%%%%%%%%%%%%%%%%%%%%%%%%%%
%%%%%%%%%%%%%%%---TA system---%%%%%%%%%%%%%%%
%%%%%%%%%%%%%%%---GaN---%%%%%%%%%%%%%%%%%%%%
%%%%%%%%%%%%%%%%%%%%%%%%%%%%%%%%%%%%%%%%%%%%%%%%%%%

%%%-----------------------------------------------------------%%%
% The following script outputs the THz time-domain traces
% obtained by performing THz time-domain spectroscopy
% measurements on GaN. The Fourier Transform of the
% time-domain traces are obtained as well. The experimental
% data is obtained using the TA system.
%%%-----------------------------------------------------------%%%

%%%%%%%-----Clear environment-----%%%%%%
clear
clc
close all
%%%%%%%-----End sub-----%%%%%%

%%%%%%%-----Define parameters-----%%%%%%
L = 150;  % Number of points
NFFT = 2^nextpow2(1000); % Next power of 2 from length of y
dt=0.08;
f = 1/2/dt*linspace(0,1,NFFT/2+1);
file1='refractive_index.xlsx';
%%%%%%%-----End sub-----%%%%%%

%%%%%%%-----Import text files-----%%%%%%
s1 = 'TA_system_n-_GaN.txt';
s2 = 'TA_system_n+_GaN.txt';
s3 = 'TA_system_free_space_GaN.txt';
s4 = 'TA_system_sapphire.txt';
s5 = 'TA_system_free_space_sapphire.txt';
%%%%%%%-----End sub-----%%%%%%
```

```
%%%%%%%%-----time domain signals-----%%%%%%
y1=dlmread(s1, '\t', 'A1..B150');
y2=dlmread(s2, '\t', 'A1..B150');
y3=dlmread(s3, '\t', 'A1..B150');
y4=dlmread(s4, '\t', 'A1..B150');
y5=dlmread(s5, '\t', 'A1..B150');
%%%%%%%%-----End sub-----%%%%%%

%%%%%%%%-----Export FULL time domain signals-----%%%%%%
warning('off','MATLAB:xlswrite:AddSheet')
aa=0.01;
bb=0.016;
xlswrite(file1,{'time'},'GaN_td_full','K1');
xlswrite(file1,y1(:,1),'GaN_td_full','K2');
xlswrite(file1,{'TA_system_N- GaN'},'GaN_td_full','L1');
xlswrite(file1,y1(:,2)+aa,'GaN_td_full','L2');
xlswrite(file1,{'TA_system_N+ GaN'},'GaN_td_full','M1');
xlswrite(file1,y2(:,2)+bb,'GaN_td_full','M2');
xlswrite(file1,{'TA_system_free space'},'GaN_td_full','N1');
xlswrite(file1,y3(:,2),'GaN_td_full','N2');
%%%%%%%%-----End sub-----%%%%%%

%%%%%%%%-----cut-off time domain signals-----%%%%%%
y1(1:63,2)=0;
y1(120:L,2)=0;
y2(1:63,2)=0;
y2(120:L,2)=0;
y3(1:23,2)=0;
y3(85:L,2)=0;
y4(1:65,2)=0;
y4(145:L,2)=0;
y5(1:30,2)=0;
y5(108:L,2)=0;
%%%%%%%%-----End sub-----%%%%%%

%%%%%%%%-----Export CUT-OFF time domain signals-----%%%%%%
xlswrite(file1,{'time'},'GaN_td_co','K1');
xlswrite(file1,y1(:,1),'GaN_td_co','K2');
xlswrite(file1,{'TA_system_N- GaN'},'GaN_td_co','L1');
xlswrite(file1,y1(:,2)+aa,'GaN_td_co','L2');
xlswrite(file1,{'TA_system_N+ GaN'},'GaN_td_co','M1');
xlswrite(file1,y2(:,2)+bb,'GaN_td_co','M2');
xlswrite(file1,{'TA_system_free space'},'GaN_td_co','N1');
xlswrite(file1,y3(:,2),'GaN_td_co','N2');
%%%%%%%%-----End sub-----%%%%%%

%%%%%%%%-----FT of signals-----%%%%%%
Y1 = fft(y1(1:L,2),NFFT);
Y2 = fft(y2(1:L,2),NFFT);
Y3 = fft(y3(1:L,2),NFFT);
Y4 = fft(y4(1:L,2),NFFT);
Y5 = fft(y5(1:L,2),NFFT);
%%%%%%%%-----End-----%%%%%%

%%%%%%%%-----Relative signal-----%%%%%%
Yrel_1=Y1(1:NFFT/2+1)./Y3(1:NFFT/2+1).* ...
```

```
Y5(1:NFFT/2+1)./Y4(1:NFFT/2+1);
Yrel_1(:,1)=real(Yrel_1(:,1))-i*imag(Yrel_1(:,1));
Yrel_2=Y2(1:NFFT/2+1)./Y3(1:NFFT/2+1).* ...
Y5(1:NFFT/2+1)./Y4(1:NFFT/2+1);
Yrel_2(:,1)=real(Yrel_2(:,1))-i*imag(Yrel_2(:,1));
%%%%%%%%-----End-----%%%%%%

%%%%%%%%-----Export FT amplitude-----%%%%%%
xlswrite(file1,{'frequency'},'GaN_fd_amp','I1');
xlswrite(file1,f(:),'GaN_fd_amp','I2');
xlswrite(file1,{'TA_system_amp_N-'},'GaN_fd_amp','J1');
xlswrite(file1,abs(Yrel_1(:)),'GaN_fd_amp','J2');
xlswrite(file1,{'TA_system_amp_N+'},'GaN_fd_amp','K1');
xlswrite(file1,abs(Yrel_2(:)),'GaN_fd_amp','K2');
%%%%%%%%-----End-----%%%%%%

%%%%%%%%-----Export FT phase-----%%%%%%
xlswrite(file1,{'frequency'},'GaN_fd_phase','I1');
xlswrite(file1,f(:),'GaN_fd_phase','I2');
xlswrite(file1,{'360_phase_N-'},'GaN_fd_phase','J1');
xlswrite(file1,unwrap(angle(Yrel_1(:))),'GaN_fd_phase','J2');
xlswrite(file1,{'360_phase_N+'},'GaN_fd_phase','K1');
xlswrite(file1,unwrap(angle(Yrel_2(:))),'GaN_fd_phase','K2');
%%%%%%%%-----End-----%%%%%%
```

GAN_REFRACTIVE_INDEX.m

```
function Nf = GAN_REFRACTIVE_INDEX(V, n3p, d2, d3, d3_ref, ...
lower_limit, upper_limit, f, Yrel)
%%%-----------------------------------------------------------%%%
% The following code uses experimental data obtained by THz
% time-domain spectroscopy experiments (performed on
% thin film GaN grown on sapphire substrates) to determine
% the GaN refractive index.
%
% Input parameters:
% -V is the number of points that are solved for
% -n3p is the refractive index of the sapphire substrate
% -d2 is the thickness of the GaN
% -d3 is the thickness of the sapphire substrate on the GaN sample
% -d3_ref is the thickness of the bare sapphire (reference) wafer
% -lower limit is the minimum GaN refractive index the
%  solver considers
% -upper limit is the maximum GaN refractive index the
%  solver considers
% -f is the frequency of the radiation
% -Yrel is the experimental measurements
%
% Output parameter:
% -Nf is the vector containing the GaN refractive index
%%%-----------------------------------------------------------%%%

%%%%%%%%-----Define parameters-----%%%%%%
n1p=1;   %refractive index of air
```

```
syms n2p;
n4p=1;   %refractive index of air
c=299792458;   %speed of light in a vacuum
%%%%%%%%-----End sub-----%%%%%%

%%%%%%%%-----Find refractive index of SI GaN-----%%%%%%
Nf=zeros(V,1);
for ii=1:V
    fi=f(ii)*10^12;   %frequency
    w=2*pi*fi;   %angular frequency
    k0=w/c;   %free space wavevector
    k2=w/c*n2p;   %GaN wavevector
    k3=w/c*n3p;   %sapphire wavevector
    t12=2*n1p/(n1p+n2p);   %transmission at air/GaN interface
    t23=2*n2p/(n2p+n3p);   %transmission at GaN/sapphire interface
    t13=2*n1p/(n1p+n3p);   %transmission at air/sapphire interface
    r12=(n1p-n2p)/(n1p+n2p);   %reflection from air/GaN interface
    r23=(n2p-n3p)/(n2p+n3p);   %reflection from GaN/sapphire inter.

    t=t12*t23/t13*exp(i*k2*d2)*exp(i*k3*d3)/ ...
    (1+r12*r23*exp(2*i*k2*d2))*exp(i*k0*d3_ref)/exp(i*k0*d3)/ ...
    exp(i*k0*d2)/exp(i*k3*d3_ref); %transmission through GaN sample

    if t~=0
        n_temp=vpasolve(Yrel(ii)==t,n2p, ...
        [lower_limit(ii) upper_limit(ii)])
    end

    if length(n_temp)>0
        Nf(ii)=n_temp;
    end

end
%%%%%%%%-----End sub-----%%%%%%

end
```